1 2 Don Ames
STAFF VICE PRESIDENT
MCR

NASA Technical Memorandum 86321

1400 11 DEC 1984

DO NOT DESTROY
RETURN TO LIBRARY
DEPT. 022

Research and Technology

1984 Annual Report of the Langley Research Center



29 JUL 1985
MCDONNELL DOUGLAS
RESEARCH & ENGINEERING LIBRARY
ST. LOUIS

NASA

NATL AERONAUTICS AND SPACE ADM; NASA-TM-86321

BRN3163
LM101325E

Foreword

The role of the Langley Research Center is to engage in the basic and applied research necessary for the advancement of aeronautics and space flight, to generate new and advanced concepts for the accomplishment of related national goals, and to provide research advice, technological support, and assistance to other NASA installations, other government agencies, and industry. This Langley Research Center 1984 Annual Report on Research and Technology contains highlights of our major accomplishments and applications made during the past year. The highlights illustrate both the broad range of the research and technology activities at the Langley Research Center and the contributions of this work toward maintaining United States leadership in aeronautics and space research. For further information about the report contact Jerry C. South, Chief Scientist, Mail Stop 103, Langley Research Center, Hampton, Virginia 23665, (804) 865-3316.



Donald P. Hearth
Director

DIRECTOR
AERONAUTICS & TECHNOLOGY
13452 7 NOV 1984

Availability Information

The NASA program office and the corresponding Agency-wide Research and Technology Objectives and Plans (RTOP) work breakdown structure are listed for each research and technology accomplishment in the Contents. OAST designates the Office of Aeronautics and Space Technology; OSSA designates the Office of Space Science and Applications; AD designates the Deputy Administrator; OER designates the Office of External Relations; and OSF designates the Office of Space Flight.

For additional information on any summary, contact the individual identified with the highlight. This individual is generally either a member or a leader of the research group submitting the highlight. Commercial telephone users may dial the listed extension preceded by (804) 865. Telephone users with access to the Federal Telecommunications System (FTS) may dial the extension preceded by 928.

Contents

Foreword i
Availability Information ii

Aeronautics Directorate

Aeronautics Directorate 1
Görtler Vortex Experiment 1
AD (307-03-01)
Spectral Methods for Aerodynamic Problems 2
OAST (505-31-03)
Numerical Simulations of Transition 3
OAST (505-31-03)
Navier-Stokes Solutions of Subsonic Compressible Base Flow 3
OAST (505-31-03)
Large-Eddy Substitution Via Vortex Cancellation for Wall Turbulence Control 4
OAST (505-31-13)
Heat Transfer Efficiency Increases for Riblet Drag Reducing Surfaces 5
OAST (505-31-13)
Vortex Breakdown Theory 5
OAST (505-31-23)
Three-Dimensional Navier-Stokes Code for Exhaust Plume Flow Field 6
OAST (505-40-90)
Advanced Design Rotor for the AH-64 6
OAST (505-42-23)
Advanced Powered-Lift STOVL Fighter Configuration 7
OAST (505-43-03)
Tumbling Studies of an Advanced Fighter Configuration 7
OAST (505-43-13)
Free-Flight Tests of Vortex Flaps on a 0.15-Scale F-106B Model 8
OAST (505-43-13)
Unsteady Flow Separation at High Angles of Attack 8
OAST (505-43-13)
F-16XL Model Flight Tests 9
OAST (505-43-13)
Automatic Engine-Out Trim System for Light Twin Aircraft 9
OAST (505-43-23)
Numerical Simulation of Inlet/Diffuser System Flows 10
OAST (505-43-23)
Propulsive Wing/Canard Fighter for STOL Operations 11
OAST (505-43-23)
Low-Speed Aerodynamics of an Advanced Fighter Employing High-Lift Devices and Multifunction Nozzles 11
OAST (505-43-23)
SWINT Code Application to Advanced Missile Configuration 12
OAST (505-43-23)
Wing Design Including Leading-Edge Thrust 12
OAST (505-43-23)

Application of a Full-Potential Method for Analysis of Complex Aircraft Geometries 13
OAST (505-43-23)
Approximate Entropy Correction to a Three-Dimensional Supersonic Full-Potential Flow Code 14
OAST (505-43-23)
Combustion Diagnostics 15
OAST (505-43-83)
A Simplified Hydrocarbon Reaction Mechanism for Combustion Applications 16
OAST (505-43-83)
Navier-Stokes Solution for Flow Inside Two-Dimensional Thrust Reversing Nozzles 16
OAST (505-43-90)
Application of an Outboard Leading-Edge Droop for Stall/Spin Resistance on a Natural Laminar Flow Wing 17
OAST (505-45-23)
Wing-Tip-Mounted Turboprop 17
OAST (505-45-43)

Electronics Directorate

Electronics Directorate 19
Tunable-Diode Laser Heterodyne Spectrometer Demonstrated 19
OSSA (147-13-01)
Nonintrusive Simultaneous Measurement of Three Flow Parameters in a Supersonic Flow. 20
OAST (505-31-53)
Laser Doppler Velocimeter Measurements of a Juncture and Taylor-Görtler Vortices Flow Fields 21
OAST (505-31-53)
Spline Smoothing of Data With Variable Tension Between Knots 21
OAST (505-31-83)
Algebraic Grid Generation for Wing-Fuselage Bodies 22
OAST (505-31-83)
Frequency Response Analysis for Sampled Image Systems 22
OAST (505-31-83)
Ultrasonic Sensor for Optimizing Resin Cure 23
OAST (505-33-23)
Shuttle Wheel Bolt Stress Measurements 23
OAST (505-33-23)
Residual Stress Measurement Technique 24
OAST (505-33-23)
Experimental Confirmation of Acoustic Radiation Stress in Solids 24
OAST (505-33-23)
Effects of Metal Ions on Positronium Formation in Polymers 25
OAST (505-33-90)
Parameter Estimation Applied to a Highly Augmented Airplane 25
OAST (505-34-03)
A Fault-Inferring Nonlinear Detection System (FINDS) Algorithm for Integrated Avionics Sensor Configurations 26
OAST (505-34-13)
Development of the Semi-Markov Unreliability Range Evaluation (SURE) Program 26
OAST (505-34-13)

Advanced System/Subsystems Monitoring Interface 27
OAST (505-34-13)
Pilot/Autopilot Interface Using Hands-On Throttle and Stick Concept 27
OAST (505-34-13)
Real-Time Smoothing of Rolled Symbology in All-Raster Electronic Flight Displays 28
OAST (505-34-13)
Raster Graphic Display Generator Integrated With Thin-Film Electroluminescent (TFEL) Display Panel 29
OAST (505-34-13)
High-Resolution Large-Screen TFEL Flat-Panel Display Using Monolithic Drivers 29
OAST (505-34-13)
Effects of Digital Altimetry on Pilot Workload 30
OAST (505-35-13)
Advanced Display Used for Precise Flight Control 31
OAST (505-35-13)
Advanced Avionics Systems Pilot Interface Study 31
OAST (505-35-13)
Expert System for Aircraft Engine Fault Diagnosis 32
OAST (505-35-13)
Four-Dimensional Guidance Concept for Airborne Terminal Areas 32
OAST (505-45-33)
Control/Display System Problem and Solution Verified by Model Analysis 33
OAST (505-45-33)
Oculometric Indices of Simulator and Aircraft Motion 34
OAST (505-45-33)
Integrated Digital/Electric Aircraft Has Performance Potential 34
OAST (505-45-73)
Remote Solar-Powered Data Acquisition Module 35
OAST (506-53-63)
Evaluation of Quantum-Well Lead Salt Tunable-Diode Lasers 35
OAST (506-54-23)
Pushbroom Microwave Radiometer Technology for Soil Moisture Measurement 36
OAST (506-54-23)
Co:MgF_2 Lidar System 36
OAST (506-54-23)
Kinematic Control of Robot Arms 36
OAST (506-54-63)
Distributed Artificially Intelligent System for Interacting With the Environment 37
OAST (506-54-63)
Teleoperator Interface Research 38
OAST (506-57-23)
Fast Initialization of Bubble Memory Systems 38
OAST (506-58-13)
AlGaAs Phased-Array Semiconductor Lasers for Space Communications 39
OAST (506-58-23)
Fiber Optics Wavelength Division Multiplexing 39
OAST (506-58-13)
15-Meter Hoop-Column Antenna Tests 40
OAST (506-62-43)

Space Directorate

Space Directorate 41

Measurements of Trace Gases in the Remote Troposphere: Gaining Insight Into the Tropospheric Ozone Budget 41
OSSA (176-10-05)

Biospheric-Atmospheric Coupling 42
OSSA (176-20-02)

Aerosol Optical Extinction in Atmospheric Mixed Layers by Airborne Lidar 42
OSSA (176-40-04)

Airborne Lidar Observations of a Tropopause Fold Event 43
OSSA (176-40-04)

Methane Flux From Coastal Salt Marshes 44
OSSA (199-30-26)

Use of Radiative Transfer Modeling to Correct for Angle-of-View Effects on Remote Sensing of Vegetation 44
OSSA (199-30-36)

Nebulization Reflux Concentrator 45
AD (307-04-02)

Calculation of Heating on Shuttle Lower Surface 46
OAST (506-51-13)

Direct Simulation of Transitional Flow for Hypersonic Reentry Conditions 46
OAST (506-51-13)

Engineering Flow Field Method With Angle-of-Attack Applications 47
OAST (506-51-13)

Experimental Investigation of a Transatmospheric Vehicle at Mach 20 47
OAST (506-51-13)

Orbiter Boundary Layer Transition Visualization 48
OAST (506-51-13)

Orbiter Shock-Interaction-Induced Heat Transfer 48
OAST (506-51-13)

Space Shuttle Orbiter Side Fuselage Heating Study 49
OAST (506-51-13)

Temperature-Dependent Reaction Rate Expression for Oxygen Recombination on Shuttle Heatshield Tiles 50
OAST (506-51-13)

Box Truss Antenna Structure 50
OAST (506-62-23)

An Analytical Method for Assessment of Space Station Rigid Body Control Dynamics With Articulating Appendages 51
OAST (506-64-13)

Atmospheric Model Implementation for Space Station Orbital Control and Decay Assessments 52
OAST (506-64-13)

Space Station Environmental Control and Life Support System Technology Assessment Analysis 53
OAST (506-64-13)

Space Station Systems Analysis Through Phased Emulation/Simulation 54
OAST (506-64-14)

MAPS Shuttle-Borne Remote Measurements of Carbon Monoxide 54
OSSA (618-22-31)

Bidirectional Cloud Models 55
OSSA (619-12-30)

Airborne Lidar Observations of Polar Stratospheric Clouds Over the North Pole 55
OSSA (665-10-40)
Aircraft Window Crazing Explained by SAM II Observation of Volcanic Material in Polar Stratosphere 56
OSSA (665-10-40)
Altitudinal and Latitudinal Variation of Aerosol Sizes Inferred From SAGE Data 57
OSSA (665-40-40)
Aerosol Measurements in the Arctic 57
OSSA (672-21-13)
Lidar Measurements of Arctic Haze During the 1984 Winter Polar Mission 58
OSSA (672-21-14)
Comparison of Satellite-Observed and Modeled Clear-Sky Albedos 58
OSSA (672-22-04)
Cloud Remote Sensing 59
OSSA (672-22-06)
Atmospheric Lapse Rate Regimes 60
OSSA (672-40-05)
Clouds in Climate Models 60
OSSA (672-40-05)
CO_2 Greenhouse Effect and Infrared Radiation 60
OSSA (672-40-05)
Ozone International Reference Models for the Middle Atmosphere 61
OSSA (673-41-07)
Polar Night NO_2 Measurements From LIMS 62
OSSA (673-41-10)
Distribution of Total Odd Nitrogen in the Stratosphere 63
OSSA (673-62-02)
Analysis and Application of Fourier Transform Spectroscopy in Atmospheric Remote Sensing 63
OSSA (678-12-04)
Computer-Aided Controllability Assessments of Space Station Conceptual Configurations . 64
OSF (906-84-40)

Structures Directorate

Structures Directorate 65
Effects of Flight on Shock-Associated Noise 65
OSSA (505-31-33)
Improved Failure Prediction Method for Cracked Metal Structures 66
OAST (505-33-23)
Rapid Adhesive Bonding 67
OAST (505-33-33)
Improved Metal Matrix Composites 67
OAST (505-33-33)
Off-Axis Tensile Coupon Requires High Aspect Ratio To Measure Shear Modulus Accurately 68
OAST (505-33-33)
Fracture Criteria for Adhesives 68
OAST (505-33-33)
Optically Transparent/Colorless Polyimide Films 69
OAST (505-33-33)

Forward-Swept-Wing/Body-Freedom Flutter Studies at Transonic Speeds 69
OAST (505-33-43)
Unsteady Aerodynamic Pressures and Instability Boundary Determined for Elastic Wing . 70
OAST (505-33-43)
Transonic Code Extended to Multiple Airfoil Configuration 71
OAST (505-33-43)
Method for Reducing Stress Concentration in Diffusion-Bonded Joints 71
OAST (505-33-53)
Validation of Sidewall Noise Reduction Theory 72
OAST (505-33-53)
Transmission Loss of Finite Composite Panels 72
OAST (505-33-53)
Curved-Cap Beaded-Web Corrugation 73
OAST (505-33-53)
Annoyance of Advanced Turboprop Aircraft Flyover Noise 74
OAST (505-33-90)
TDT Test Provides Essential Data Base for JVX Preliminary Design 74
OAST (505-42-23)
Helicopter Community Noise Study 75
OAST (505-35-13)
Superplastic Forming and Weldbrazing of Titanium Compression Panels 76
OAST (505-43-43)
Load-Limiting Subfloor Concepts Reduce Aircraft Crash Loads by 50 Percent 76
OAST (505-53-33)
Analysis Predicts Tire Carcass Temperature During Braked Rolling 77
OAST (505-45-14)
Single- and Counter-Rotation-Propeller Noise Comparison 77
OAST (505-45-43)
Automatic Finite-Element Mesh Refinement 78
OAST (506-51-23)
Siloxane-Modified Polyimide for Space Applications 78
OAST (506-53-23)
Metal Matrix Composite Processing To Minimize Thermal Strain Hysteresis 79
OAST (506-53-23)
Durable Thermal Protection System Concepts 79
OAST (506-53-33)
Emittance/Catalysis Enhancement of Superalloys for TPS Applications 80
OAST (506-53-33)
Three-Dimensional Architectures Improve Mechanical Properties of Carbon/Carbon Composites 80
OAST (506-53-33)
Underwater Neutral Buoyancy Tests Prove One-Man Assembly Concept Effective 81
OAST (506-53-43)
Thermal Protection System for Nose Cap of Aeroassisted Orbital Transfer Vehicle 82
OAST (506-53-43)
Fastener Concept Developed for High-Temperature Composite Materials 83
OAST (506-53-43)
Carbon-Carbon Hot Structure Shuttle Body Flap Design 83
OAST (506-53-43)
Photogrammetric Measurement System Meets Solar Array Experiment Requirements ... 84
OAST (506-62-49)

Damage Containment Demonstrated for Compression Panel With Tough Resin 84
OAST (534-03-23)
Prediction of Noise and Aerodynamics of Supersonic Propellers 85
OAST (535-03-12)
Aeroacoustic Computation of Blade/Vortex Interaction 86
OAST (532-06-13)
Optimization Methods Applied to Rotor Blade Aerodynamic Design 86
OAST (532-06-13)

Projects Directorate

Projects Directorate 88
Technology Integration for Supersonic Cruise V/STOL Fighters 88
OAST (505-43-43)
Laminar Flow Control Technology 88
OAST (505-45-63)
Advanced Composite Structures Technology 89
OAST (534-06-13)

Systems Engineering and Operations Directorate

Systems Engineering and Operations Directorate 90
Nose Boom Development for the Global Tropospheric Experiment 90
OSSA (176-20-14)
Fastener Retention Systems for Cryogenic Wind Tunnel Models 91
OAST (505-31-53)
Explosively Severed Composite Panels for Aircraft Safety 91
OAST (505-42-23)
Field Repair of AH-1G Helicopter Window Cutting Assemblies 92
OAST (505-42-23)
Fabrication of Research Model Components Using Thermoplastic Composite Material ... 92
OAST (505-45-23)
Pultrusion Fabrication Technology 93
OAST (506-53-53)
Quartz Cable/Steel Bead Bond Joint for Hoop-Column Antenna 94
OAST (506-62-43)
Video Processor for Dynamic Analysis of Large Structures 94
OAST (506-62-49)
Optimal Design of a Thermally Stable Optical Bench 95
OSSA (618-32-33)
Thermal-Vacuum Testing and In Situ Optical Alignment Measurements of the HALOE Telescope and Sun Sensors 95
OSSA (678-12-04)

Technology Utilization Program

Technology Utilization Program 97
Water Quality Monitoring System 97
OER (141-20-10)

Collagen Phase Transition in Thermal Skin Death 97
OER (141-20-20)
Noninvasive Lung Diagnosis Through Sound 98
OER (141-20-21)

Aeronautics Directorate

The Aeronautics Directorate at NASA Langley is composed of approximately 300 scientists and engineers engaged in research in the various aeronautics disciplines. The Directorate is organized into three research divisions, which conduct aeronautical research to advance the state of the art throughout the complete aerodynamic speed range.

The Low-Speed Aerodynamics Division conducts research in the areas of basic fluid mechanics, low-speed aerodynamics, flight dynamics, and flight management, aircraft operations, aviation safety, and improved test methods. The Division develops and validates theoretical aerodynamic methods for subsonic conditions and design methodology required to improve subsonic aerodynamic performance, stall/spin behavior, handling qualities, and takeoff and landing performance.

The High-Speed Aerodynamics Division conducts research to advance the state of the art for supersonic aircraft, hypersonic aircraft, and missiles, and to support the development of high-performance military aircraft, advanced cruise and tactical missiles, the Space Shuttle, and follow-on advanced space transportation systems. New analytical methods for design and analysis are derived and applied to advanced high-speed aircraft and missile concepts. Key experiments are conducted to validate the analytical methods, explore the potential of advanced concepts, and provide a data base for use by industry design teams. Conceptual designs for advanced high-speed vehicles are conceived and analyzed in order to determine the performance payoff from the application of advanced research results.

The Transonic Aerodynamics Division conducts research to advance the state of the art of transonic aircraft technology in the areas of fundamental aerodynamics, with particular emphasis on Reynolds number effects, laminar-flow concepts, stability and control, performance analysis, configuration concepts, and related aerodynamic phenomena. Particular areas of emphasis include improving the efficiency and reducing the fuel consumption of conventional jet transports, developing the technology for advanced military combat aircraft, developing theoretical and analytical methods for predicting aerodynamic characteristics in separated and in transonic flows, developing advanced airfoils for low-speed and transonic aircraft and for helicopters, and developing advanced experimental techniques, including advanced wall concepts, for transonic wind tunnels, cryogenic wind tunnel technology, and magnetic suspension and balance systems. Research analysis is performed using advanced analytical techniques with Langley's large computer complex. These research results are obtained from tests conducted in Langley's unique experimental facilities, which span the range from subsonic through transonic (including the new National Transonic Facility) to supersonic.

Görtler Vortex Experiment

Görtler vortices arise in boundary layers along concave surfaces due to centrifugal effects. These streamwise vortices are one of the three known principal sources of instability that lead to transition from laminar to turbulent flow. There are a number of flow situations where the fluid encounters concave curvature; e.g., the lower surface of an LFC supercritical wing. This experiment was the first of its kind to study the development of Görtler vortices on an airfoil with a pressure gradient.

A 6-ft-chord experimental model was tested in the Low-Turbulence Pressure Tunnel (LTPT). Görtler vortices were first visualized using sublimating chemicals. The streamwise vortices were observed as alternating light and dark streaks on the surface due to the differential shear stress pattern of the vortex layer. Each pair of light and dark streaks together indicated one wavelength of the counterrotating streamwise vortex layer. A five-beam laser velocimeter was



Görtler vortex model in wind tunnel.

used to measure the three velocity components in the boundary layer and a dedicated computer system was used to record and process the data.

Theoretical studies of the Görtler instability have shown that the vortex amplification varies with free-stream velocity (i.e., with Reynolds number and Görtler number). An experimental investigation would be expected to show a vortex spacing corresponding to the theoretically predicted maximum amplified wavelength. However, previous experiments which were conducted in curved channels with zero pressure gradient did not find this correlation. Indeed, the wavelength was found to be almost independent of free-stream velocity which probably indicates that some portion of the test apparatus, such as turbulence damping screens, had "selected" the wavelength.

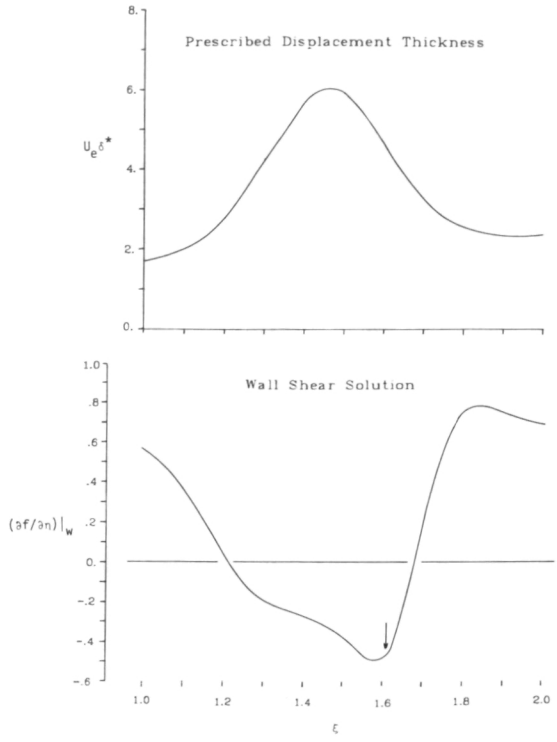
In the present experiment, the Görtler number was varied by changing the free-stream velocity. The experimentally determined wavelength fell near the theoretically predicted maximum amplified wavelength and clearly varied with Görtler number as predicted. These expected results probably were obtained because of the excellent low-turbulence environment and the absence of the opposite channel wall in this experiment.

J. Ray Dagenhart, 4514

Spectral Methods for Aerodynamic Problems

The accuracy and efficiency of the spectral collocation method for the solution of partial differential equations have been assessed over a wide range of problems of aerodynamic interest. Among the problems considered at LaRC were transonic potential flow past an arbitrary lifting airfoil, supersonic potential flow about a conical body, and a two-dimensional boundary layer flow with either external pressure gradient or displacement thickness prescribed. The methods developed in this study were straightforward, easy to apply, and robust; in many cases, a clear advantage in accuracy and/or efficiency over corresponding finite-difference techniques was seen.

In the airfoil application, the spectral-multigrid algorithm developed at LaRC was significantly more efficient than state-of-the-art finite-difference codes for subcritical flow cases. Despite a reduction of efficiency due to the shock-capturing technique required when transonic flow was present, the spectral method still offered high accuracy for overall properties such as lift for these cases. In the application to supersonic conical flow, however, the extensive regions of supersonic flow and strong shocks precluded any such advantage. This problem was, however, a good test of the robustness and range of applicability of the methods developed.



Wall shear for a separated boundary layer.

Good results were obtained in the application to boundary layer problems. As an illustration, a difficult separated-flow test case is shown. Solution was accomplished using the so-called inverse form of the boundary layer equations, in which displacement thickness distribution as a function of streamwise distance ξ is prescribed, and external pressure and wall shear are part of the solution. In the example, the wall shear solution $(\partial f/\partial \eta)|w$ at the point indicated by the arrow was accurate to three decimal places on a grid with only 26 points in the streamwise direction and 28 points in the normal direction. Estimates indicate that this is a factor-of-50 savings in total points over a corresponding second-order finite-difference method.

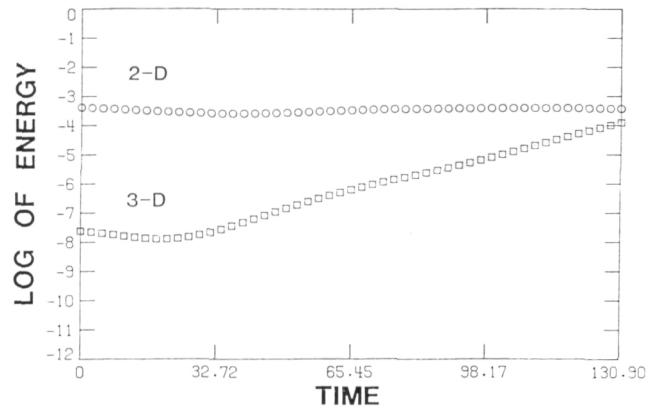
Craig L. Streett, 2627

Numerical Simulations of Transition

Fully spectral three-dimensional incompressible Navier-Stokes codes have been developed for simulating transition to turbulence in a channel and in a parallel boundary layer. The latter code has the capability of including the effects of laminar flow control techniques such as pressure gradient, suction, or heating. The distinguishing feature of the new algorithm is the ability to treat implicitly vertical variations (in both space and time) in viscosity. This capability is especially important in the case of heating, for the temperature-induced fluctuations in viscosity would otherwise lead to a severe time step limitation which would greatly increase the cost of the calculations.

Extensive tests have been performed to validate both codes. One such test involves the computation of very low amplitude disturbances known as Tollmein-Schlichting waves. An elaborate linear theory is available for these waves. Both codes are able to reproduce these waves to better than 0.01-percent accuracy over several wave periods.

A second test involves nonlinear effects. For both channel flow and boundary layer flow, linear theory predicts that all Tollmein-Schlichting waves should decay if the Reynolds number of the flow is smaller than a critical Reynolds number. Nevertheless, instabilities have been observed in subcritical situations. The codes reproduce previously observed subcritical instabilities in the channel and the boundary layer. Moreover, we have demonstrated that the same phenomenon occurs in a heated boundary layer, as illustrated. The calculation starts with a 10-percent two-dimensional wave plus a 0.1-percent-amplitude three-dimensional wave. (Both waves decay in the absence of one wave.) As the figure shows, the three-dimensional wave is unstable.



Evolution of the energy for subcritical heated boundary layer flow.

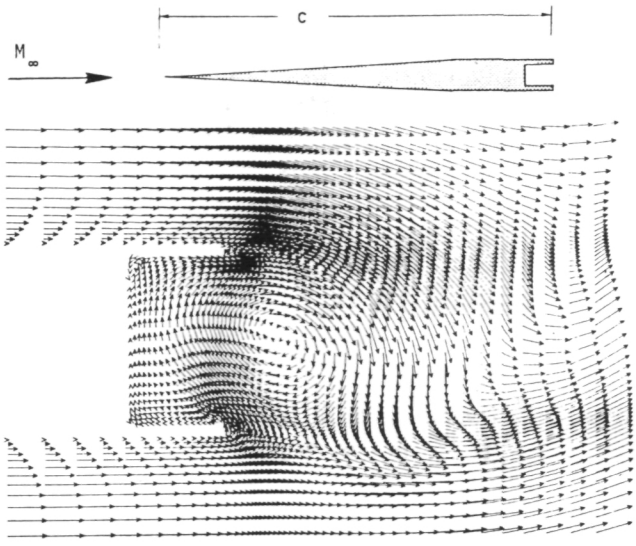
These codes are now being employed in an extensive series of calculations which are intended to clarify the basic nonlinear mechanisms responsible for the early stages of transition. A parametric study of secondary instability is under way.

Thomas A. Zang, 3171

Navier-Stokes Solutions of Subsonic Compressible Base Flow

The separated flow in the base region of a bluff body produces a drag force which can contribute significantly to the total drag of the body. In general, the nature of the near-wake flow is strongly dependent upon the geometry of the body and the Mach number regime and Reynolds number of the external flow. For example, a two-dimensional bluff body in a subsonic stream generates a wake dominated by a regular array of alternately shed vortices for a wide range of Reynolds numbers. Since the base drag in this case is associated with the vortex shedding, methods for reducing the base drag must be directed toward eliminating or weakening the vortex shedding or delaying the formation of the vortices. Two of the methods that have been found to reduce base drag in wind tunnel experiments are being studied numerically using solutions of the time-dependent two-dimensional compressible Navier-Stokes equations. These two methods are the use of a base cavity and the injection of mass through the base into the wake. The finite-difference scheme used in the present study is the unsplit MacCormack explicit predictor-corrector technique with an option for fourth-order accurate differencing of the convective terms. This scheme was selected because it could be vectorized to efficiently utilize the CDC CYBER-203 computer at Langley.

Calculations have been made for subsonic flow past the slender body configuration shown at the top of the figure for cases with unmodified bases as well as with the cavity and for the blunt base with mass injection into the wake. The figure shows velocity vectors in the near-wake region for Mach 0.6 external flow with a Reynolds number based on chord length of 9.62×10^3 at a point in time after periodic flow had been established. The presence of the cavity allows the vortex formation region to extend into the cavity. As a result, the



Velocity vectors for near-wake flow for model with cavity.

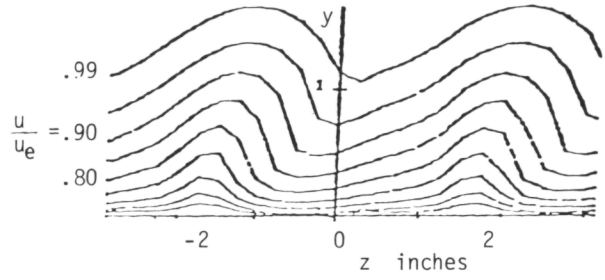
pressure along the rear wall of the cavity is now higher than along the base of the unmodified configuration at the corresponding point in the shedding cycle, and thus the base drag is reduced. In calculations with mass injection into the wake with sufficiently large velocity, the vortex formation region was moved downstream, resulting in higher base pressure and less base drag. For both types of base modification, the laminar-flow solutions have shown qualitative agreement with experimental turbulent-flow observations and have demonstrated the drag reduction capability possible with these types of base modifications. Further calculations are being made to extend the Mach number and Reynolds number range of the present results.

David H. Rudy

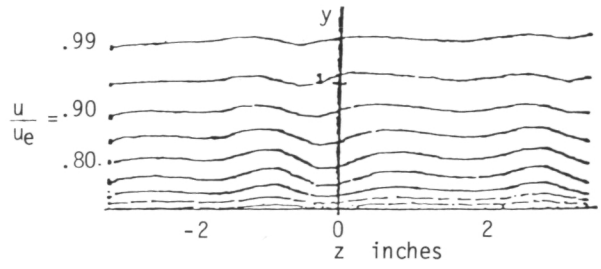
Large-Eddy Substitution Via Vortex Cancellation for Wall Turbulence Control

The substitution of longitudinal vortices for the large eddies of a turbulent boundary layer (and their subsequent removal) is being studied as a means of turbulence control. An initial experiment proves that longitudinal vortices created by flat-plate vortex generators can be cancelled downstream by vortex generators (unwinders) set to produce the opposite sign circulation. This is evidently the first successful attempt to cancel longitudinal vortices in a turbulent boundary layer.

The test was performed in the 2- × 3-Foot Boundary Layer Channel located at Langley Research Center. Seven co-rotating vortex generators were set at 3° angle to the flow whereas the unwinders were set at only −1.5° to allow for the viscous decay of vortex strength. The figures show the spanwise velocity profiles of the boundary layer at 3.87 ft from the vortex generators. The first figure shows the distortion of the boundary layer isobars (presented in terms of the ratio of the local velocity to the velocity at the edge of the boundary layer) due to the vortex generators alone. The second figure shows the relaxation of the isobars due to the unwinders placed 1.33 ft from the generators. The same results (i.e., "permanent removal") were found as far as 10 ft downstream from the vortex generators.



Vortex generators alone.



Vortex generators and unwinders.

The results of this research are applicable to vortex control as well as wall turbulence control. Besides altering the turbulent structure, this unwinding method may be useful in removing "necklace" vortices which interfere with propulsive efficiency and create noise on submarines. The unwinder method when applied to wall turbulence control has various possible applications which include optimization of laser windows, infrared sensors, sonar domes, and aircraft fuselages, as well as possible net drag reduction.

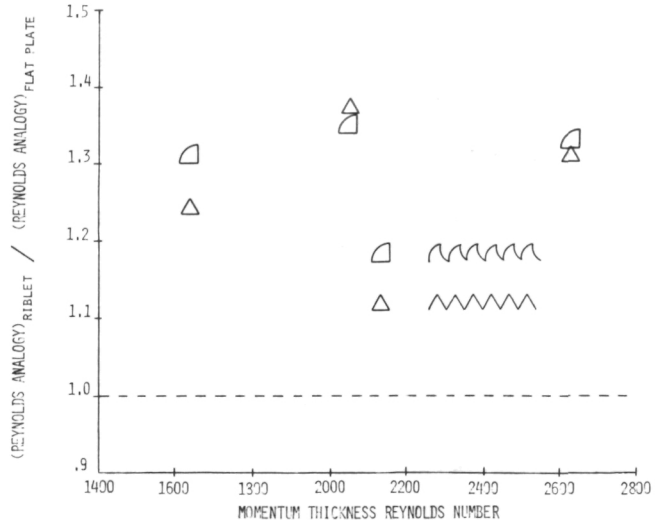
Catherine B. McGinley, 3736

Heat Transfer Efficiency Increases for Riblet Drag Reducing Surfaces

Tests conducted in the Langley 7- by 11-in. low-speed wind tunnel have provided measurements of the convective heat transfer efficiencies (i.e., Reynolds analogy factors) for a variety of riblet surfaces. Riblets are small, flow-aligned longitudinal grooves whose height/spacing relationships have been shown to influence fluid drag; in fact, riblets with a range of nondimensionalized height/spacing ratios have been clearly shown at NASA Langley to reduce drag.

Experimental heat transfer efficiency factors in this research relate each test surface's average convected heat transfer to its associated drag. To appreciate the test results, it is important to consider that most conventional rough surfaces exhibit Reynolds analogy factors below the flat-plate value. Typically, in these cases, although the roughness itself induces increased heat transfer, the attendant drag increase is proportionately greater, and the corresponding Reynolds analogy efficiency factor falls below the flat-plate reference factor.

Different kinds of nonplanar surface microgeometries apparently alter the boundary conditions of the flow at the wall differently. Current measurements of riblet surfaces show selected increases in Reynolds analogy factors of up to 36 percent above the flat-surface value. The largest increases in efficiency were produced by the two riblet surfaces depicted in the figure. Despite the shape variation in the riblet geometries (as suggested by the symbol shape), the data indicate that it is the nearly similar height/spacing relationship, scaled according to given flow conditions, which primarily determines the riblet heat transfer efficiencies. For the test flow regime, the riblet surfaces included in the figure also reduced drag by as much as 8 percent (riblet height/spacing > 1, absolute riblet height ≃ 0.020 in.).



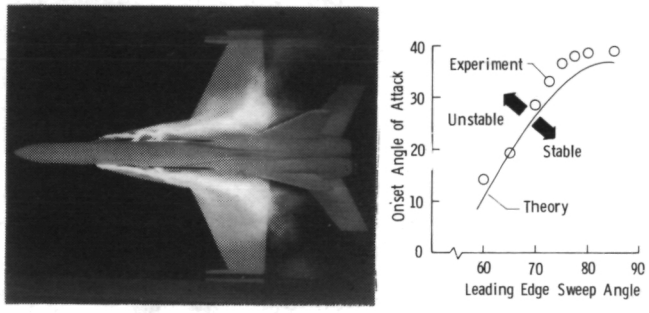
Sample Reynolds analogy data.

A potential engineering application of surfaces such as these riblets, whose observed Reynolds analogy factor increases result from both increased heat transfer and decreased drag, might include heat exchanger optimization; i.e., reduced size, weight, and cost.

A. Margrethe Lindemann, 3993

Vortex Breakdown Theory

Separation-induced leading-edge vortices can dominate the flow about slender wings at moderate to high angles of attack, often with favorable aerodynamic effects. However, as angle of attack is increased, the vortices can break down or "burst" in the vicinity of the configuration, causing many adverse effects such as lift loss, pitch up, and buffet. The water tunnel photograph illustrates strake vortices bursting over the wing of a YF-17 model and in the vicinity of the tail surfaces.



Vortex stability boundary; delta wings.

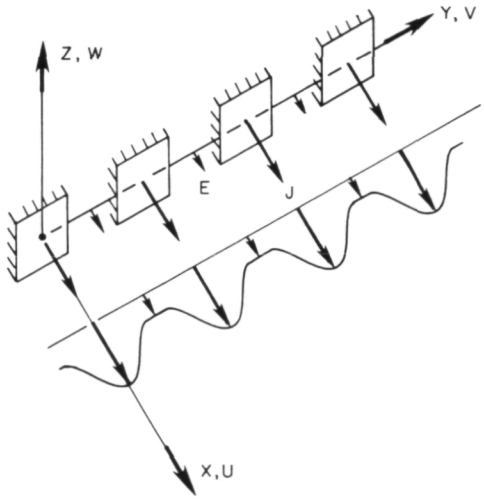
A theory has recently been developed at Langley for studying the vortex breakdown phenomenon. The three-dimensional method couples a nonlinear model of the inner vortex core with the (nonlinear) free vortex sheet theory, which models the outer portion of the vortex. Preliminary findings show reasonable correlation for the onset of vortex breakdown at the trailing edge of delta wings of differing leading-edge sweep angle, as illustrated. A similar correlation has been

found for trailing-edge sweep effects. Documentation of the theory is under way and extensions to the theory for additional flow effects are being studied.

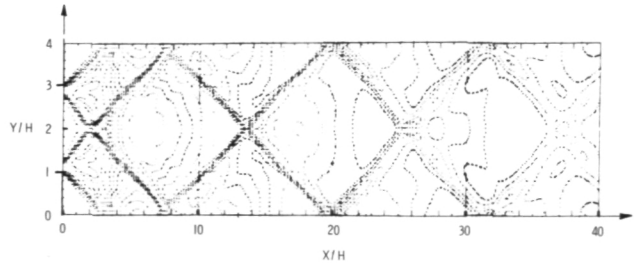
James M. Luckring, 2601

Three-Dimensional Navier-Stokes Code for Exhaust Plume Flow Field

A computer code for analyzing exhaust plume flow fields from nonaxisymmetric nozzles in subsonic and supersonic free streams has been developed by the Princeton Division of Science Applications, Inc., under contract to NASA Langley. The code solves the parabolized form of the three-dimensional Navier-Stokes equations by a hybrid steady-state marching procedure. In supersonic regions, a fully coupled shock-capturing procedure is used, while subsonic regions are solved with a pressure-split formulation. New procedures have been developed for the subsonic pressure-split solution which improve significantly the accuracy and speed of the computations.



Schematic of multiple square nozzles.



Parabolized Navier-Stokes pressure contours; multiple nozzles. Aspect ratio = 1; supersonic underexpanded jet.

The code is designed to analyze supersonic overexpanded or underexpanded nonaxisymmetric jets exhausting into subsonic or supersonic streams. Predictions have been made for both single and multiple, square and rectangular nozzles. A calculation representing an infinite array of square underexpanded jets in a supersonic free stream is shown schematically. The jets are initially 2×2 (dimensionless units) and their axes of symmetry have a spacing of 4. The calculations were performed using symmetry conditions on the $z = 0$ planes at $y = 0$ and $y = 2$. Pressure contours are shown in the x-y centerplane ($z = 0$) which clearly exhibit the formation of jet-induced bow shocks traversing the flow in the spanwise direction. The strength of these shocks is gradually weakened downstream due to the multiple-jet shock shear layer interactions. The ability to predict such complex flow fields is needed to understand both aerodynamic and acoustic interactions in modern aircraft nozzle installations. The code is currently being coupled with other external flow codes to predict these interactions.

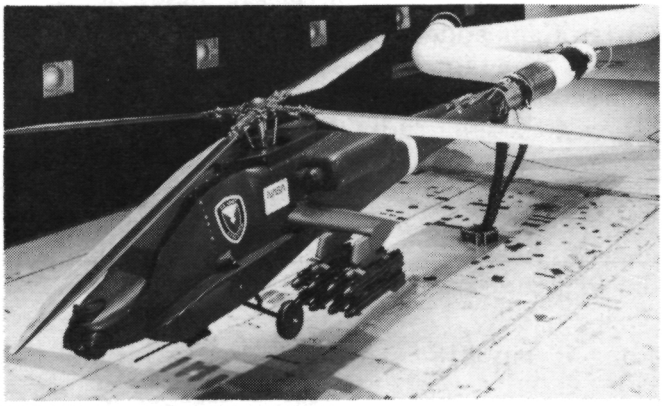
R. G. Wilmoth, 2673

Advanced Design Rotor for the AH-64

A 27-percent scale model of the AH-64 main rotor and fuselage was tested in the Langley 4- by 7-Meter Tunnel. Two different rotors were evaluated during the test program. The first rotor was an aeroelastically scaled model of the current flight rotor and the second was an advanced configuration designed by Army researchers. The aerodynamic design of the advanced blades incorporated technology which was developed and successfully demonstrated during an earlier UH-1 configuration study. The advanced blades utilize three airfoils developed at Langley especially for helicopter rotor application; thin tapered tips were used to reduce drag, and the blade twist was 12° (compared to 9° for the standard AH-64 blade). The blade is rectangular to 0.8 radius and then tapered to the tip with a taper ratio of 5. The nonrectangular planform is made practical by the use of composite materials.

Test data indicate performance improvements in hover and forward flight with an increase in figure of merit of 6 percent at design gross weight, sea level standard. This result indicates a power saving of 6 percent in hover and a corresponding fuel savings of 3 percent in hover, or a 4-percent (580-lb) increase in lift capability. These values are judged to be conservative because of model scale effects. Improvements in forward-flight performance have been measured (fuel savings and range) and the data are currently being analyzed to quantify the gains. The results of this research can now be coupled with other recent technology developments in advanced rotor design to enhance not only hover performance but high-speed flight and maneuverability as well.

J. C. Wilson, 3611



Model of advanced rotor for AH-64 helicopter.

Advanced Powered-Lift STOVL Fighter Configuration

An advanced powered-lift short takeoff and vertical landing (STOVL) fighter concept (General Dynamics E-7 configuration) was tested in the Langley 4- by 7-Meter Tunnel. The concept uses an in-wing-mounted augmentor in tandem with a vectoring main nozzle to provide powered lift. The purpose of the investigation was to determine the augmentor performance in hover and the overall configuration aerodynamics (with the augmentor and a flowing engine inlet) from hover through transition to forward flight. The model was tested from static conditions (Mach = 0) to a free-stream Mach number of 0.20. The angle of attack was varied from 0° to 25° and sideslip angles were varied from -15° to 15°. The augmentor was operated up to a nozzle pressure ratio of 3.5. In addition, elevon deflections were tested together and differentially from −20° to 20° to determine control effectiveness (pitch and roll) with and without the augmentor operating.



E-7 model in Langley 4- by 7-Meter Tunnel.

Preliminary results indicate that the augmentor performance will allow hovering when used in combination with a vectoring main nozzle. The overall configuration aerodynamics and control effectiveness, both with and without the augmentor operating, indicate that the configuration can transition from hovering to wingborne forward flight.

D. W. Banks, 3611

Tumbling Studies of an Advanced Fighter Configuration

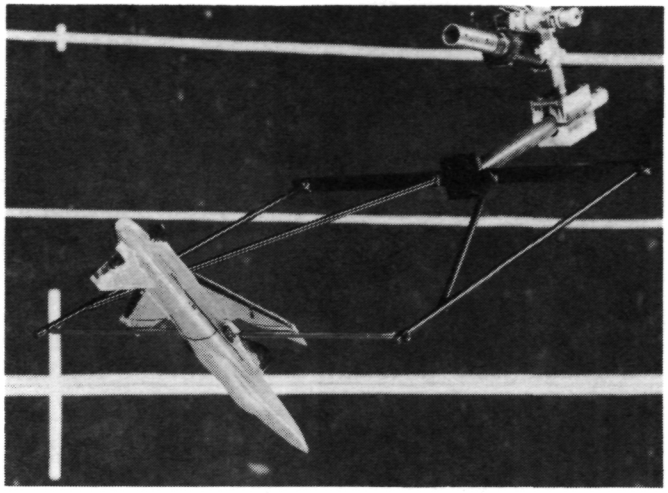
Certain modern aircraft design trends, such as relaxed static stability and the elimination of aft-mounted horizontal tails, combined with an unprecedented demand for pitch agility, have established the need to study the phenomenon of tumbling, an autorotative pitching motion. Tumbling has not been observed in airplane model tests since the flying wings and other unconventional designs of the late 1940's.

Dynamic model tests conducted in the Langley Spin Tunnel on one such modern configuration, the X-29A Forward-Swept Wing Demonstrator, have shown the existence of this phenomenon for the unaugmented airframe. Both free-tumbling tests and single-degree-of-freedom free-to-pitch tests have demonstrated autorotation in pitch which cannot be controlled by the canard surfaces. The strake flaps are effective during the tumbling motion. Static and dynamic aerodynamic data were also obtained for the X-29A configuration over a 360° angle-of-attack range for use in analysis of tumbling and to aid in the develop-

ment of a mathematical model for follow-on simulator studies.

The eventual goal of the tumbling studies is to conduct a piloted simulation investigation to assess susceptibility to tumbling and to develop control laws for providing resistance to tumbling motions.

Raymond D. Whipple, 2244



X-29A model undergoing tumbling tests in the Langley Spin Tunnel.

Free-Flight Tests of Vortex Flaps on a 0.15-Scale F-106B Model

In recent years there has been growing interest in the application of the vortex flap concept on advanced fighter configurations. Through extensive research efforts largely at NASA Langley, theoretical and experimental studies have shown that leading-edge vortex flaps can provide increased maneuver performance on advanced fighter configurations with slender wing design. The beneficial effects of vortex flaps are derived primarily from the control of vortical flow on the forward-facing surface of a leading-edge flap. In anticipation of demonstrating the vortex flap concept in flight, a 0.15-scale model of the F-106B was flown using the free-flight test technique in the 30- by 60-Foot Tunnel. The primary purpose of the free-flight tests was to assess the impact of vortex flaps on the stability and control characteristics up to stall.

In the free-flight tests, the basic F-106B configuration exhibited good flying characteristics except near the stall where a directional divergence occurred at an angle of attack of about 30°. With vortex flaps added to the basic leading edge, the F-106B free-flight model exhibited good flying characteristics. The addition of the vortex flap reduced the longitudinal stability, but additional pitch damping or forward shift in center-of-gravity location provided good pitch stability characteristics. Vortex flaps improved the lateral-directional characteristics such that the yaw divergence was delayed to $\alpha = 36°$.



Free-flight model of F-106B airplane with leading-edge vortex flaps installed.

Long P. Yip, 2184

Unsteady Flow Separation at High Angles of Attack

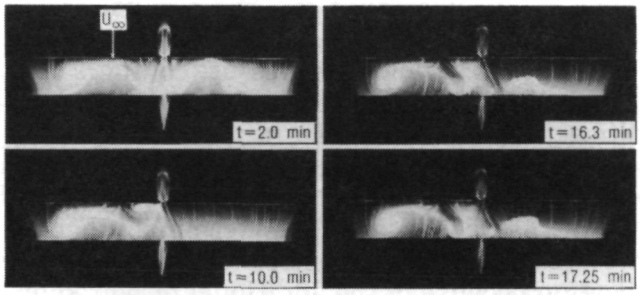
A wind tunnel investigation was conducted in the 4- by 7-Meter Tunnel to investigate the stall characteristics of an aspect ratio 7 wing-body model. The wing had an NACA 0012 airfoil with a 14-in. chord. Flow visualization data were obtained using fluorescent oil for angles of attack ranging from 7.5° to 20° at a Reynolds number of 1.0×10^6.

The test results indicate that complex asymmetrical and unsteady flow patterns can develop on a wing over a relatively small angle-of-attack range past $C_{L\max}$. At most angles above $C_{L\max}$, the vortices which form at the junction of the wing and body tend to wash over either the left or the right wing. A stable but asymmetrical stall pattern occurs at 16° angle of attack with the left wing separated and the right wing attached. At $\alpha = 20°$, the separation pattern is stable and

somewhat symmetrical with both wings separated. At 17° angle of attack, however, an unsteady separation phenomenon occurs, as illustrated. In the early stages of the test the separation pattern is symmetrical. Ten minutes into the test, the separation abruptly shifts to an asymmetrical pattern with the right wing essentially attached and the left wing separated. Sixteen minutes into the test the separation shifts again to a case where both wings are separated to differing degrees. The right wing at this time is separated over only a limited portion of the wing.

The test results show that for even a relatively simple configuration, the flow field associated with three-dimensional separation is extremely complex and provides a graphic illustration of the nature of the problem.

William L. Sellers III, 4646

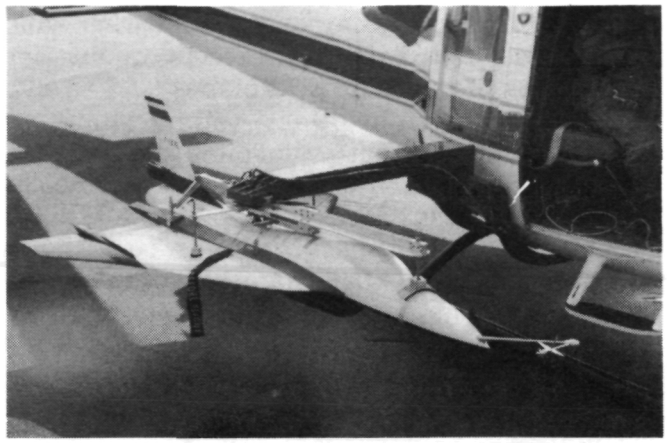


Oil flow pattern on NACA 0012 wing. Angle of attack = 17°; Reynolds number = 1.0 × 10^6.

F-16XL Model Flight Tests

NASA Langley Research Center has been involved for several years in the development of automatic flight control systems to provide high-angle-of-attack stability and enhanced maneuvering capability for advanced fighter configurations. The F-16XL is an example of an advanced design that employs such a system. Although designed with a moderate level of relaxed stability, a set of automatic flight control laws has been developed at Langley to provide the F-16XL with positive angle-of-attack control and high levels of resistance to departure and spin entry.

Flight testing of a dynamically scaled, remotely piloted model of the F-16XL has provided an effective assessment of the control system performance. This test model, as shown in the figure, is unpowered and is dropped from a helicopter for each test. The 18-percent scale model is fitted with



Test model of 18-percent scale model of F-16XL.

a complete motion-sensing and air data package that provides, via radio link to ground receivers, the feedbacks required by the control system. A ground-based minicomputer is programmed with the flight control laws and simulates the control system as used on the full-scale aircraft.

During simulated tactical maneuvering and aggressive high-angle-of-attack flight the automatic flight control system has been found to be very effective in providing the desired high-angle-of-attack characteristics. These results correlate well with other model tests and piloted simulations that have been conducted on this configuration.

David J. Fratello, 2244

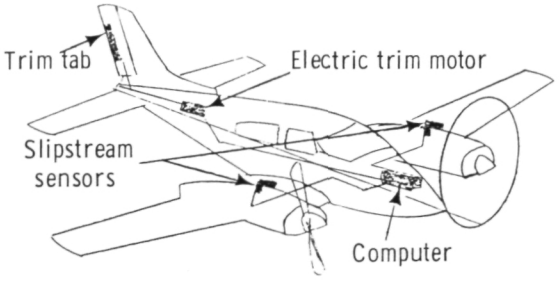
Automatic Engine-Out Trim System for Light Twin Aircraft

The failure of an engine is a major cause of fatal accidents on current light twin aircraft. As part of a research program at the NASA Langley Research Center addressing this problem, an automatic control concept was developed to improve safety under this condition. The concept, which could be integrated into an autopilot, is illustrated in the figure. Total pressure sensors in each slipstream sense any differential thrust condition and command changes in rudder, aileron, and elevator trim tab positions to compensate for the asymmetric power. The concept is being evaluated in piloted simulation using the Langley General Aviation Simulator. The simulation aerodynamic model represents a generic light twin

and was developed using data from earlier wind tunnel tests and from more recent qualitative flight tests of two NASA airplanes.

The evaluation pilots found that the automatic trim system lowers pilot workload and makes the airplane easier to control precisely. The system is of most benefit for coping with engine failures after takeoff but it has also been shown to be beneficial for single-engine landing maneuvers in which large power changes are required. Flight tests of a light twin airplane with a slipstream sensor will be conducted in the near future to validate the basic design concepts of the system.

Eric C. Stewart, 2184



Automatic engine-out trim system.

Numerical Simulation of Inlet/Diffuser System Flows

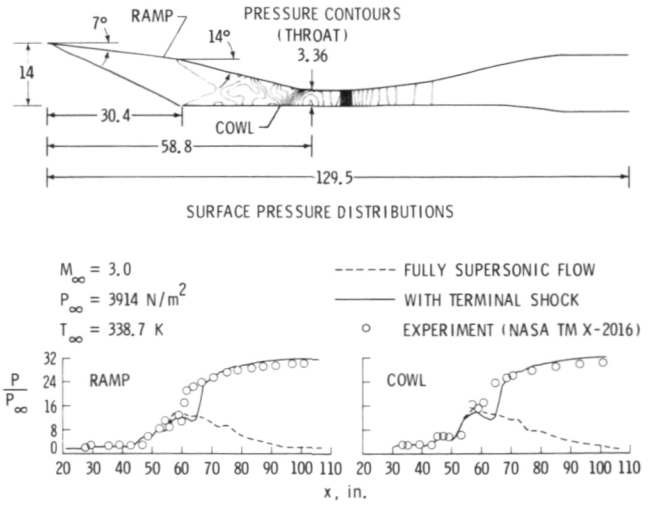
An attempt has been made to numerically simulate terminal shock region flows in two-dimensional supersonic inlet configurations using a Langley-developed two-dimensional Navier-Stokes code that employs a two-layer eddy viscosity model for turbulent flow calculations (NASA TM-85708). Boundary layer bleed modeling is employed to control and stabilize the terminal shock.

An inlet/diffuser design that has been extensively tested is illustrated. Results from tests at a design Mach number of 3 are documented in NASA TM X-2016. In the experimental test, boundary layer bleed was used upstream as well as downstream of the throat. In addition, vortex generators were used in the diffuser section for forced mixing of the flow to avoid flow separation and to provide more uniform flow at the engine face station. Results are presented here for the calculations made at the design Mach number of 3.0, 0° angle of attack, and a Reynolds number per foot of 2.2×10^6. The free-stream (inflow) pressure and temperature were 3914 N/m^2 and 338.7 K, respectively.

In simulating the preceding flow, a fully supersonic flow solution was obtained through the configuration at the design inflow Mach number of 3. A significant amount of bleed was required through the ramp and cowl (both ahead of and behind the throat) even to obtain the supersonic solution. The bleed locations and magnitudes were selected to match the experimental values. Several calculations were required to adjust bleed rates to minimize separation on the ramp and cowl. The supersonic solution was then used to establish a terminal shock in the diffuser by imposing an experimentally measured back pressure of approximately 32 times the free-stream pressure. Since the numerical calculations could not simulate the vortex generators employed in the experiment, a slightly higher amount of bleed was used in the calculation to avoid flow separation in the diffuser.

The figure shows the pressure contours in the inlet with the terminal shock clearly evident in the diffuser. The surface pressure distributions on the ramp and cowl surfaces are compared with the experimental data and are in good agreement with the measured levels. The terminal shock is predicted slightly downstream of the measured location because of the additional bleed required in the calculations in the absence of vortex generators.

Noel A. Talcott, Jr., 3294



Numerical simulation of flow through a two-dimensional inlet.

Propulsive Wing/Canard Fighter for STOL Operations

A wind tunnel investigation was performed at Langley to determine the effects of chordwise blowing on the aerodynamics of a propulsive wing/canard fighter configuration. Most STOL fighter configurations use some form of powered lift to provide the low approach speeds for STOL operations. At these low speeds, the control power of the canards or horizontal tails to trim the nose-down pitching moment generated by the high lift is reduced. This limits the powered-lift concepts. In this investigation, the configuration uses chordwise blowing on the wing flap to generate high lift and on the canard flap to generate nose-up pitching moment for trim.

A systematic study was conducted to quantify the effects of the canard and wing locations, thrust coefficients, trailing-edge flap deflections, and blowing jet width on the configuration aerodynamics. The results indicated that as the blowing span was increased on either the canard or the wing, the thrust-induced lift increments were increased. The configuration with a high canard and low wing location was considered best for overall performance. The blown canard produced significant nose-up pitching moments. If the blowing rates of the canard and the wing were adjusted slightly, the canard would maintain trim across the angle-of-attack range tested.

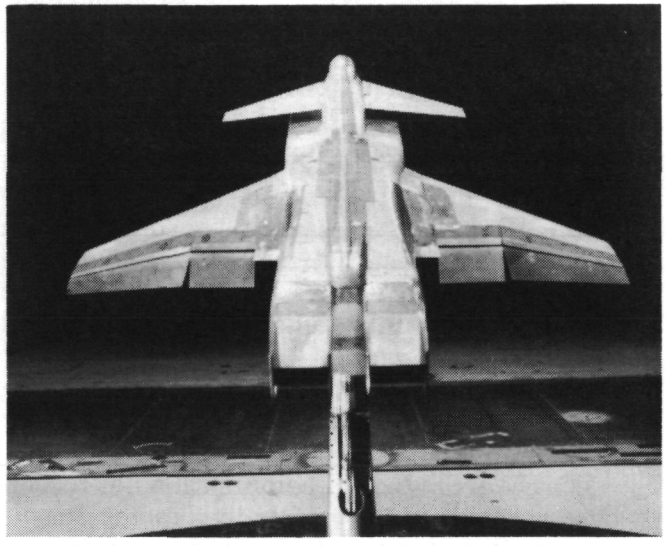
P. F. Quinto, 3611



Wing-canard model in 4- by 7-Meter Tunnel.

Low-Speed Aerodynamics of an Advanced Fighter Employing High-Lift Devices and Multifunction Nozzles

A joint wind tunnel investigation was conducted by NASA with McDonnell-Douglas and the U.S. Air Force to determine the low-speed aerodynamics of an advanced fighter configuration with various high-lift devices and multifunction nozzles. It was of prime interest in the investigation to determine if the configuration could generate high lift and have the multifunction nozzle maintain trim and proper lift-to-drag ratio for landing with the thrust level at military power. Also of interest was the exhaust plume pattern when the configuration was in ground effect, to determine when gas reingestion might be a problem during full-thrust reversing.



Advanced fighter with high-lift devices and multifunction nozzles.

The configuration was tested with full-span slotted trailing-edge flaps and leading-edge vortex and Krueger flaps for high lift. The multifunction nozzles could be vectored for trim and partially reversed for thrust spoiling at approach conditions with military power. Finally, one of the thrust reverser nozzles had splay doors which directed the exhaust plume outboard to reduce the possibility of gas reingestion. The testing was conducted at angles of attack from $-4°$ to $28°$ and tunnel dynamic pressures from 8 to 50 psf both in and out of ground effect with various deflections of flaps and nozzles.

Results indicate that the configuration with a vortex flap deflected $45°$ down would have the

best takeoff performance (i.e., highest lift-to-drag ratio), whereas a vortex flap deflected 45° up would have the best landing performance (high lift and high drag). The multifunction nozzles can trim the configuration at approach conditions with military power by both thrust vectoring and partial thrust reversing. The thrust reverser with splay doors diverted the exhaust plume outboard, which would reduce the probability of gas reingestion during reverse thrust operation. This nozzle, although losing some reverser effectiveness, can allow shorter landing ground rolls compared to the configuration without the splay door because the splay door reverser can be employed to lower velocities before gas reingestion becomes a problem.

G. M. Gatlin, 3611

SWINT Code Application to Advanced Missile Configuration

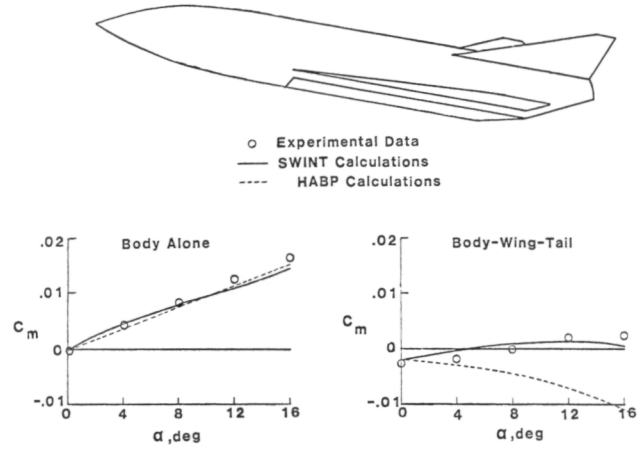
The SWINT (Supersonic Wing Inlet Tail) Euler code, developed by the Naval Surface Weapons Center, is designed to compute the aerodynamic characteristics of missile-type configurations. The code has recently been made operational at Langley and has been combined with the QUICK-geometry system developed by the Grumman Aerospace Corporation under contract to Langley to greatly simplify its geometry input requirements for advanced body shapes.

The SWINT/QUICK combination has recently been applied to the Langley hypersonic missile configuration illustrated. A common computational problem with configurations of this type is the inability of the traditional computational methods to accurately predict the control effectiveness of the tail fins. Since these fins are located in the leeside flow field of the body, experimental data have shown that they lose their control effectiveness at high angles of attack. By contrast, the traditional method of calculating these effects, the Hypersonic Arbitrary Body Program (HABP), developed by the Douglas Aircraft Corporation, predicts that the controls remain effective even in the leeside flow.

In order to investigate the ability of the Euler code to predict these effects, SWINT normal-force and pitching-moment calculations were made on the configuration shown at a Mach number of 6 and an angle of attack of 16°. It was found from the force calculations that SWINT predicted very little normal force on the tail fins compared to the large contributions from the body and wings, and that the overall predicted normal force was in excellent agreement with experimental data.

Since the large tail fins on this configuration are designed primarily as control surfaces, the small predicted normal force from SWINT results in very little control effectiveness, as can be seen from the pitching-moment calculations shown in the figure. Both the data and SWINT calculations show that the configuration is unstable in pitch even with the large tail fins. In contrast, this figure also shows results from the HABP code, which incorrectly predicts a stable trend in pitching moment from the tail fins.

Jerry M. Allen, 2196



SWINT results in hypersonic missile configuration.

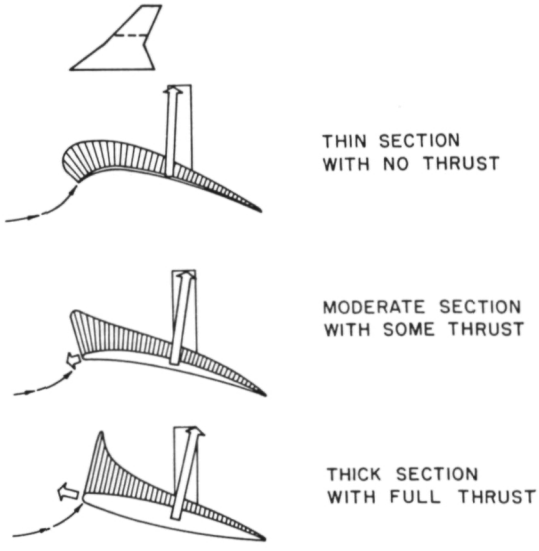
Wing Design Including Leading-Edge Thrust

Because full theoretical leading-edge thrust is seldom achieved and the amount actually attainable is difficult to predict, it has become common practice to design wings with twist and camber distributions which do not require any leading-edge thrust. In this approach, the twist and camber are tailored to a specific design point, and of course will give less than optimum performance at off-design points. Performance gains resulting from appreciable levels of actual leading-edge thrust, on the other hand, are not nearly as sensitive to flight conditions. Thus, it would be desirable to include attainable leading-edge thrust

considerations in the design process so as to strike a balance between performance gains associated with twist and camber and those attributable to attainable thrust, and in the process obtain a wing with a more moderate camber surface.

In earlier work, a study of the factors which place limits on the theoretical leading-edge thrust was made, and an empirical method for estimation of attainable leading-edge thrust was developed. This established the groundwork for a linearized-theory wing design computer program including attainable thrust considerations, which was developed by Kentron International under contract to NASA Langley.

The way in which attainable leading-edge thrust affects wing design may be illustrated with the aid of the figure. At the top of the figure is a typical mid-semispan wing section for a converged program solution for a thin wing with a leading-edge radius of zero. Such a design will display a considerable amount of camber to generate an appreciable portion of the total lift on forward portions of the wing where distributed thrust can be generated. For a thick wing section with a relatively large leading-edge radius, such as that shown at the bottom of the figure, an appreciable amount of thrust can be generated, and there may be no need to resort to twist and camber. For intermediate section thicknesses and radii, as shown in the middle of the figure, a design with considerable variation of the severity of camber across the wing semispan could result. For inboard stations of a swept wing, little or no camber would be required, but for stations near the wing tip, the camber could approach that required for the thin wing with no leading-edge thrust. These examples show how the present design method may be used to define a wing with the mildest twist and camber capable of achieving performance levels comparable to those attainable with full theoretical thrust. Such a wing design should offer advantages in structural simplicity and in aerodynamic performance at off-design flight conditions.



Effect of attainable thrust on program-generated wing surfaces.

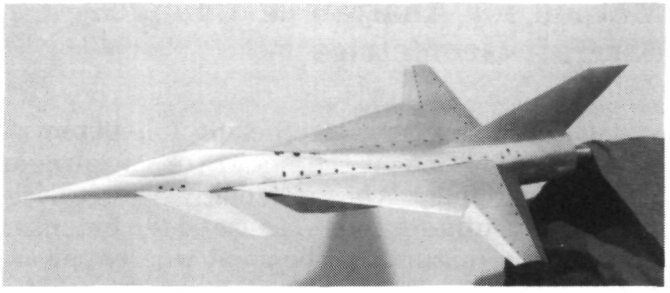
Christine M. Darden, 3294

Application of a Full-Potential Method for Analysis of Complex Aircraft Geometries

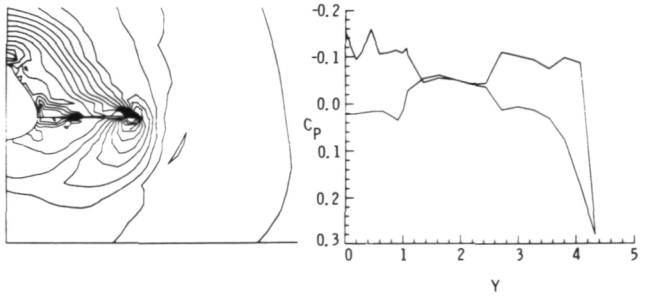
The development of efficient full-potential solvers now permits accurate nonlinear aerodynamic analysis of supersonic flow over fairly complex configurations. These full-potential solvers have matured to the point where they are in many cases competitive with the more complex Euler solvers. A nonlinear aerodynamic prediction technique which was developed by Rockwell International under contract to NASA and solves the conservative full-potential equation is currently being evaluated for the analysis of supersonic flow fields over aircraft geometries. The application of this method to complete aircraft configurations identified several areas where modifications and/or enhancements to the code were required. Recent modifications to the code now permit the analysis of fully three-dimensional flows as well as supersonic flows with embedded subsonic pockets.

The major objective behind the development of this full-potential method is to fill the need for a nonlinear supersonic technique which will produce accurate results for complex geometries while making efficient use of computational resources as well as minimizing the required level of user sophistication. The photograph shows a supersonic fighter model currently under study at NASA Langley. This is an example of the type of configuration that the full-potential code was and is being developed to analyze. The method is not yet capable of solving the entire fighter configuration but it has been used to analyze the forward portion of the vehicle, namely the forebody-canopy-canard portion of the fighter. A typical result is shown from the analysis of the forward portion of the fighter at the cruise condition of $M = 2$, $\alpha =$

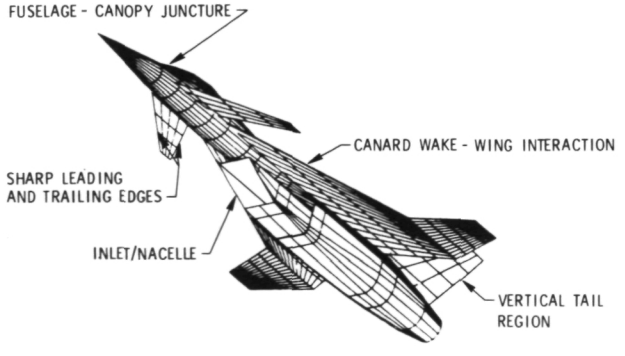
4^0. This is a plot of the surface pressure distribution as well as pressure contours of the flow field at a cross-section located at 31 percent of the fighter body length. At this location, just downstream of the canard root chord trailing edge, a "double-body" problem arises—that is, the canard appears to be detached from the body in the cross-section plane. The wake treatment in the code has been modified to permit such situations where a wake region separates the body and a lifting surface. The surface pressure distribution clearly demonstrates a typical lifting pressure profile on the body and canard and no lift (i.e., no pressure differential) being produced in the wake region.



NASA Langley advanced fighter configuration.



Pressure contours and surface distribution on a fighter forebody-canard configuration at x/l = *0.31.*



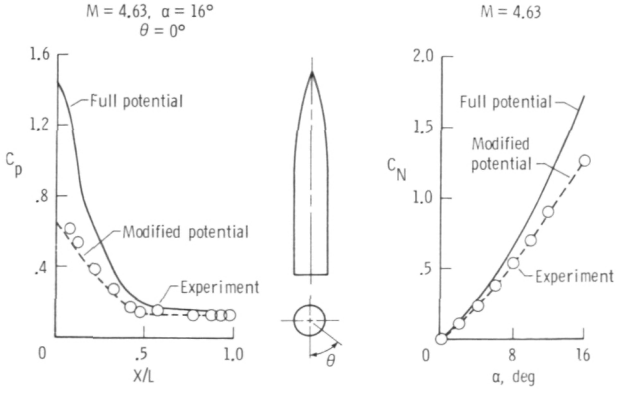
Problem areas in the analysis of an advanced fighter configuration.

To complete the analysis of the entire supersonic fighter configuration requires that the method address several additional problem areas, as illustrated. Once these are resolved, the full potential code will be capable of analyzing a complex, realistic aircraft.

Kenneth M. Jones, 3294

Approximate Entropy Correction to a Three-Dimensional Supersonic Full-Potential Flow Code

The range of applicability of any potential flow code is limited in both Mach number and angle of attack to conditions in which the entropy changes across the bow shock are small. This limit has been removed for the NCOREL full-potential code, which was developed under NASA contract by the Grumman Aerospace Corporation, by making an approximate entropy correction. In the correction procedure, the bow shock location and strength are determined from the nonisentropic Rankine-Hugoniot conditions instead of the usual isentropic conditions. The remainder of the solution procedure is unchanged and the resulting surface pressures are corrected for entropy effects according to an expression which is a function of the entropy jump across the bow shock and the velocities as computed in the full-potential code. Because the entropy jump across the bow shock is determined using the same solution procedure as the full-potential code and because the surface pressures are corrected by simply post-processing the isentropic pressures, the total entropy correction is obtained for essentially no additional com-



Generic missile body.

putation cost and without any change to the full-potential flow code formulation.

An example illustrating the accuracy and extended capability is presented in the figure. Pressure and normal force results are shown for a generic missile body at $M = 4.63$. Pressure data at $\alpha = 16°$ are shown along the lower surface centerline, which is where the entropy effect is largest. The entropy effect is the difference between the full-potential solution and the modified potential solution. Note that the modified potential result agrees well with the experimental data. The integrated effect of the entropy correction is shown by the normal force results. The change in normal force due to entropy correction is approximately 30 percent at $\alpha = 16°$.

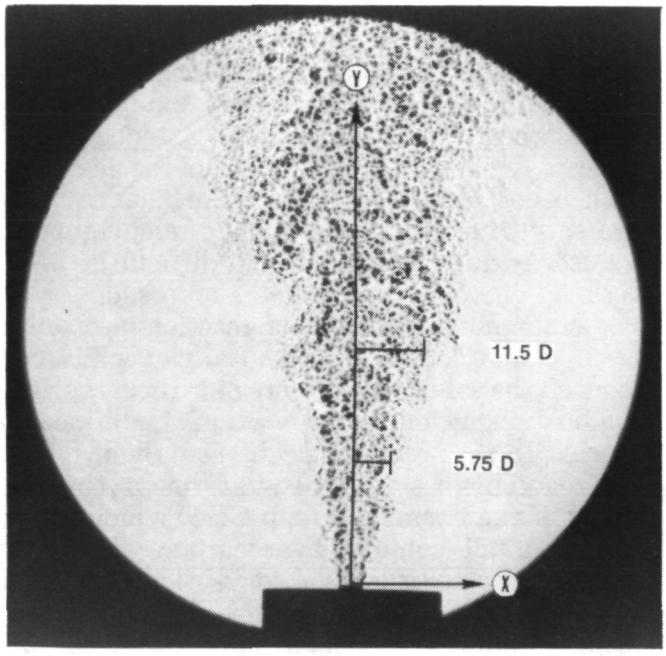
James L. Pittman, 3181

Combustion Diagnostics

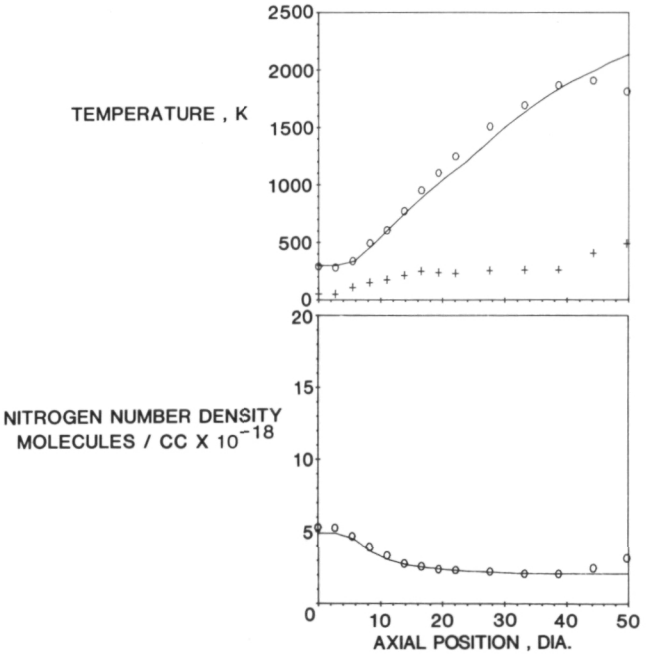
Nonintrusive (optical) measurement techniques for temperature and major species in supersonic combustion flow fields are highly desirable due to the extreme temperatures and velocities encountered. Conventional probe techniques with cooled hardware designed to withstand the harsh thermal environment have the inherent disadvantage of significantly altering the properties that are to be measured. A nonintrusive technique based on coherent anti-Stokes Raman spectroscopy (CARS) has been developed, and calibration experiments were conducted in a flat-flame burner to demonstrate the accuracy of the temperature and concentration measurements.

The motivation for detailed measurements in reacting flows is the generation of a good data base that will allow the assessment of complex computational fluid dynamics (CFD) computer codes that attempt to model turbulence and finite-rate chemical kinetics. Recently the CARS system was used to determine temperature and species profiles in a turbulent diffusion flame. The photograph is a spark shadowgraph of the diffusion flame with the location of CARS axial and radial profiles. The temperature and nitrogen concentration distributions (circular data points) along the centerline of the diffusion flame burner are compared with CFD results (lines) in the plots. The CARS values plotted are the average of 200 laser pulses, and the crosses indicate the rms values of the temperature fluctuations due to turbulence. Except at far axial positions, agreement between the measured and calculated values is remarkably good considering that a parabolized Navier-Stokes code with equilibrium chemistry and a two-equation turbulence model was used for the calculations. A supersonic coaxial burner is being designed to extend the velocity range of the measurments.

G. Burton Northam, 2803



Shadowgraph of the subsonic diffusion flame showing locations where data were taken.

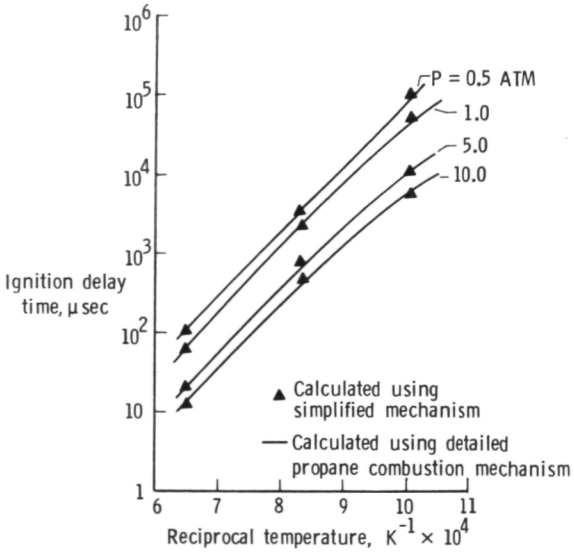


Centerline survey.

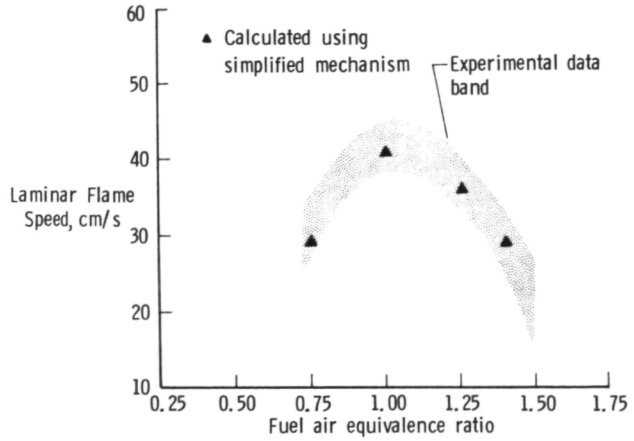
A Simplified Hydrocarbon Reaction Mechanism for Combustion Applications

Numerical modelling of combustion processes in air-breathing propulsion systems such as gas turbines, ramjets, and scramjets has become an important element in many combustion research programs. An essential component in many of these models is a chemical kinetic reaction mechanism which describes the oxidation of a hydrocarbon fuel. Current numerical models which attempt to combine a description of the chemistry with other processes such as turbulence, mass transport, fuel vaporization, and quenching, encounter serious computational difficulties when detailed chemical mechanisms are used.

A simplified hydrocarbon reaction mechanism has been developed at NASA Langley which contains all the essential elements of hydrocarbon fuel combustion, including the reaction of intermediate species. In the proposed mechanism the hydrocarbon reactions are described in terms of the reactivity of the chemical group CH_2, which is contained in all common-hydrocarbon species including the constituents of conventional hydrocarbon fuels. The observed kinetic behavior of propane combustion as determined in shock tube studies, and the calculated kinetic behavior of propane-air mixtures as derived from the detailed propane combustion mechanism, were used as a data base for constructing and refining the simplified mechanism. The mechanism contains 13 chemical species and 26 chemical reactions. Numerical studies revealed that the simplified mechanism can reproduce the observed kinetic behavior of propane-air mixtures, including laminar flame speeds, over a wide range of temperatures and pressures. It is anticipated that the simplified mechanism, when incorporated into numerical combustor models, will provide a more realistic description of the combustion process than can be achieved using the previously available reaction mechanisms.



Calculated ignition delay times as a function of temperature and pressure for a stoichiometric fuel-air mixture.



Comparison of measured and calculated flame speeds in propane-air mixtures at T = *289 K and* P = *1 atm.*

C. J. Jachimowski, 2803

Navier-Stokes Solution for Flow Inside Two-Dimensional Thrust Reversing Nozzles

A computer program has been written to predict the flow inside two-dimensional convergent-divergent nozzles operating in the thrust reverser mode. The computer program, developed by Dr. Robert W. MacCormack of the University of Washington under contract to NASA, is a solution of the Reynolds-averaged time-dependent compressible form of the Navier-Stokes equations. The equations are solved numerically on a generalized nonorthogonal coordinate mesh using the implicit computational method of MacCormack. Turbulence effects are simulated using an algebraic eddy viscosity model. The turbulence model used should be adequate for

attached flows and for flows with small regions of boundary layer separation.

Calculations have been made for configurations with a rounded lip and a sharp lip at the reverser port that are in excellent agreement with experiment. The code has the capability of computing the flow inside nozzles with thrust reversers fully deployed or partially deployed. The code can also be used to predict the flow for nozzle configurations and asymmetric thrust reversing; that is, with the upper and lower reverser ports operating at different angles.

Efforts are under way to further enhance the capabilities of this code by allowing the effects of external flow on thrust reverser performance to be computed.

Lawrence E. Putnam, 2673

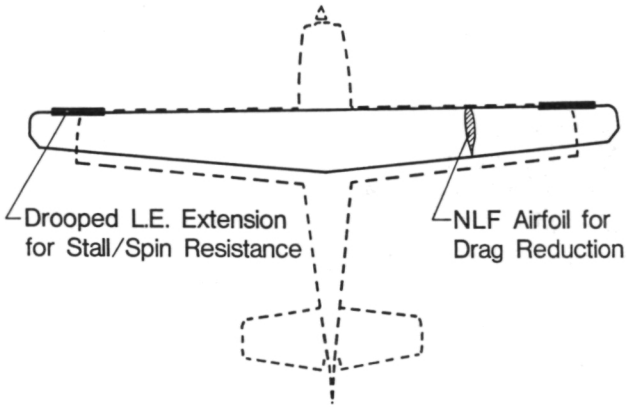
Application of an Outboard Leading-Edge Droop for Stall/Spin Resistance on a Natural Laminar Flow Wing

The NASA Langley Research Center has been engaged in a research effort to develop the technology required to improve the stall departure/spin resistance characteristics of general aviation aircraft. One concept that has proved extremely effective for improving the characteristics of such aircraft has been the wing outboard leading-edge droop. This modification has been developed for a variety of aircraft configurations and tested using static and dynamic wind tunnel investigations, radio-controlled models, and flight test validations. A more recent area of interest in general aviation has been the development of airfoils designed for extensive regions of natural laminar flow. This technology provides for the improved performance and fuel efficiencies desired for advanced general aviation designs.

A logical extension of the research effort in the general aviation field is to combine the natural laminar flow airfoil with the outboard leading-edge droop modification. A study to evaluate this combination has been pursued as a cooperative effort between Langley and industry. Langley has been responsible for developing the outboard droop design during tests in the 12-foot and 30- by 60-foot low-speed wind tunnels. A new natural laminar flow airfoil designed at Langley was used. This airfoil was designed for 70 percent natural laminar flow on both the upper and lower surfaces. Since the previous outboard droop designs have not been concerned with natural laminar flow, a design approach using another NLF airfoil as the droop airfoil geometry was used. This approach assured natural laminar flow on the drooped as well as the undrooped portions of the wing. The design procedure was further validated by use of the Eppler airfoil analysis code to examine the pressure distributions for conditions conducive to natural laminar flow. Shown in the figure is a comparison of the planform with the advanced NLF airfoil wing and leading-edge modification.

Results of static and dynamic force tests have shown the NLF wing with modified leading edge to have improved stall departure resistance characteristics without adversely affecting the natural laminar flow to 70 percent wing chord.

Joseph L. Johnson, Jr., 2184



NLF advanced wing design for drag reduction and stall/spin resistance.

Wing-Tip-Mounted Turboprop

It has been proposed that the recently developed high-speed turbopropeller designs may offer an increase in propulsive performance of approximately 20 percent over that of the present-day turbofan engines. A turboprop/airframe integration investigation has been initiated to determine the installation interference effects associated with interaction of the propeller wake and the aircraft. To minimize these effects and take advantage of favorable aerodynamic flows that exist on an aircraft, it was proposed that the turbo-

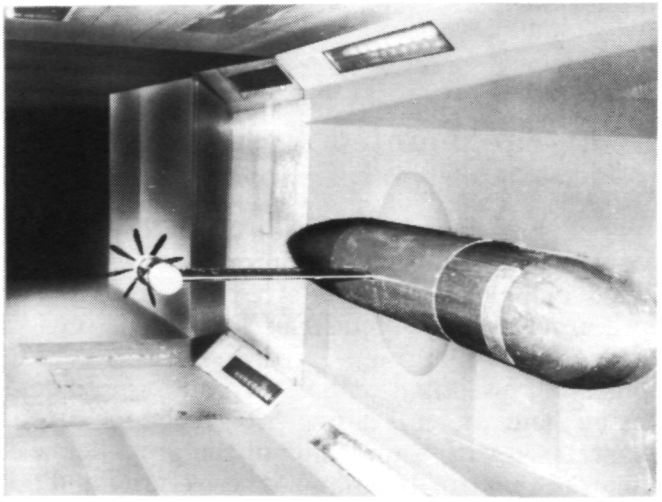
prop be installed on the wing tip as a pushed configuration.

Wind tunnel tests have been conducted at 0.70 Mach using a semispan model that has an unswept untapered wing with a symmetrical airfoil section and an aspect ratio of 6.3. An eight-bladed SR-2 high-speed propeller was mounted on a force balance which was located in the nacelle with the air-driven motor. This nacelle was mounted on the wing tip and set at -3° incidence.

Results were obtained at a constant thrust level throughout the positive-angle-of-attack range where the direction of rotation of the lift-induced vortex flow at the wing tip is opposite to that of the propeller. The propeller RPM required for constant thrust decreases through the positive-angle range from approximately 15,100 at $\alpha = 0°$ to 13,000 at $\alpha = 3°$. With the propeller blade pitch angle fixed, the increase in the vortex flow relative to the propeller with increase in angle of attack of the wing effectively increases the propeller pitch angle, resulting in a reduction of 2100 RPMs while maintaining the same thrust level. The horsepower values required to maintain a constant thrust output from the propeller are, therefore, less at $\alpha = 3°$, due to the vortex flow, than at $\alpha = 0°$, where no vortex exists. This represents a 23-percent reduction in power required for the same turboprop thrust output.

In addition, there is a reduction in the induced drag of the wing which results from an injection of the high-energy propeller wake into the vortex core, disrupting its axial flow and causing the vortex to dissipate. This high-energy wake is introduced into an already weakened or lower energy vortex behind the wing, having just passed through the propeller, which is a benefit. The reduction in induced drag achieved at a lift coefficient of 0.30, for example, is approximately 25 percent relative to the induced drag of the basic wing.

J. C. Patterson, Jr., 2673



Wing-tip-mounted turboprop model.

Electronics Directorate

The Electronics Directorate conducts basic research and technology development activities in the areas of aircraft flight management, aircraft flight control systems, spacecraft theoretical dynamics and control, spacecraft information handling systems, remote sensing systems, fault-tolerant systems, electromagnetics, computer science, measurements technology, and simulation technology. These electronics-related research and technology development activities are focused toward application to the next generation of aircraft and spacecraft.

The Analysis and Computation Division provides computational support for all theoretical and experimental aerospace research activities performed at Langley. The Division conducts research and development required to provide mathematical and computer techniques, procedures, and equipment for numerical analysis, problem formulation and programming, electronic computation, simulation, data recording, transcription, transmission, and presentation. Additional responsibilities include conception, design, implementation, and management of advanced centralized data processing systems, flight software systems, and flight simulators, as well as providing consultation on Langley application of computer technology.

The Instrument Research Division provides instrumentation and measurement support for all experimental aerospace research activities performed at Langley, with primary responsibility for the instrumentation of ground-based facilities. The Division conducts research and development programs on sensor materials, components and devices, nonintrusive (optical) and immersion sensing systems, nondestructive measurement of materials, and measurement devices for operating in a cryogenic or reentry environment, and in instrument areas where data requirements exceed capabilities. Additional responsibilities include providing engineering and application expertise to support computer-based data acquisition and control requirements, developing and maintaining measurement standards, calibrating and repairing instruments, and managing an instrument pool.

The Flight Control Systems Division conducts research on flight systems technology for the next generation of aerospace vehicles. The activities of the Division encompass concept formulation, analytical studies, and flight evaluation for flight management capabilities and flight-crucial applications. Specific research involves investigation of fault-tolerant system architectures and their implementation; advanced crew station concepts, including configurations, display media, and input/output technology; and applied controls technology. Flight systems integration and validation research is conducted in AIRLAB, a major new NASA national laboratory. Additional major research efforts are directed to provide more efficient operations of transport aircraft in the evolving national airspace system, cockpit systems to improve crew-vehicle interfaces, aircraft systems and procedures to reduce operating cost and complexity, and improved techniques for performance analysis, workload assessment, and simulation.

The Flight Dynamics and Control Division conducts research on flight control technology for the next-generation aircraft and spacecraft using analysis, simulation, and flight testing. The Division develops and applies new and improved mathematical and optimization techniques to control problems, develops and evaluates manual and automatic digital control system concepts for aircraft and spacecraft, conducts generic research in dynamic system modeling, and performs analysis and simulation studies of the optimal trajectories of flight vehicles. Other research performed in the Division contributes to the technology base required for the design, development, and utilization of teleoperator and robotic devices for space operations.

The Flight Electronics Division conducts research and technology development activities in the areas of environmental sensors, laser components and systems, solid-state electronics, antenna and microwave components, subsystems and systems, and related disciplines for application to sensor, communication, and information processing and data management systems. This technology development is directed toward conceptual design, breadboard fabrication, and proof-of concept evaluation of ground and flight electronics for incorporation in spacecraft and aircraft flight programs.

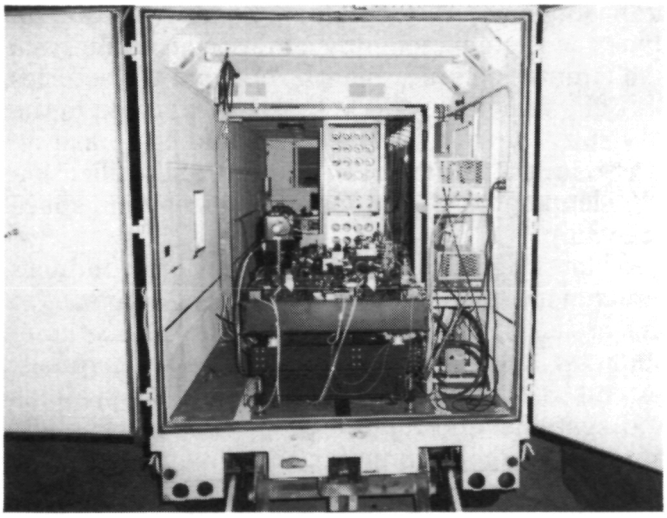
Tunable-Diode Laser Heterodyne Spectrometer Demonstrated

The Langley Research Center's Laser Heterodyne Spectrometer (LHS) has successfully demonstrated the heterodyne technique of detection of atmospheric ozone using a tunable-diode laser. The demonstration was performed in

the LHS laboratory at Langley (near sea level) with the solar signal directed into the instrument by a solar tracker and mirrors. It was demonstrated that a tunable-diode laser could be successfully used as a local oscillator in a heterodyne system, providing both tunability and very high resolution (10^{-4} cm^{-1}). The computer-controlled dual-channel LHS was designed to allow the simultaneous measurement of two gases from either a CV 990 aircraft platform or a stationary site such as Mt. Evans in Colorado.

Having been successfully demonstrated at Langley, the LHS has been integrated into a van and transferred to the University of Denver, where it will be used to acquire atmospheric transmission data in the 9- to 11-μm spectral region for the Air Force Geophysical Laboratory. Besides ozone measurements, the LHS is also capable of measuring nitric acid and other trace species as well as performing auroral measurements.

Herb Kowitz, 3535



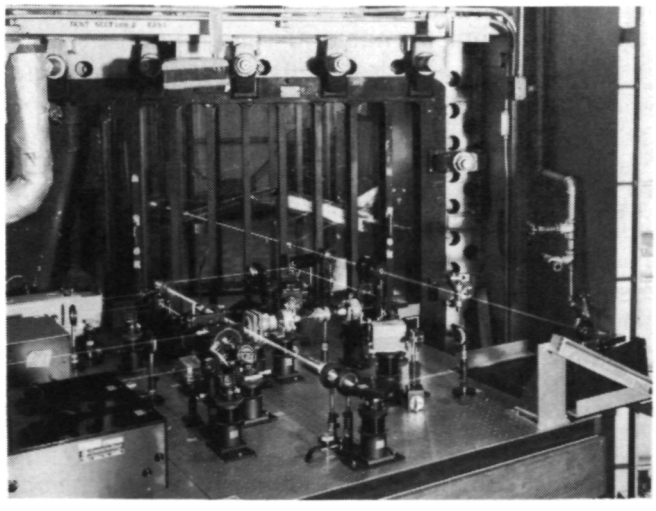
LHS instrument integrated into van. Optical instrument is shown in the foreground with support electronics behind (center).

Nonintrusive Simultaneous Measurement of Three Flow Parameters in a Supersonic Flow

Coherent Raman spectroscopy has been used for the first time to remotely and simultaneously measure the (particle-free) flow velocity in nitrogen, the static pressure, and the translational temperature in the LaRC Unitary Plan Wind Tunnel (UPWT). These three quantities were measured simultaneously at a single point using nonintrusive laser techniques. The system employs two lasers, one C.W. (continuous wave) probe and one pulsed pump, arrayed on a single optical table along with an optical retrometer located on the opposite side of the flow. The retrometer yields a vibration-free optical system which has the additional advantage of simultaneously capturing both the forward and backward (counter-propagating laser beams) Raman scattering. Spectral line shape analysis of the forward- and backward-scattered nitrogen spectra allows the temperature and pressure to be determined, while the Doppler shift between the two yields the velocity of the nitrogen molecules.

The system was deployed in an inverse Raman mode with a laser resolution of 190 MHz. This resolution represents an order of magnitude improvement in spectral resolution since the first UPWT measurements and has enabled pressure to be added to the system capability. The UPWT demonstration of the concept included measurements of velocity and temperature—and hence Mach number—over the Mach number range from 2.50 to 4.63, static pressure measurements (at Mach 2.50) corresponding to a Reynolds number per foot range of 1 to 5×10^6, and measurements behind the shock wave of a flat-plate model.

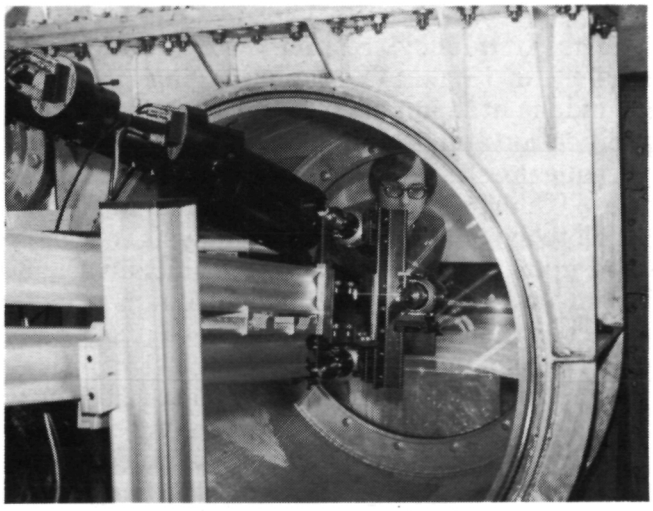
Reginald J. Exton, 2791



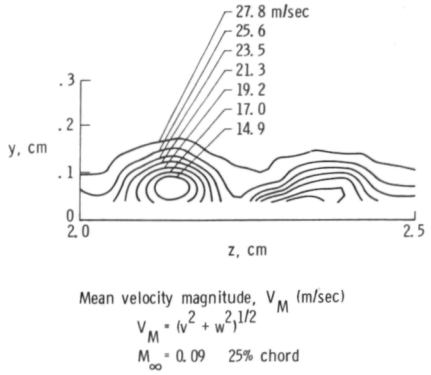
Inverse Raman spectroscopy at the Unitary Plan Wind Tunnel.

Laser Doppler Velocimeter Measurements of a Juncture and Taylor-Görtler Vortices Flow Fields

A specialized single-axis five-beam three-component laser velocimeter was constructed and used to study juncture and Taylor-Görtler vortices in Langley's Low Turbulence Pressure Tunnel. The juncture was defined by a blunt-leading-edge vertical splitter plate and a sharp-leading-edge horizontal plate. The Taylor-Görtler vortices were generated in the flow field above a supercritical airfoil model. The juncture flow field measurements were performed at 50-, 75-, and 95-percent chord positions covering a 3- by 3-cm area normal to the directed tunnel flow. The closest point of approach was 3.5 mm to the vertical surface and 1.0 mm to the horizontal surface. The LDV sample volume was 80 um in diameter and 120 um in length.



Laser Doppler velocimeter installation in Low Turbulence Pressure Tunnel.



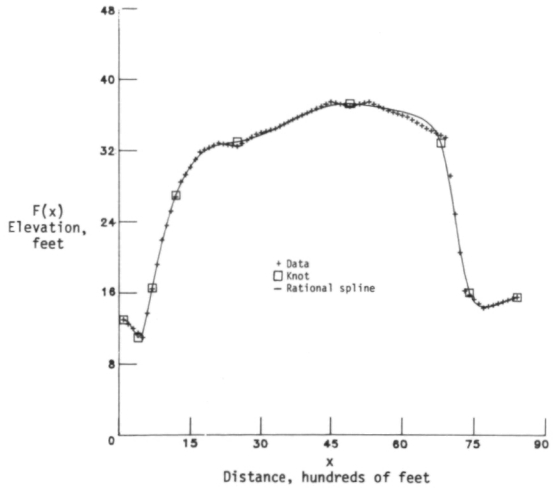
Contour map of velocity magnitude.

Measurements of the Taylor-Görtler vortices were made over a chord range of 15 to 32.75 percent every 0.25-percent chord. Typical survey ranges were 1.5 to 4.5 cm from the centerline along the span direction and from 0.3 to 3.0 mm above the model surface. The photograph shows the model and the multiple-component velocimeter laser beams with respect to the model. Typical results of the Taylor-Görtler vortices measurements are shown in the figure, which presents the resultant two-component (v and w) velocity magnitude contours at the 25-percent chord position for the Mach 0.09 run condition.

James F. Meyers, 2791

Spline Smoothing of Data With Variable Tension Between Knots

Cubic spline functions for interpolating and smoothing data have been available for a number of years. One difficulty with these functions is that if the slope of the data changes drastically at one point, the spline exhibits undesirable and fictitious fluctuations in the neighborhood of that point. A. K. Cline, at the University of Texas at Austin, developed the spline under tension in order to reduce these fluctuations. With the spline under tension, a tension factor is applied to the entire data range, including intervals where no tension is needed. More recently an interpolating spline, the rational spline, was developed which applies tension independently between each pair of knots.



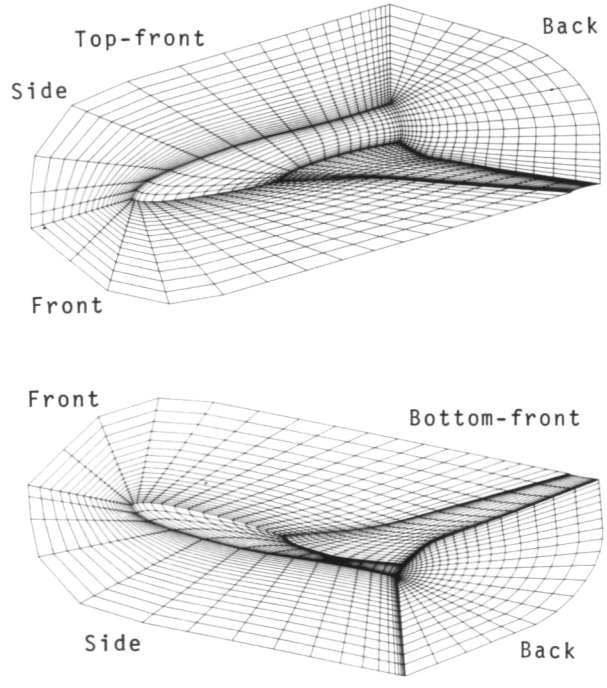
Rational spline fit to terrain elevation data.

An efficient algorithm for smoothing data with the rational spline has been developed at Langley. A least-squares fit is made to the data with the tension factor between each pair of knots either specified by the user or adjusted to constrain the deviation between the rational spline and the straight line joining the knots to a user-specified value. The figure illustrates smoothing of elevation data in which the tension was fixed in the first four intervals and the seventh and adjusted in the remaining intervals.

James R. Schiess, 2747

Algebraic Grid Generation for Wing-Fuselage Bodies

An algebraic procedure for the generation of boundary-fitted grids about wing-fuselage configurations has been developed at Langley. A wing-fuselage configuration is specified by cross sections and mathematically represented by Coons' patches. A configuration is divided into sections so that several grid blocks that either adjoin each other or partially overlap each other can be generated, and each grid has six surfaces that map into a computational cube. Grids are first determined on the six boundary surfaces and then in the interior. Grid curves that are on the surface of the configuration are derived using plane-patch intersections, and single-value functions relating approximate arc lengths along the curves to computational coordinates define the distribution of grid points. The two-boundary technique and transfinite interpolation are used to determine the boundary surface grids that are not on the configuration, and transfinite interpolation with linear blending function is used to determine the interior grids.



Surface grids for the front of an aircraft configuration.

Robert E. Smith, 3978

Frequency Response Analysis for Sampled Image Systems

The frequency response or modulation transfer function (MTF) of an imaging system is of fundamental importance both in the initial specification and design of the system and in any subsequent detailed analysis of the images it produces. Unfortunately, the traditional MTF approach to system performance analysis (which is based upon point source images, shift-invariant system assumptions, and continuum mathematics) is not directly applicable to many contemporary imaging systems; i.e., electro-optical line scan and sensor array devices. That is, because of the discrete nature of sampled imaging systems, whenever these systems form the sampled image of a point source, the appearance of the image may depend upon the location of the point source relative to the sampling (i.e., pixel) grid. This sample scene phasing phenomenon is familiar to those who analyze the appearance of small, high-contrast objects in a digital image. For such systems the basic problem then is this: how can the traditional MTF approach to systems performance analysis be modified and extended to account for the effects of sampling?

Recent research at Langley and in conjunction with researchers at the University of Arizona has produced a solution to this problem. A stochastic technique has been developed which accounts for the combined effects of imaging, sampling, and reconstruction by using a point source system input randomly located relative to the pixel grid and averaging the system output over all possible point source locations. This technique produces an

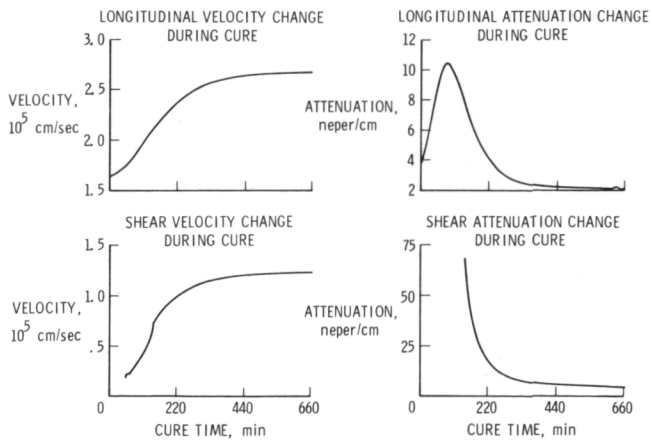
analytic expression for the average system MTF which has general applicability and provides a numerical measure of system performance which can be evaluated easily. This random sample scene phase approach is an extension of a technique previously developed by the same researchers and successfully applied to an analysis of the radiometric error in remote sensing imagery introduced by the combined effects of sampling and reconstruction.

Stephen K. Park, 2070

Ultrasonic Sensor for Optimizing Resin Cure

A new ultrasonic sensor has been developed at Langley to characterize the degree of cure in resins. The concept has direct application to dynamic measurements for feedback and process control, thus improving the curing of composite materials. At present, no satisfactory system exists to determine the precise condition of polymerization, which is necessary for autoclave pressurization control. Application of pressure too early results in resin-poor material, whereas late pressurization results in poor densification.

This technique involves measurements of the acoustic velocity and attenuation for longitudinal and shear wave propagation. The figure shows a classical resonance relaxation for the compressional wave case with a more complex situation for the transverse wave. From these measurements of neat resins, effective loss and storage moduli may be determined from the ultrasonic attenuation and ultrasonic velocity, respectively. In addition, the ultrasonic velocity can be used to obtain the resin viscosity. An integrated sensor for autoclave operation now appears feasible and is being pursued based on these results.



Ultrasonic research sensor for monitoring resin curing.

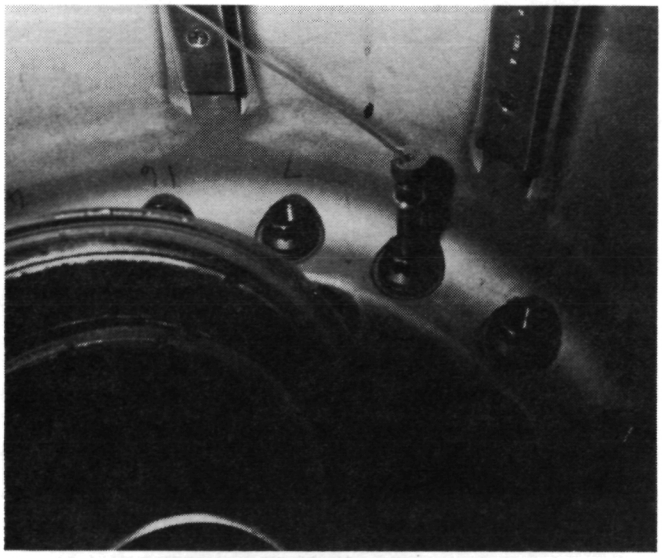
William P. Winfree, 3036

Shuttle Wheel Bolt Stress Measurements

The LaRC bolt stress measurement system was sent to Wright-Patterson Air Force Base for use on the Shuttle wheel bolts. With the aid of LaRC technicians, details of loading were examined which uncovered several bolt irregularities. This discovery prevented possible failures during rolling tests of the wheel assembly. The ultrasonic measurement system measures the acoustic phase length of the bolt, reducing the errors present in torquing control systems to less than 2 percent. Changes in phase length are interpreted as changes in bolt preload.

These tests proved the value of using an ultrasonic "stress" measurement instead of a torque measurement to eliminate errors caused by frictional variations. Further tests will examine a total flange preload system based on the ultrasonic method.

Joseph S. Heyman, 3036

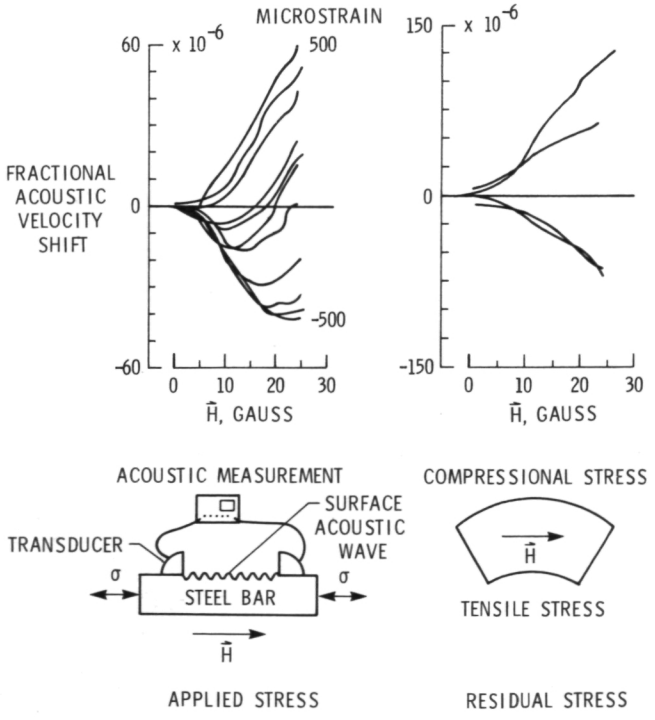


LaRC bolt stress measurement system.

Residual Stress Measurement Technique

Residual stress is one of the most difficult material states to determine nondestructively. To date, only X-ray scattering has been successfully used to characterize stress. Other techniques have had only limited practice, and X-ray measurements have a limitation in detecting surface conditions. Laboratory results at LaRC indicate that an exciting new concept has promise for obtaining residual stress measurements in steel. The technique uses a magnetic derivative of an ultrasonic wave velocity.

The technique has only recently been possible, thanks to another LaRC development called the ultrasonic pulse phase-locked loop (P^2L^2), which was selected as the NASA Invention of the Year in 1982. The high resolution of the P^2L^2 was able to detect small variations caused by stress in magnetic material behavior. Shown at the left in the figure are the changes in acoustic velocity caused by the applied magnetic field. Applied stress influences the magnetic derivative of the acoustic natural velocity (measured as a fractional velocity shift) for stresses that produce 500 to -500 microstrain. At the right in the figure, measurements on a plastically deformed sample containing residual stress show that the expected tensile side (two upper curves) indicates tensile stress, whereas the compressive side (two lower curves) shows compressive stress. This technique holds promise for determining residual stress in ferromagnetic materials. An important application of this technique is described in the preceding highlight.



Magnetic/acoustic residual stress measurement.

Joseph S. Heyman, 3036

Experimental Confirmation of Acoustic Radiation Stress in Solids

Of particular importance to quantitative nondestructive evaluation is the determination of the stress state of materials. A comprehensive theoretical and experimental investigation performed at LaRC of the nonlinear interaction between ultrasonic waves and the stress state has led to a significant breakthrough in the understanding of acoustic radiation stress in solids.

Four critical tests of the theory were incorporated into the experimental investigation with the purpose of separating out stresses resulting from external causes from those resulting from internal causes and measurement systems. The results of these investigations have confirmed an important link between mechanical stresses in solids and general nonlinear behavior leading to such thermodynamic phenomena as thermal expansion.

These investigations have established that quantities called nonlinearity parameters are related to the nonlinear processes in a very direct way. In the presence of sound waves these quantities cause a slight expansion of the material when positive and a slight contraction of the material when negative. Very sensitive tests, capable of measuring dimensional changes on the order of 0.01Å made it possible to confirm the predictions in samples of silicon (positive nonlinearity parameter) and vitreous silica (negative nonlinearity parameter).

The results of the investigation have significant and far-reaching implications to a number of related research areas, including strength of materials and specific heats of solids.

William T. Yost, 3036

Effects of Metal Ions on Positronium Formation in Polymers

The changes in environmental stability, electrical conductivity, and mechanical properties that can be affected by the incorporation of selected metal ions in polymeric chains have been the subject of increasing research interest in recent years. Of special interest at Langley have been the properties of epoxide resins containing chromium and cobalt ions. For example, a mole ratio of only 1:10 Cr ion to the polymer repeat unit reduces the saturation moisture content of epoxies by 6 to 30 percent without affecting their structured properties. Cobalt ions, on the other hand, increase the saturation moisture content in epoxies but at the same time increase their structured strengths. Positron annihilation characteristics have been investigated in the metal-ion-containing epoxide resins in order to elucidate the mechanisms responsible for these different effects.

It has been observed that the presence of Cr ions in epoxies results in the inhibition of positronium (Ps) formation and the acceleration of its decay rate. Co ions, on the other hand, do not affect the Ps formation probability but do increase its decay rate. These results indicate that more free electrons are accessible to positrons in Cr-containing epoxies than in Co-containing epoxies. However, positronium annihilation rates are equally affected by the Cr and Co additives, suggesting that their unpaired spins, rather than their effects on the matrix structure, are the more important factor in determining their suitability.

Jag J. Singh, 3907

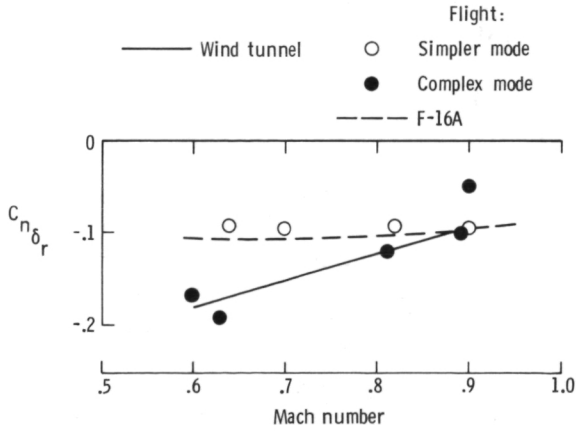
Parameter Estimation Applied to a Highly Augmented Airplane

The introduction of high-speed, highly maneuverable, statically unstable aircraft presents new problems in the field of system identification. These aircraft may have many control surfaces which interact through a flight control system (FCS). Such systems can preclude certain control inputs which would be optimal for the estimation of stability and control derivatives. Moreover, correlations among several control surface movements can degrade the accuracy of associated control derivative estimates. It is for such aircraft, however, that the importance of a good model is paramount since the FCS must be based on an adequate mathematical model of the airplane. As a step toward understanding the identification procedure that should be employed for such aircraft, a project was undertaken to identify the stability and control derivatives of the Advanced Fighter Technology Integrator (AFTI) F-16 airplane. The AFTI/F-16 is a derivative of the F-16A. Significant airframe changes from the F-16A were the addition of maneuverable twin vertical canards mounted beneath the engine inlets and a slight dorsal hump behind the cockpit canopy. The effect of these changes should be seen when results of the current analysis are compared with flight test results from the F-16A.

Flight data from two FCS modes have been analyzed. In the simpler mode, lateral control is accomplished through rudder and flaperons with vertical canards locked. In the more complex mode, lateral control depends on a combination of flaperons, differential horizontal tail, rudder, and vertical canards.

The figure shows the vertical canard effect on the rudder effectiveness derivative, $C_{n_{\delta r}}$. It is seen that in the simpler mode, the $C_{n_{\delta r}}$ estimated from flight data agrees with the F-16A. However, the $C_{n_{\delta r}}$ in the more complex mode shows an augmentation due to movement of the vertical canards. Because of correlations between the canard and rudder motion, separate canard and rudder effectivenesses are not identifiable. Hence, an effective $C_{n_{\delta r}}$ is estimated for the complex FCS mode.

James G. Batterson, 4591



Rudder effectiveness derivative determined from flight and wind tunnel tests as a function of angle of attack.

A Fault-Inferring Nonlinear Detection System (FINDS) Algorithm for Integrated Avionics Sensor Configurations

Integrated avionics concepts are being implemented in designs for future aircraft which stress maximum efficiency through relaxed static stability and require flight-crucial information from the avionics sensors. Reliability and safety requirements for these aircraft mandate automatic selection of operational sensors with quick rejection of failed components. Accordingly, current research at NASA Langley has been directed toward fault-tolerant concepts for sensor arrays in the integrated avionics context. In particular, a fault-inferring nonlinear detection system (FINDS) algorithm has been developed to provide detection, isolation, and compensation for failures in ground-based navigation aids and on-board flight control and navigation sensors. FINDS also provides sensor fault-tolerant estimates for the aircraft states which are used by aircraft automatic guidance and control systems. FINDS monitors for failures by evaluating all sensor outputs simultaneously and with the use of analytic relationships between the various sensor outputs derived from the aircraft equations of motion. Therefore, FINDS is an integrated sensor failure detection and isolation system.

The problem is cast in the context of simultaneous state estimation and failure identification in discrete time nonlinear stochastic systems. The fault-tolerant system algorithm consists of a no-fail estimator implemented as an extended Kalman filter, which provides estimates for aircraft state variables and normal sensor biases; a bank of detectors which are first-order filters for estimating sensor failures; likelihood ratio computers; and a decision function, which selects the most likely failure mode based on the likelihood ratios.

The FINDS algorithm has been tested in a six-degree-of-freedom nonlinear digital simulation of commercial transport in a Microwave Landing System environment. The aircraft state and bias estimation performance of the algorithm compared favorably with other methods, and the failure detection performance, particularly for navigation-aid sensors, was shown to be excellent.

Frederick R. Morrell, 3291

Development of the Semi-Markov Unreliability Range Evaluation (SURE) Program

The traditional methods of computing the state probabilities of a semi-Markov model either are applicable to only a small subclass of models or must be programmed independently for each problem. For example, existing programs are unable to analyze the nonexponential recovery distributions as encountered in the FTMP (fault-tolerant multiprocessor) fault injection experiments. Also, the traditional methods typically require significant computer resources. Recently at NASA Langley a new mathematical theorem was proved which enables the efficient computation of the system failure state probabilities of a large family of semi-Markov models useful for the analysis of the reliability of fault-tolerant architectures. This mathematical theory was implemented in a flexible interactive computer program named SURE.

A mathematical model is entered into the SURE program via a simple but flexible command language and is displayed graphically on a Megatek monitor in AIRLAB. Once the math model is entered, the program automatically finds every path to a system failure state in the model and computes upper and lower bounds on the probability of traversing the path. Bounds on the system reliability are obtained from analyzing every path in the model. Bounds on the total probability of system failure are plotted on the Megatek as a function of any specified parameter of the system; for example, mean recovery time.

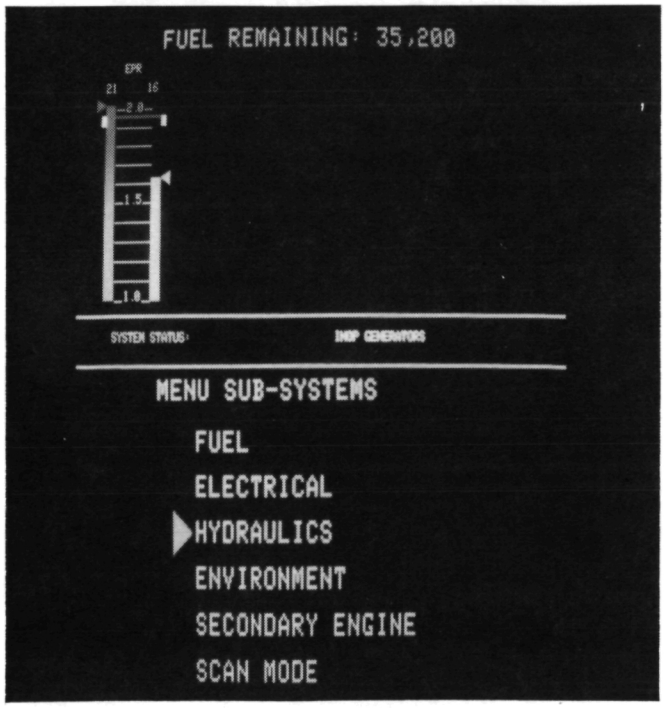
The first version of the SURE program has been developed. The user interface was found to be quite flexible and easy to use—for example, mathematicians with little or no computer experience were able to use the tool with only 15 to 20 minutes of instruction. The SURE program was found to be extremely fast even for models with hundreds of states and the upper and lower bounds were found to be extremely close for most systems. The graphical display of the mathematical model was found to be useful in detecting model input errors.

Ricky W. Butler, 3681

Advanced System/Subsystems Monitoring Interface

The accelerated use of digital avionic systems and the related increase in available sensor outputs provide the modern transport aircraft crew with a plethora of information on system/subsystem performance. The potential benefits that arise from this wealth of information are as obvious as the need to effectively display the information in digestible forms. Not as immediately obvious is the need for an information management system with an effective crew interface that will not further increase either crew training requirements or crew workload.

The Crew Station Technology R&T base program has developed an information management/interface concept that incorporates these goals as well as an additional goal of consolidated multipurpose controls. Although current display technology is providing fewer cockpit displays/meters through the use of multipurpose displays, the number of dedicated controls/switches has continued to increase. In order to combat this trend of increasing numbers of dedicated controls, the concept is designed around a programmable display pushbutton device (a technology fostered under the Crew Station Technology program) as a multifunction display/switch for pilot input/output.



Engine/subsystems monitoring display with warning messages and subsystem menu.

The completed control/display interface concept has been implemented in a transport flight simulator for pilot evaluation/enhancement with representative system/subsystem displays. The concept provides continuous display of the primary engine system variables and advisory caution and warning system messages, with various pilot-selectable subsystem formats, on one display. The concept incorporates intelligent automation and piloting-aiding strategies within the information management system and also provides an automatic subsystem scanning mode to ease pilot workload.

Russell V. Parrish, 2259

Pilot/Autopilot Interface Using Hands-On Throttle and Stick Concept

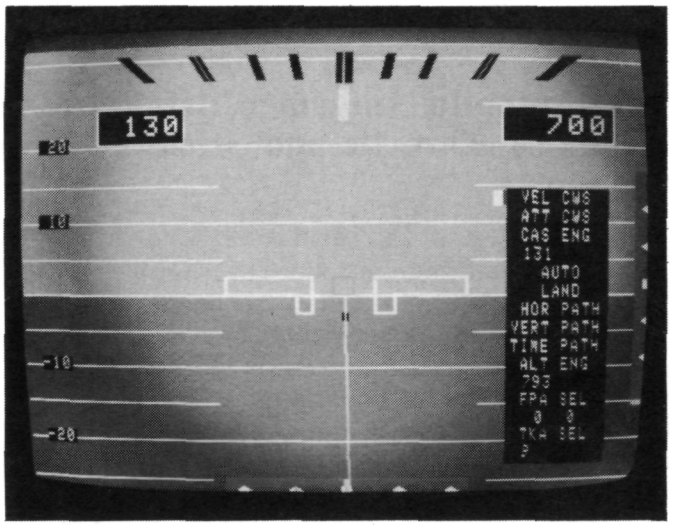
Almost all segments of the flight management research community are concerned with reducing crew workload within the modern aircraft cockpit. These reductions are being sought in various ways, including the reduction of cockpit clutter through use of multipurpose, integrated displays and consolidated keyboards/controls which utilize programmable-legend/multifunction switches. These concepts are also intended to improve pilot performance and efficiency, particularly during critical operations. The Air Force has been actively pursuing a concept known as hands-on throttle and stick (HOTAS) for the high-workload arena of the fighter cockpit. This concept involves the activation of various flight and weapons systems/subsystems by the pilot without the necessity of releasing the flight controls. This is accomplished by the use of switches and buttons built into the throttles and stick handles.

A similar concept is being evaluated within the Crew Station Technology program for transport aircraft applications. The initial application has been developed around a pilot/autopilot interface, comparing a conventional, dedicated control/display unit for an advanced autopilot to a HOTAS implementation. The HOTAS implementation allows the pilot to select the various combinations and levels of automatic flight control assistance by activating a cursor-selectable menu choice. The menu can be erased or superimposed over the primary flight display at the push of a button on the hand controller. Cursor move-

ment and numerical changes to flight parameters are commanded through use of a multiposition thumbwheel slide within the throttle handles.

Initial pilot reaction has been highly favorable, with particular emphasis being placed on the ease of sharing attention between the primary flight display and menu operations. More formal simulator evaluations to determine effects on tracking performance as well as physical workload are planned, and additional applications of the HOTAS concept to other cockpit functions are under way.

Russell V. Parrish, 2259



Primary flight display with superimposed advanced autopilot menu.

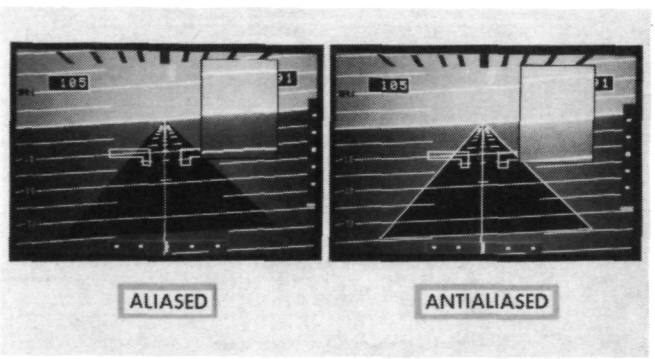
Real-Time Smoothing of Rolled Symbology in All-Raster Electronic Flight Displays

Raster scan electronic display systems (resembling television) have many potential advantages for flight applications. They permit efficient shading of large areas, making "windows" to display information against backgrounds, prioritizing symbology such that overlapping shapes do not change colors, and generally achieving photographic-like clarity for the pictorial integration of flight information. Further, they permit the utilization of simpler, less costly resonant deflection systems within CRT display devices, which reduces power consumption by 50 percent when compared to stroke display devices. They are also compatible with emerging flat-panel display technology. However, when vectors or lines are rolled to near-horizontal or near-vertical orientations, current raster systems portray them as a series of straight lines (stairsteps), depending on the picture element resolution. This effect, called aliasing, can be objectionable at times, depending on the display format and symbology.

The Crew Station Technology R&T base program has developed a smooth (antialiased) line-drawing algorithm and has validated it in a real-time applications program which generates an advanced primary flight display. The display was evaluated within a cockpit simulator which permitted the experimentor to "fly" the aircraft while the line-drawing algorithm was switched between aliased and antialiased modes. In the antialiased mode, the algorithm smooths the stairstepping by filtering the high spatial frequency content and shading gently toward the background color. Thus, each vector is broadened and made bolder.

The experimental results have indicated an unmistakable improvement in line quality with the antialiasing algorithm. (Note the insets in the figure, which show a magnified view of the horizon and pitch scale.) This algorithm gives excellent line quality with only a slight loss in execution speed. Timing tests were performed using the primary flight display shown. The results indicated that the antialiasing algorithm reduces the update rate for the display by only 17 percent. Further, the dynamic quality of the display was quite acceptable.

M. Jack Neubauer, 3457

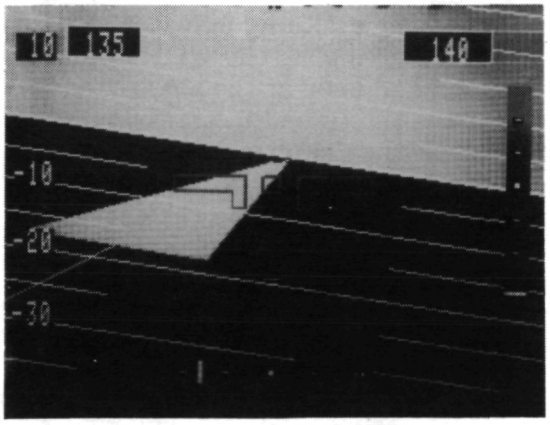


Advanced all-raster programmable display generator performance showing capability for real-time smoothing of rolled symbology.

Raster Graphic Display Generator Integrated With Thin-Film Electroluminescent (TFEL) Display Panel

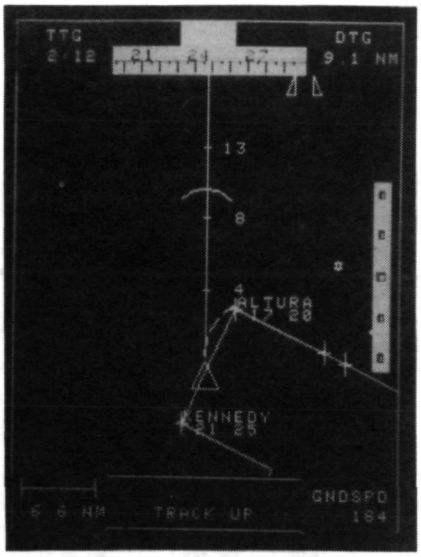
As part of the Crew Station Technology research effort at Langley Research Center, a monochrome thin-film electroluminescent (TFEL) flat-panel display has been integrated with an Adage-3000 high-performance raster graphics programmable display generator (PDG) and a VAX 11/780 host computer for the generation and display of primary flight displays. This successful integration of these two technologies is important because each offers unique capabilities for the flight deck environment. Raster graphics PDG technology offers the capability for shaded pictorial display generation for the consolidation and integration of display functions. Flat-panel display technology offers the potential to save space, weight, and power while providing higher reliability and graceful degradation.

Existing software for the PDG produced an electronic attitude director indicator (EADI) and a horizontal situation indicator (EHSI). These display formats, intended for use with high-resolution color CRT displays, were output as 512 × 512 picture elements of resolution. Since the TFEL panel required NTSC monochrome composite video as input for digitizing the video and displaying it on the 240 × 320-line electroluminescent panel, the PDG output signal formats had to be adjusted. In order to display the EADI and EHSI on the video graphics exerciser, the formats had to be scaled to 240 × 320 picture elements (525-scan-line 60-Hz noninterlaced video), the PDG computer program had to be modified to support the appropriate channeling of pixels to required regions of the color look-up tables, the PDG video amplitude parameters had to be adjusted to match those of the TFEL display, the RGB color maps had to be converted to gray-scale color maps, and the green output had to be used as a monochrome NTSC signal. The EADI and EHSI are shown displayed on the TFEL panel. These displays showed no missing lines and almost no discernible effect of missing pixels within lines, and gray scale performance was good. In addition, dynamically there were no smearing, streaking, or flicker effects.



240 X 320 PIXELS
60 HZ, NONINTERLACED

Raster-addressed EADI.



240 X 320 PIXELS
60 HZ, NONINTERLACED

Raster-addressed EHSI.

Jack J. Hatfield, 2171

High-Resolution Large-Screen TFEL Flat-Panel Display Using Monolithic Drivers

Matrix-addressed thin-film electroluminescent (TFEL) displays hold the promise of replacing the cathode ray tube (CRT) as the primary display

device in future flight decks. TFEL displays must be matrix-addressed, which requires extensive addressing circuitry. This circuitry must be integrated for TFEL to remain a low-volume, low-cost display. TFEL addressing, however, requires up to 200 V, and the technology for integrating large numbers of circuits capable of this high voltage onto single clips did not exist. In addition, it was required that the display be addressed at TV rates and in 16 gray shades (i.e., 16 levels of brightness).

Supertex, Inc., under a contract funded by NASA Langley Research Center and U.S. Army ERADCOM, was able to develop integrated circuits, called row drivers and column drivers, that met these requirements. This development required the merging of DMOS high-voltage transistors with standard 5-V CMOS circuitry. The row drivers are capable of switching from −140 V to +200 V. The column drivers allow the selection of any of 16 output levels from 3.75 to 56.25 V.

The success of these new high-voltage integrated circuits was recently demonstrated by using them to present live television in 16 shades of gray in a 512 row × 640 column TFEL display panel.

James B. Robertson, 3716



First laboratory tests of a high-resolution large-screen TFEL display using monolithic drivers.

Effects of Digital Altimetry on Pilot Workload

With the proliferation of cathode ray tubes and associated microprocessor hardware, the capability now exists to place almost any type of information on a pilot's display. A general effort is under way to determine the effects of the various types of information and information placements on pilot visual scanning behavior and workload. One information problem area has been that of altimetry. In spite of numerous attempts to find the best altimeter, incidents still occur as a result of missing an altitude assignment.

Seventy-two VOR-DME (VHF omni range/Distance Measurement Equipment) landing approaches were flown in the NASA Langley fixed-based Full-Workload Simulator to evaluate the effects of using a digital altimeter on pilot scanning behavior and workload. Six pilots used conventional counter-drum-pointer altimeter (CDPA) and a digital altimeter (DA), which consisted of five seven-segment LED digits 0.28 in. high. Pilot scanning data were collected with Langley's oculometer system. The oculometric data were reduced to dwell percentages, average dwell times, transition matrices, and dwell time histograms, and were analyzed statistically.

The results showed only slight differences in pilot scanning behavior with the DA versus the CDPA. Although the average dwell time on the DA was slightly shorter, there were more transitions to altitude information with the DA. The average dwell time on the attitude indicator was 0.2 sec shorter after looking at the CDPA than if the previous look had been at the DA. After looking at the DA, the pilots had to think longer about the digital altitude information than they did when using the CDPA. Pilot comments were generally negative toward the DA because of the lack of needle motion cues, the difficulty of forming a mental picture of altitude when using the DA, and the necessity for the pilot to perform mental arithmetic to estimate the distance to his assigned altitude. This research suggests that digital display of altitude requires more cognitive processes on the part of the pilot than conventional altimeter displays.

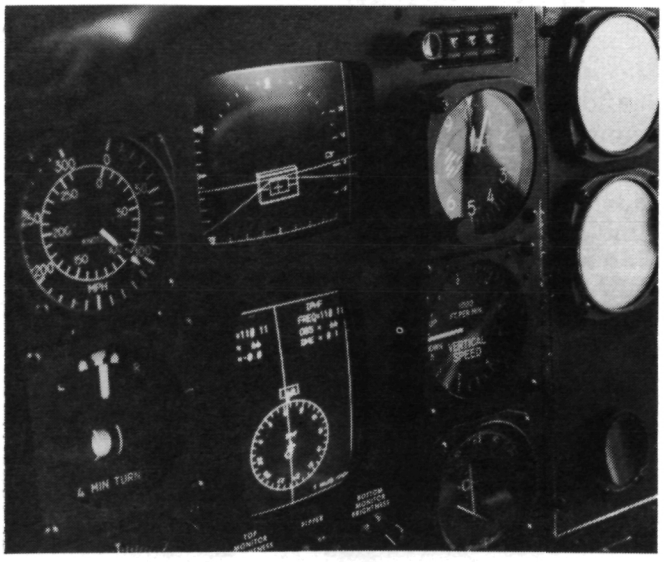
Randall L. Harris, 3917

Advanced Display Used for Precise Flight Control

The desire for increased airspace capacity, reduced delays, and improved efficiency dictates a need for more precise control of aircraft position than has been possible with conventional displays. The ability to land an aircraft when no out-the-window information is available has been a research goal for some time. The computer-drawn pictorial path-in-the-sky "follow me" box display concept has been shown to result in lateral and vertical positioning of the aircraft that is eight times more precise than that obtained with conventional displays. This attribute of the display format should provide an increase in flight safety by reducing the excursions of the aircraft, and should also allow landing approaches to be made with lower ceilings. This hypothesis has been tested in a study that combined a low-accuracy moving-map with the "follow me" box to form a combination display that would satisfy all performance requirements for IFR flight, and in a second study that concentrated on instrument touchdowns.

The study that combined the box display with a moving-map display covered most phases of an instrument flight in an operational environment. The simulator that was used for the test was detailed enough that the subject was able to make a realistic evaluation of the system. Thunderstorm conditions, frequent unexpected flight plan changes, and a ceiling of 60 ft were used to generate a difficult task. In the touchdown study the subjects had no out-the-window information and had to use the box display as the only source of information. The results showed that the tasks could be successfully performed because of the precise position control of the aircraft that was obtained. However, some pilots noted an increase in the workload created by the box display format compared to that of conventional instruments for enroute navigation. Shown in the photograph is the instrument panel with the box display above and the map display below.

James J. Adams, 3917

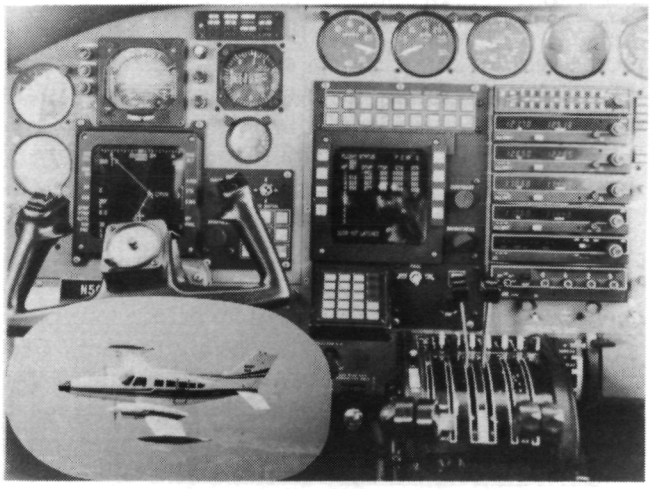


Instrument panel with CRT displays.

Advanced Avionics Systems Pilot Interface Study

Digital, integrated avionics systems offer numerous advantages over conventional, separate system installations. Concern exists, however, about the impact on pilot workload of managing and using highly capable avionics systems.

An experimental, integrated digital avionics system, built by Honeywell and King Radio, was installed in a Langley Cessna 402 research aircraft and utilized in a series of flights to study the benefits and problems of the pilot interface with advanced systems. The test system provided for flight plan storage, automatic radio tuning, CRT-based moving-map display, and autopilot capabilities. The flights consisted of realistic IFR scenarios flown by professional research pilots. The test system provided numerous benefits to the pilot, such as the moving-map display and a continuous display of flight status. The integrated system provided capabilities that would not have



Experimental avionics system.

been feasible with nonintegrated avionics installations. Areas were identified where improvements are needed in the pilot interface with the level of avionics capability. Blunders were made with the system that related to data management, loss of awareness of system state, and difficulty in forming a mental system model. These blunders sometimes created excessive pilot workload.

The test results suggested numerous guidelines for the design of pilot/avionics interfaces. These guidelines include minimizing the number of possible system states, allowing the pilot to choose the level of system capability to use, and providing pictorial information, on a moving map-display, of active waypoint/course and autopilot mode.

David A. Hinton, 3917

Expert System for Aircraft Engine Fault Diagnosis

Onboard fault diagnosis requires flight crews to assimilate a great deal of information in situations that are often time-critical. Recent advances in expert-systems technology for applications such as medical diagnosis have demonstrated that expert-systems techniques have a great deal to offer to aid the human in the system. Research was conducted to determine how expert-systems techniques could be used to perform aircraft fault diagnosis. A turbofan aircraft engine was chosen as a representative subsystem for which faults had to be diagnosed. The result of this research is a prototype expert system that demonstrates the concepts for aircraft fault diagnosis.

Aircraft pilots were interviewed as the main source of knowledge on engine fault diagnosis. Several commonalities were noted that differed greatly from the procedures described in pilot handbooks. Pilots described the symptoms they looked for in qualitative terms, such as "epr fluctuating" and "egt decreasing," rather than using specific quantitative information. They used causal knowledge to reason about how the system behaved, about failures causing certain symptoms to occur, and about how those symptoms could cause other behavioral changes within the system. The pilots used time-based information for diagnosis. They looked for the behavior of the symptoms over time for certain patterns that they recognized as representative of particular faults.

The results of the pilot interviews were incorporated into an expert system capable of reasoning as the pilots do. The system can diagnose single and multiple faults in the engine system. It performs qualitative reasoning and uses causal and time-based information to diagnose failures and to estimate likelihood of a particular fault. The engine fault diagnosis expert system has been demonstrated to diagnose faults accurately and quickly.

Kathy H. Abbott, 3621

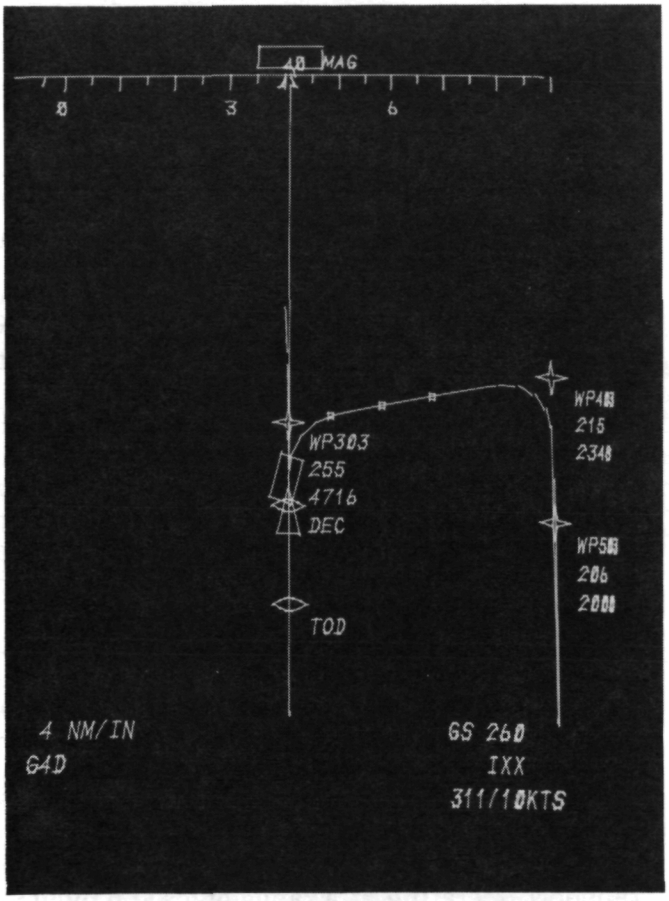
Four-Dimensional Guidance Concept for Airborne Terminal Areas

Four-dimensional guidance of aircraft in the Terminal Maneuvering Area (TMA) would allow more precise control of minimum longitudinal separation of aircraft and thus more efficient use of the available approach capacity of the respective airport. In a cooperative effort with the German government, a visiting engineer from the DFVLR Institute of Flight Dynamics is adapting and extending a four-dimensional guidance concept, originally developed at the DFVLR Institute, for flight tests in 1985 with the Advanced Transport Operating Systems Research Program Boeing 737. The development includes control modes integrated with navigation information and the automatic flight control system. Initial tests were performed on this system using the DFVLR's HFB 320 test aircraft.

The four-dimensional guidance mode is designed for that portion of the flight starting up to 50 miles from the runway (the metering fix) and continuing to a point on the runway-extended centerline (the merge gate). Under this concept, the time of arrival at the merge gate is controlled only by altering the path (called a delay fan), allowing airspeed and altitude to be chosen separately to minimize fuel consumption. Algorithms compatible with this concept have been developed to provide descent and deceleration at idle thrust. Additional features of the system allow the pilot to check or enter necessary data such as altitude and airspeed for the intermediate approach or the planned time of arrival at the merge gate assigned by ATC. The planned time-accurate flight path is presented on a cathode ray tube, as illustrated. Features of the presentation include a time box

symbol, which gives the desired position of the aircraft, and an airplane symbol, which shows the present position. The time error will be accommodated by path adjustments occurring prior to interception of the extended centerline. TOD (top of descent) and DEC (deceleration) symbols indicate the beginning of the idle-descent and idle-deceleration phase, which ends when the airplane reaches the end of the last curve onto the extended runway centerline.

William E. Howell, 2132



Electronic map display showing planned time-accurate flight path.

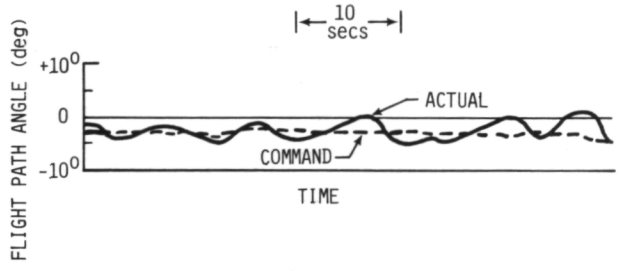
Control/Display System Problem and Solution Verified by Model Analysis

Control wheel steering, appropriate display information, and its format have been under investigation in the Advanced Transport Operating Systems (ATOPS) Program as a means of reducing pilot workload. One problem area which has been given attention is coupling the appropriate display information with control wheel steering. ATOPS-supported research has shown that control difficulties and even pilot-induced oscillations (PIOs) result when the display is not matched well with the control mode.

A Langley-developed pilot model of the TSRV advanced flight deck has been employed to analytically evaluate the advantage of using velocity vector control wheel steering coupled with a predictive display of inertial flight path angle. The curve labelled "actual" in the figure presents a model time history segment of inertial flight path angle during an instrument approach to landing in turbulence with velocity vector control wheel steering and raw flight path angle displayed. The large amount of oscillation is a result of the incompatibility of the flight path angle display with the control system, and resulting PIOs. The curve labelled "command" presents model results for flight under similar conditions with a display of reference flight path angle presented, which is the flight path angle command signal that the control augmentation system is attempting to maintain. With this signal displayed, the model pilot allows the control system to damp out perturbations due to turbulence. Model-measured pilot workload is greatly reduced and system performance is improved.

The result of this model analysis helps validate a previous finding which emphasizes the importance of flight control system and display compatibility. As the ATOPS-developed velocity vector control wheel steering mode is introduced into the cockpits of the next generation of aircraft, an appropriate display of reference flight path angle should be presented to the pilot to continuously inform him of what that control system is attempting to accomplish.

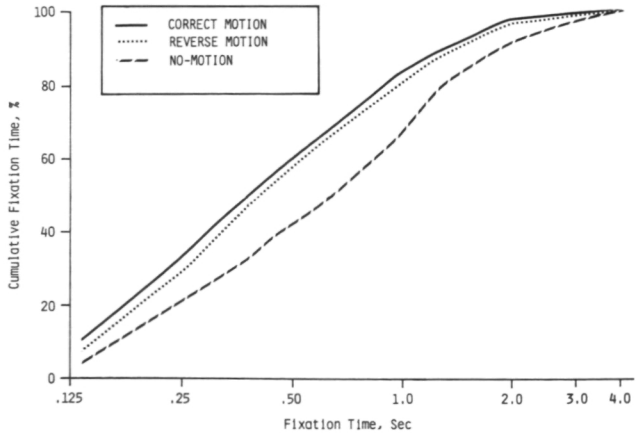
Marvin C. Waller, 3917



Aircraft path with actual and command flight path angle displayed.

Oculometric Indices of Simulator and Aircraft Motion

Because of the importance that motion and eye scan interaction may play in providing high-fidelity flight simulation, oculometer studies were performed under the Advanced Transport Operating Systems (ATOPS) Program to investigate differences in pilot eye scan behavior between actual and simulated motion and simulation with no motion. In these studies, fixation time, defined as the time the eyes spend at a particular location before moving on (saccade) to another fixation point, was found to be sensitive to motion effects. The first experiment investigated simulator motion and no motion during a series of simulated ILS (instrument landing system) approaches. The mean fixation time with no-motion was found to be significantly longer than for the motion condition, particularly on the cockpit Flight Director. A second experiment investigated eye scan parameters based on data collection in flight and during fixed-base simulation. Motion effects were most evident when the subject was viewing a display of attitude and flight path information. A third study employed a part task, with motion in only one dimension (pitch). Subjects were tested in no motion, correct motion, and reversed direction motion conditions. The mean fixation times for the no-motion condition were significantly longer than for either motion condition, whereas the fixation time with either motion did not differ significantly. The figure shows the relationship between fixation time and cumulative percentage of total fixation time for this experiment, and portrays the differences between the three motion conditions.



Effect of motion cues on eye fixation time.

The results of the experiments support the hypothesis that motion serves an alerting function to the pilot that "something happened." The results do not support the hypothesis that direction of motion is conveyed through this type of motion information. The results suggest that simulation without motion cues may yield an understatement of the true capacity of the pilot.

James R. Comstock, Jr., 3917

Integrated Digital/Electric Aircraft Has Performance Potential

Emerging fault-tolerant controls technologies coupled with recent advances in rare-earth magnet materials have led to the concept of an Integrated Digital/Electric Aircraft (IDEA) with flight-critical digital fly-by-wire controls and all-electric secondary power. The application of these new technologies and materials in the IDEA would result in substantial performance gains and fuel savings. To quantify these expected benefits, contracts were awarded to the Boeing Commercial Airplane Co. and the Lockheed-California Co. Both contracts had a common statement of work which called for establishing a baseline commercial transport aircraft that used 1990 technologies in all areas except systems. After calculating the predicted performance of the baseline, flight-critical fly-by-wire controls and all-electric secondary power were substituted to establish the IDEA concept and the performance was recalculated.

The results from both contractors showed substantial performance gains. In the case of Lockheed, for a three-engine 350-passenger transport operating at a range of 2500 n.mi., the IDEA aircraft saved 11.3 percent on fuel and 8.2 percent in direct operating costs (DOC) when compared to the baseline. The Boeing results showed a 3-percent fuel savings and a 1.8-percent reduction in DOC for a twin-engine 197-passenger transport at a range of 1000 n.mi. when compared to the baseline. It is important to note, however, that in the Boeing study the baseline aircraft already included analog fly-by-wire controls, which means that the benefits realized by the application of IDEA concepts would be somewhat lower than those in the Lockheed study.

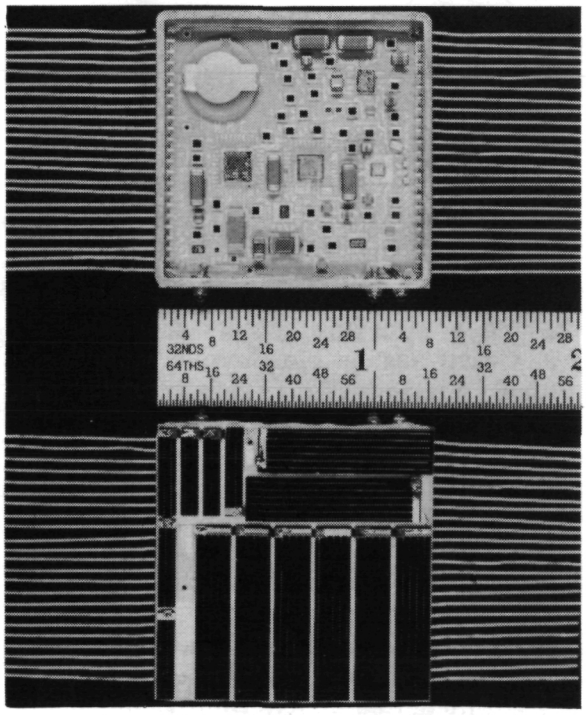
The results of the studies also included a series of research program recommendations for NASA

to insure that the agency would play a major role in spurring the timely development of the Integrated Digital/Electric Aircraft.

Cary R. Spitzer, 3318

Remote Solar-Powered Data Acquisition Module

Hybrid solar-powered sensor modules featuring an optical, bidirectional communications link compatible with UART (universal asynchronous receiver transmitter) data formatting in a 1.25- by 1.25- by 0.16-in. module have been demonstrated. The modules consist of four sections: power supply, control, data acquisition, and communication. The power supply is an array of gallium arsenide solar cells typically exhibiting 16 to 18 percent efficiencies. The data acquisition section consists of a sensor, or signal source, and a 12-bit A/D converter. The control section coordinates the overall functions, including timing. The communications section is responsible for recognizing an interrogation command and responding with a serial transmission of digitized data. Both interrogation and data transmission communications occur over an infrared light beam. A remote command and control console furnishes the interrogation signals and displays the results. This development of a small solar-powered data acquisition module, which can be activated remotely from a central station via an optical link and can respond with data measurements on a return optical link, should have widespread remote sensing applications. The module was developed for LaRC by the Solid State Division of Hughes Aircraft Co.



Data acquisition module.

Harlan K. Holmes, 3446

Evaluation of Quantum-Well Lead Salt Tunable-Diode Lasers

A breakthrough in the state of the art of lead salt tunable-diode lasers was achieved by General Motors Research Laboratory's construction of the first successful quantum-well lasers using lead salts. These diode lasers have a narrow stripe geometry, large optical cavity, PbTe quantum-well active region, and PbEuSeTe lattice-matched confinement layers, and were grown by molecular-beam epitaxy at GM. They can be used to cover the 2.6- to 6.6-μm wavelength region.

These lead salt quantum-well diode lasers exhibit remarkable characteristics—record high-temperature operation, markedly low threshold currents, single-mode production, and week-to-week reproducibility of lasing frequencies. Lasing was achieved at 174 and 281 K under CW (continuous wave) and pulsed (approximately 1 μsec) operation, respectively. These temperatures are well within the thermoelectric cooling range and simplify effective use of these lasers. The effective use of lead salt lasers (non quantum well) has previously been limited by their inability to generate two or more modes simultaneously and by the day-to-day variability of the current and temperature required to generate specific laser frequencies. In heterodyning against a CO laser, a quantum-well laser produced beatnotes which were reproducible week after week for several months simply by adjusting the currents and temperatures to previously used and recorded values. Because of these and similar results, quantum-well structures represent a breakthrough in the state of the art of lead salt diode lasers. These quantum-well lasers were provided by GM to MIT Lincoln Labs, who performed extensive characterization tests on them under NASA Grant NAG-1-164.

Stephen J. Katzberg, 4469

Pushbroom Microwave Radiometer Technology for Soil Moisture Measurement

A Pushbroom Microwave Radiometer (PBMR) has been developed at Langley and successfully flown aboard NASA aircraft. The pushbroom concept combines the fine spatial resolution of individual radiometer beams with the wide coverage afforded by arranging several beams fanning out to form a wide swath across the subtrack of the aircraft or spacecraft. With a center frequency of 1.4 GHz and a bandwidth of 25 MHz, the PBMR has application to Earth surveys of the moisture content of soils. Such surveys were flown over agricultural test sites in Maryland, Delaware, Virginia, and Texas during 1983 and 1984 in cooperation with Goddard Space Flight Center, the U.S. Department of Agriculture, and various state agencies. Those surveys were coordinated with simultaneous ground-based measurements of the soil moisture, taking advantage of whatever recent rainfall was available. In late 1984 the PBMR will be flown over nearly rain-free fields in California, where the amount of moisture will be controlled by irrigation.

Advanced Microwave Integrated Circuit (MIC) techniques were employed in the design of the PBMR's front end, and the signal processing is accomplished through digital means. This provides the ability to change the number and configuration of the beams without making extensive hardware modifications. Thus, the PBMR is not only a useful tool for remotely sensing soil moisture, but serves as a testbed for the study of pushbroom concepts in general.

The obvious extension of this technology is to orbital remote sensing of the Earth. An experiment has been proposed whereby a dual-frequency pushbroom radiometer would be installed on the Space Shuttle with a large (3- by 6-m) phased-array antenna system to provide a 100-km swath across the orbiter's subtrack. The swath would be made up of four beams, each making its own measurements of soil moisture over land and sea surface temperature over the ocean.

R. W. Lawrence, 3631

Co:MgF_2 Lidar System

A ground-based differential absorption lidar (DIAL) system has been developed at MIT Lincoln Labs which is based on the Co:MgF_2 tunable solid-state laser. The laser is tunable over the 1.5- to 2.3-μm wavelength range, allowing DIAL measurements at longer wavelengths than conventional dye lasers. Tuning is provided by an intracavity birefringent tuning filter in combination with a quartz etalon. An acousto-optic modulator is used to achieve Q-switched pulse mode operation. The receiver is a 60-cm-diameter Cassegrainian telescope with an indium antimonide detector.

Preliminary lidar measurements have included range-resolved aerosol backscatter returns out to a range of 1 km and total column content measurements using topographic targets. Water vapor absorption lines were measured in the topographic target scans. Topographic target scans of spectral regions containing HCl and methane absorption lines were performed simultaneously with gas absorption cell scans. As expected, HCl and methane were not present in measurable quantities in the atmospheric path. Predictions of HCl measurement accuracy as a function of range cell distance were made. Anticipated HCl sensitivity is a few parts per million out to 2-km-range distances, assuming a fivefold S/N improvement from pulse averaging.

Measurement sensitivities for methane are estimated at 10 to 100 parts per million, which suggests a use in detecting natural gas leaks. Range-resolved H_2O measurements from aerosol backscattering out to a 1-km range were performed.

Daniel J. Jobson, 3535

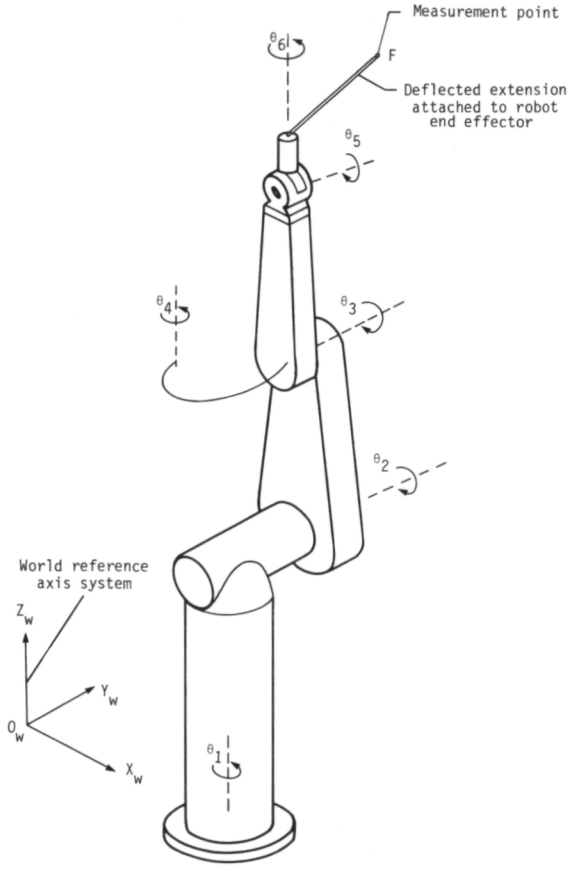
Kinematic Control of Robot Arms

In space construction and in the service and repair of satellites, a robot arm should obey movement commands from an operator or computer program as closely as possible. Singularities in the mathematical equations that translate these commands into arm movements hinder this objective. One solution is simply to avoid the position of the robot arm that causes a singularity. However, in using resolved-rate equations, an operator generally issues commands to the robot hand, and to move the hand as commanded, the arm may inadvertently pass through a singularity. Consequently, auxiliary equations have been formulated to continue controlling the robot hand when the robot arm is fully extended (singularity when $\theta_3 = 0$) and when the robot wrist is degenerate

(singularity when axes for $\theta 4$ and $\theta 6$ are collinear). Results show successful movement of a graphically simulated robot arm.

Another obstacle to kinematic control of a robot arm is unknown Denavit-Hartenberg parameters, which precisely describe the relative location of one joint axis system with respect to another. A vector-algebra approach has been developed for extracting these Denavit-Hartenberg parameters from any assembled robot arm. The only measurements required are the locations of a point on the robot hand for different joint angles. A minimum of three locations is required for each rotational joint or two for each sliding joint. This method may be useful for validation of mathematical models and also to hobbyists who build robot arms from a composite of diverse components. This method, which does not require the robot arm to be disassembled, may also be useful in the recalibration of a misaligned or bent robot arm.

L. Keith Barker, 3871



World axis system and robot arm with extension for measurements.

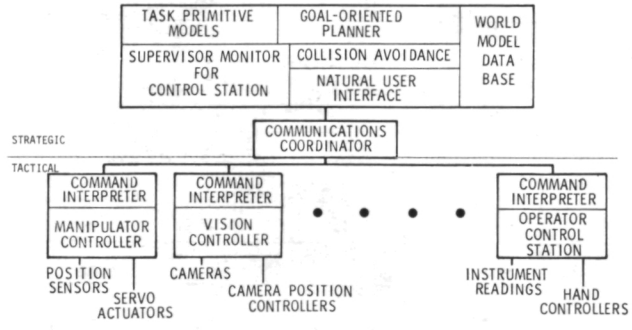
Distributed Artificially Intelligent System for Interacting With the Environment

As the complexity of space teleoperated tasks increases, there will be a growing need for shared control between man and computer to adequately perform these tasks. As a testbed for researching these control needs, Langley has designed and implemented DAISIE (Distributed Artificially Intelligent System for Interacting with the Environment), a structure that connects a distributed network of teleoperator/robotic peripherals in a hierarchical software system. The structure of DAISIE is illustrated, with the system divided into two major levels. The tactical level deals with the local control of individual sensors and actuators such as manipulator arms, vision systems, and displays. The strategic level refers to global knowledge and control of the entire structure, environment, and task at hand.

DAISIE serves two basic functions in NASA's teleoperator/robotic research. Primarily, DAISIE supports in-house research investigating the use of artificial intelligence (AI) techniques for sharing control between man and computer systems in performing a teleoperated task. Demonstrations have been performed in simple geometric environments.

The second function DAISIE serves is as a means for researchers, especially visiting professors, to test high-level AI algorithms in a realistic control environment. Examples of research efforts to date that have been interfaced to DAISIE include the dynamic generation and representation of a four-dimensional environment, collision avoidance algorithms, and robot task planning using formal logic programming.

Nancy E. Orlando, 3871



DAISIE structure.

Teleoperator Interface Research

Space operations such as construction or repair and refurbishment of satellites will be increasing in the near future. One way of performing these operations is through devices remotely controlled by humans. This method, teleoperation, offers advantages in safety, efficiency, and monetary savings. Research at Langley is being performed to enhance teleoperation capabilities with emphasis on gradually increasing the automation level of the teleoperated equipment. One critical aspect of this research is the interface between a human and the remotely controlled system. Recently, all the necessary hardware and software elements to establish and evaluate a baseline human/machine interface were assembled and initial tests were conducted. For the initial tests a direct-view control station was used as well as a reconfigurable control station. This permitted an assessment of degradation in performance resulting from loss of visual fidelity through the television link.

The tests consisted of using a Unimation Puma manipulator to pick up a peg, depress switches with it, and then insert it into a receptacle. Two different sized pegs were used, one of which cleared the receptacle by only 0.005 in. The Puma was controlled in two different ways. In one method each joint was individually addressed and caused to move. In the other, decoupled control was used to move the end effector in attitude and translation in its own axis system. Unexpectedly, no significant difference was found between the direct viewing of the task and the indirect viewing through closed-circuit TV. Control modes and peg sizes were found to affect task performance significantly. Performance was much better with the small peg and with decoupled control. These results will be used as a reference against which to assess future incremental enhancements of the teleoperator man/machine interface.

R. W. Mixon, 3871

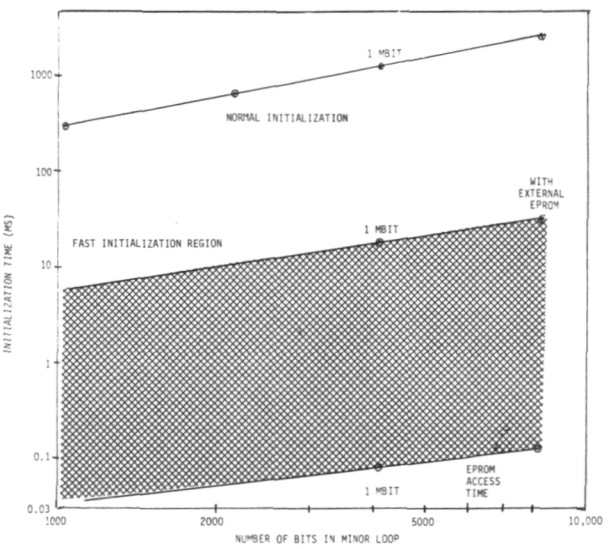


Reconfigurable control station.

Fast Initialization of Bubble Memory Systems

A faster mechanism for the initialization of bubble memory systems has been developed and demonstrated at Langley. The increased initialization speed will be particularly beneficial in enabling high-capacity bubble memory systems to provide high-speed access to arbitrary memory blocks while requiring reasonable power. Without fast initialization, power requirements will limit system capacity and arbitrary block access will be extremely slow.

Current initialization mechanisms require that data from the bootloop be read into the controller memory before read/write accesses can be made. These bootloop data indicate which loops are being used within the memory device. The bootloop is part of the bubble memory device and the data must be transferred serially from the bubble device to the controller, which is a relatively slow process. The improvement demonstrated is to initially load the bootloop data into a low-capacity but much



Initialization time for eight parallel bubbles.

faster EPROM (erasable programmable read-only memory) and, upon subsequent initializations, to transfer the bootloop from the EPROM to the controller memory. Speed improvements in excess of an order of magnitude have been realized. Initialization times for various bubble devices with and without the external storage are shown. The cross-hatched region indicates the obtainable time range using the fast initialization technique.

Karen T. Looney, 3777

AlGaAs Phased-Array Semiconductor Lasers for Space Communications

Laser communications in space provide a means for a more tightly focused beam for improved security, protection from jamming and eavesdropping, long-range communications, a high data rate, and a reduction in the size of the transmitting telescope of a full order of magnitude over microwave. As part of its electronics and communications research program, NASA Langley has been developing AlGaAs phased-array semiconductor lasers. This approach utilizes the transverse coupling of semiconductor lasers to lock the phase of arrays deposited in a narrow spacing geometry (5 μm). Once the devices are locked together, high optical power outputs (0.1 to 5 W) can be achieved. Current research is directed toward high modulation rate (0.1 to 5 GHz), high power, and diffraction-limited beams.

Currently two types of phased arrays have been demonstrated—a linear and a nonuniformly spaced array—and 50 mW per laser in the array has been achieved. Initial phased-array results have demonstrated single longitudinal mode operation to 100 MHz modulation. The thin-active-layer channelled-substrate planar large-optical-cavity device has demonstrated 120 mW of phased-array power and conditions for a diffraction-limited beam. An initial nonabsorbing mirror window design for increased optical power has been demonstrated on an AlGaAs device which gave 1.5 W peak power output. Near-term research on phased array is directed toward achieving single-mode operation with a diffraction-limited beam while the array is being modulated.

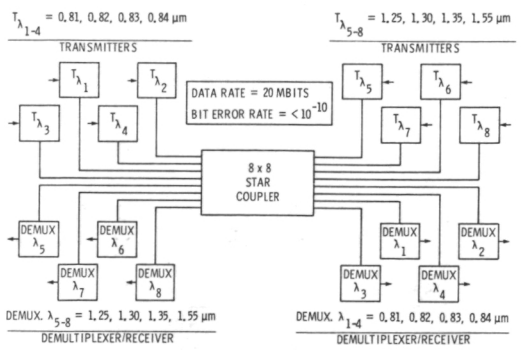
H. D. Hendricks, 3777

Fiber Optics Wavelength Division Multiplexing

Fiber optics information networks can be expandable for the growth of the space station by the use of the multiplicity of wavelengths available in wavelength division multiplexing (WDM). In addition, WDM offers a multitude of other features, including simultaneous multiple path/direction of communications, fault tolerance, and self repairing. As part of its electronics and data systems research program, NASA Langley has been developing WDM components and demonstrating WDM fiber optic networks. WDM multiplexers using a grating type wavelength dispersion have been demonstrated with resolution between channels of 5.5 nm, less than −25 dB crosstalk, and less than -5 dB insertion loss.

An eight-channel-star bus information network has been demonstrated utilizing both AlGaAs and InGaAsP semiconductor laser wavelengths. A system with four AlGaAs channels (0.8, 0.81, 0.82 and 0.83 μm and four InGaAsP channels (1.25, 1.3, 1.35 and 1.5 μm) was demonstrated at 20 megabits with a bit error rate of less than 10^{-10}. A 24-node network consisting of nine four-by-four transmission stars in a fully connected passive mesh network has been partially demonstrated for worst-case conditions at a data rate of 500 megabits and with a worst-case loss budget of less than 27 dB. Near-term demultiplexer research is directed at improving resolution (increased number of channels), reducing insertion loss, and improving cross talk isolation. Distributed-feedback (DFB) type lasers will be integrated into a single-mode optical-fiber mesh network for data systems larger than 500 megabits.

H. D. Hendricks, 3777



Eight-channel wavelength division multiplexing star bus.

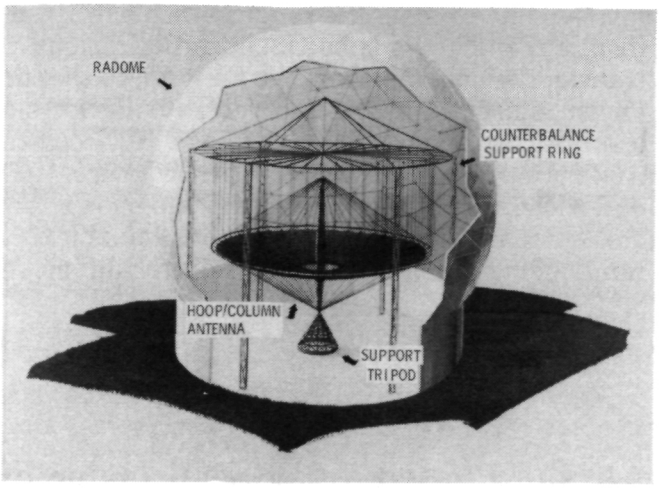
15-Meter Hoop-Column Antenna Tests

The first set of antenna kinematic deployment tests has been successfully completed at the large radome facility of the Harris Corp., Melbourne, Florida. This begins a series of structural, dynamic, and RF tests planned as part of Langley's Large Space Antenna (LSA) program using the hoop-column antenna design.

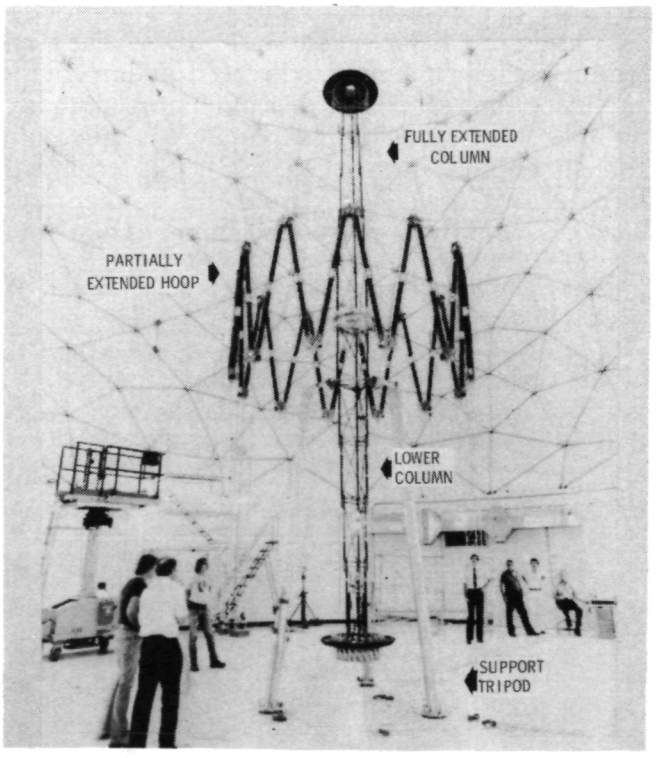
The purpose of the initial tests was to demonstrate precision deployment repeatability of the primary structural members (hoop and column) before the RF reflective mesh surface is added to the space frame. Similar tests are then planned using metric camera stereo photography and theodolite measurements to characterize the antenna surface figure. The fragile structure requires an elaborate counterbalance mechanism to allow deployment in a 1 "g" environment.

Electromagnetic tests will be conducted to determine antenna RF performance characteristics in the summer of 1985, with subsequent modal surveys planned in the Langley 16-meter thermal-vacuum facility.

T. G. Campbell, 3631



Kinematic deployment test using a counterbalanced zero-g simulator.



Partially deployed 15-m hoop-column antenna (without reflector mesh surface).

Space Directorate

The Space Directorate conducts research in atmospheric and Earth sciences, identifies and develops technology for advanced transportation systems, conducts research in energy conversion techniques for space applications, and provides the focal point for development activities for both large antenna systems technology and Space Station activities.

The Space Directorate is a leader in the area of atmospheric sciences. Its scientists are involved in seeking a more detailed understanding of the origins, distributions, chemistry, and transport mechanisms governing the regional and global distributions of tropospheric and stratospheric gases and aerosols, and in the study of the Earth radiation budget and its effect on climate processes. The research seeks to better understand both natural and anthropogenic processes. The research conducted in the Atmospheric Sciences Division covers a wide spectrum of activities, including the development of theoretical and empirical models; collection of experimental data from in situ and remote sensing instruments designed, developed, and fabricated at NASA Langley; organization of extended field experiments; and development of data management systems for the efficient processing and interpretation of data derived from airborne and satellite instruments.

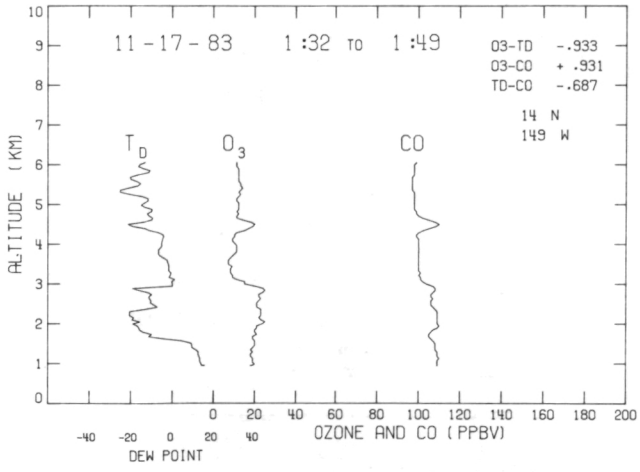
The Space Systems Division conducts research and systems analysis of advanced transportation systems, large antenna systems, and space station concepts as well as basic research into energy conversion techniques for potential space application. The Space Systems Division is a leader in the development of highly interactive and user-friendly computer-aided design (CAD) tools that enable the rapid evaluation of system concepts and the identification of high-leverage technology necessary for the development of space transportation systems, large antenna systems, and the orbiting Space Station. The evaluation of advanced space transportation systems covers a wide range of capability, including Earth-to-orbit vehicles, orbit-on-demand launches, service vehicles, and orbital transfer vehicles.

Involvement in Space Shuttle flight data and trajectory analysis is an ongoing activity that seeks improvements to increase the efficiency and cost effectiveness of the Space Shuttle. Development of orbiter experiments that utilize the Shuttle as a reentry research vehicle to study radiative heat transfer and flow field chemical kinetics and to determine the aerothermodynamic and aerodynamic characteristics of the Shuttle has been a key activity and one which will lead to the development of advanced vehicle systems.

Measurements of Trace Gases in the Remote Troposphere: Gaining Insight Into the Tropospheric Ozone Budget

As part of NASA's Global Tropospheric Experiment, measurements have been taken in remote regions of the world that will provide further insight into the global budget of tropospheric ozone and how anthropogenic activity may contribute to the observed increase in its concentration. Airplane flights during October and November 1983 produced the first concurrent high-resolution vertical profiles of dew point temperature (T_D), ozone (O_3), and carbon monoxide (CO). The CO instrument used in these flights employs a laser system that was developed at Langley; it provides a time resolution that has not been achieved by any other CO instrument in the world. The T_D and O_3 measurements shown were made by Langley researchers using conventional instrumentation.

Without the aid of the CO profile, a conclusion could be drawn upon inspection of the T_D and O_3 profiles that the origin of the O_3 band at 14°N, 149°W (near Hawaii) was from the stratosphere since higher O_3 concentrations are found concurrently with drier air (lower dew points). However,



Vertical profiles of carbon monoxide, dew point, and ozone observed on November 17, 1983.

because the vertical variability of CO and O_3 is so much in phase, it is clear that the ozone observed in these measurements did not come from the stratosphere, where CO concentrations are very low. Since CO is a tracer of air pollution, it is likely that some of the higher concentrations of O_3 seen in this profile are a result of man-made emissions that have been transported from higher and drier latitudes.

Understanding the origin of tropospheric ozone has important climatic implications. A recent report by the World Meteorological Organization notes that the observed increase in tropospheric ozone since 1960 may have two to three times more impact on the warming of the atmosphere than the observed increase in carbon dioxide since 1960.

Jack Fishman, 2294

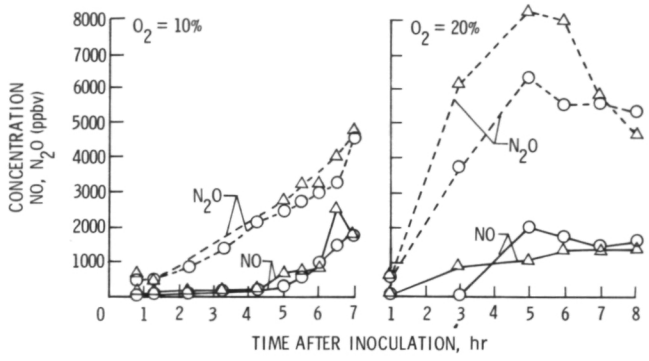
Biospheric-Atmospheric Coupling

Biochemical activity by microorganisms in soil is an important source of many atmospheric trace gases. Biochemical production is the overwhelming source of nitrous oxide (N_2O) and has been suggested as a possible source of nitric oxide (NO). N_2O, which is chemically inert in the troposphere, leads to the chemical destruction of ozone (O_3) in the stratosphere. Stratospheric O_3 absorbs solar ultraviolet radiation (200 to 300 nm) and shields the Earth's surface from this biologically lethal radiation. N_2O is also a greenhouse gas, and hence impacts the Earth's climate. Chemically active NO leads to the photochemical production of O_3 near the ground, where it is an irritant and pollutant.

Laboratory experiments and field measurements are being conducted to quantify the biogenic production of N_2O and NO and to assess how their production rates may be perturbed by anthropogenic activities. Experiments and measurements at Langley have shown clearly that NO is indeed produced by soil microorganisms and have assessed the production of these gases (NO, N_2O) as a function of various soil parameters, including moisture, temperature, acidity, nutrient level, and dissolved oxygen (O_2) level. The rates of production of N_2O and NO in soil will be used as input parameters in our photochemical models of the atmosphere to better understand the chemical coupling between the biosphere and the atmosphere.

The figure shows the simultaneous production of NO and N_2O by the common soil denitrifying bacterium *Alcaligenes faecalis* as a function of the level of dissolved O_2 in soil. Note that production of both N_2O and NO increased with the level of dissolved oxygen in the soil.

Joel S. Levine, 2187



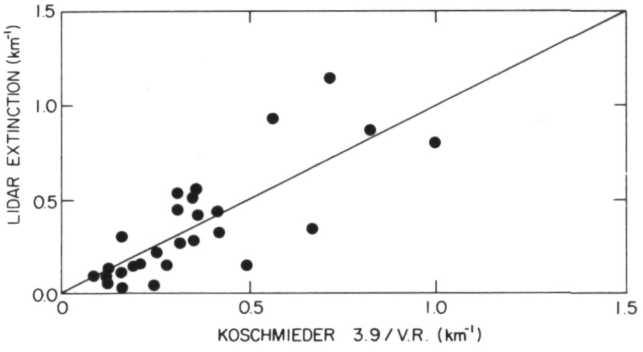
Simultaneous biogenic production of N_2O and NO by common soil bacterium as a function of the level of dissolved O_2 in soil. (The circles and triangles represent data from duplicate experiments.)

Aerosol Optical Extinction in Atmospheric Mixed Layers by Airborne Lidar

A horizontal averaging technique has been applied to airborne lidar signals from atmospheric mixed layers to derive the vertical profile of aerosol optical extinction without a priori assumptions. Mixed-layer aerosols are often responsible for severe visibility reduction near the surface and are strong indicators of manmade pollution events. The averaging technique relies on the inhomogeneous and nearly random spatial distribution of aerosol eddies to obtain an average lidar signal profile which is representative of the mean profiles for aerosol optical backscatter and extinction. Mixed-layer aerosols are distributed in turbulent eddies with dominant horizontal dimensions from 10^2 to 10^3 m and inter-eddy spacing on the order of 10^3 m. Airborne lidar obtains a horizontal sample over several eddies in a few minutes to maintain sample stationarity and can derive aerosol extinction profiles over wide geographic regions.

This horizontal averaging technique has been applied to airborne lidar data obtained during the EPA Persistent Elevated Pollution Episode/Northeast Regional Oxidant Study (PEPE/NEROS) 1980 Summer Field Experiment. As shown in the figure, the lidar-derived optical extinction profiles have been compared to surface observations of atmospheric visibility and in situ nephelometer profiles of aerosol total scattering cross sections. Surface observations of visual range (V.R.) are related to optical extinction β by the Koschmieder relation $\beta = 3.9/\text{V.R.}$ The comparison points scatter about a line of perfect correlation, where the in situ data variance appears to be directly related to the inhomogeneous vertical distribution of aerosol material. The lidar-derived profiles of aerosol extinction show significant increases in aerosol scattering at higher altitudes where relative humidities exceed 60 percent. Aerosol particles grow through the adsorption of water vapor at high but subsaturated relative humidities, the humidity growth point being related primarily to aerosol composition. The PEPE/NEROS data set shows several aerosol growth points distributed from 60 to 80 percent relative humidity, with growth points grouped by air mass type.

Scott T. Shipley, 2576



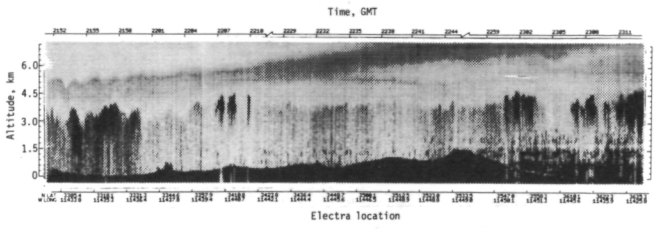
Comparison of lidar measurements with surface observation of atmospheric optical extinction.

Airborne Lidar Observations of a Tropopause Fold Event

The NASA Multipurpose Ultraviolet Differential Absorption Lidar (UV-DIAL) system was flown as part of the NASA Global Tropospheric Experiment (GTE) investigation of tropopause folding during April 1984. The UV-DIAL system was operated on board the Wallops Electra aircraft in a nadir-directed mode to obtain measurements of aerosol and ozone as a function of height. Aerosol backscattering was observed at wavelengths from 0.3 to 1.06 μm with 15 m vertical and 20 m horizontal resolution. Ozone concentrations were derived by the differential absorption technique with 100 m vertical and 2 km horizontal resolution. Primary experiment goals included the demonstration of airborne lidar techniques for the effective monitoring of tropopause fold processes.

A horizontal cross section of aerosol backscattering at 1.06 μm is shown for an 80-min flight pass covering approximately 360 km from Yuma, Arizona, to Las Vegas, Nevada, on April 20, 1984. A tropopause fold is seen in progress above a 3.0-km-high mixed layer, where high aerosol concentrations (darker shading) can be seen descending from 7.0 to 4.5 km altitude in a 1.0-km-thick layer. These stratospheric aerosols are remnants of the El Chichon eruption, and they display characteristically enhanced backscattering at 1.06 μm when compared to that at visible wavelengths. DIAL measurements of ozone show concentrations in excess of 240 ppbv in this stratospheric layer. The lidar observations are corroborated by in situ measurements of ozone and aerosol mass loading obtained as the Electra aircraft penetrated the fold at 8.0 km MSL. The results show that significant amounts of stratospheric tracers are transported well into the troposphere by tropopause folding processes. High ozone events will then occur as such stratospheric air layers fumigate the surface. Tropopause folds occur over large geographical scales, and they are readily observed by airborne lidar instrumentation.

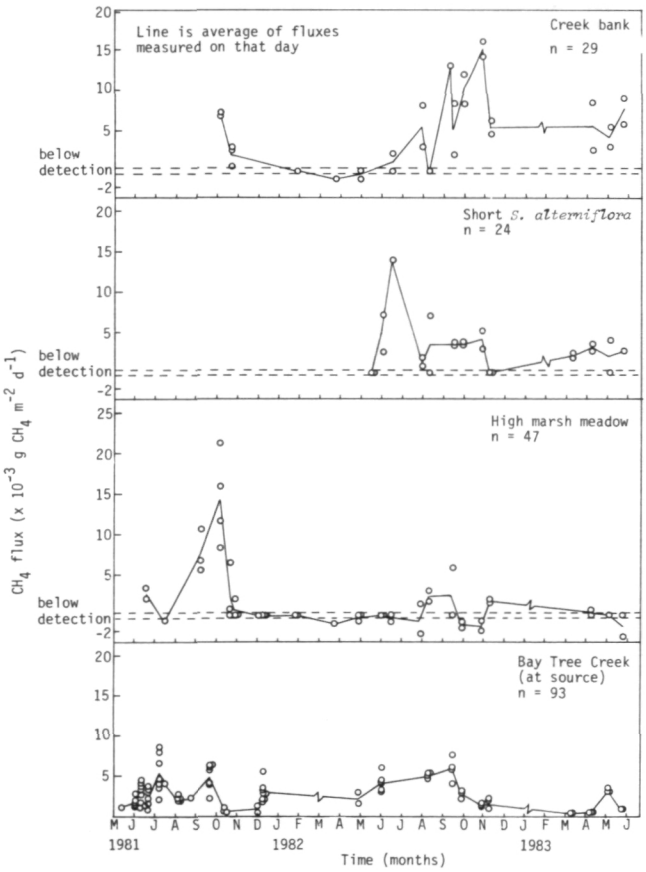
Edward V. Browell, 2576



Airborne DIAL aerosol measurement of tropopause fold event on April 20, 1984.

Methane Flux From Coastal Salt Marshes

Methane (CH_4) is an important trace gas in the Earth's atmosphere, where it is believed to have potentially critical roles in both atmospheric chemistry and radiative transfer processes. During the last several years, evidence has accumulated indicating that the concentration of CH_4 in the global atmosphere is increasing at a significant rate of 1 to 2 percent a year. Because the sources and sinks of CH_4 are poorly quantified, the reason for this increase is unclear. Research suggests that biological rather than anthropogenic sources contribute the majority of the atmospheric burden of CH_4. Wetland environments such as swamps, marshes, rice paddies, and bogs are thought to produce a considerable part of this biogenic CH_4, although the magnitude and variability of emission rates from these types of environments are only poorly known. Our research has concentrated on increasing our understanding, as well as the overall data base, of natural emissions of CH_4 from wetlands.



Methane emission rates over a 2-year period from Bay Tree Marsh and Creek. Multiple flux estimates from the creek for a single date reflect changing wind velocities and/or changing methane concentrations in the water.

The seasonal flux of methane to the atmosphere was examined from salt marsh soils in three different vegetation zones within a single marsh near Yorktown, Virginia. Maximum flux rates occurred during the summer and fall months, and emission rates ranged from -2.4 to 21.3×10^{-3} g $CH_4/m^2/d$. Estimates of annual methane losses to the atmosphere were 0.43 g CH_4/m^2 for a salt meadow, 1.3 g CH_4/m^2 for short *Spartina alterniflora*, and 1.2 g CH_4/m^2 for tall creek bank *S. alterniflora*. Flux measurements made in a variety of other coastal salt marshes along the east coast of the U.S. from Delaware to Florida were similar in magnitude to those measured at the Virginia site. Although variability was high, flux rates across the air-soil interface were found to correlate with both the measured dissolved CH_4 gradient in soil pore waters and the amount of CH_4 present in the soil.

In addition to diffusion and loss across the air-soil interface, methane can be lost from the marsh system to the atmosphere through the lateral movement of pore waters supersaturated with methane into tidal creeks, with subsequent degassing due to turbulence and diffusion. Estimates of the magnitude of CH_4 input to the atmosphere by this transport mechanism indicate that it may be on the same order of magnitude as diffusional losses across the air-soil interface. Extrapolations of the contribution that salt marshes of this type make to atmospheric methane indicate that salt marshes are only of minor global importance.

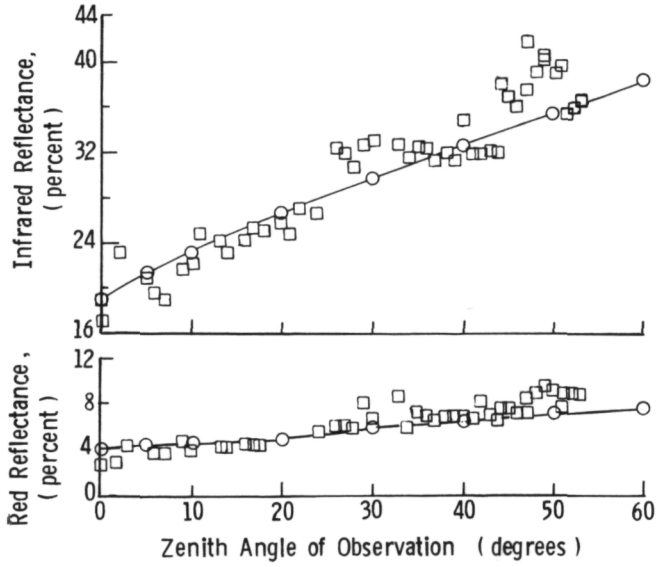
R. C. Harriss, 3237

Use of Radiative Transfer Modeling to Correct for Angle-of-View Effects on Remote Sensing of Vegetation

Assessment of global biosphere/atmosphere geochemical and physical interactions requires efficient remote sensing of vegetative cover over large areas. The NOAA 6 and NOAA 7 Advanced Very High Resolution Radiometers (AVHRRs) have emerged as important instruments for global inventories because of their wide surface swath width (3000 km), high temporal frequency of coverage, and low data volume compared with the

Landsat Earth resources sensors (Multispectral Scanner and Thematic Mapper). Quantitative spectral analysis of AVHRR data is complicated, however, by the large angular field of view (56° either side of the nadir track) of these instruments. Off-nadir viewing can have severe impacts on the detected radiance returned from a vegetated area due to anisotropic reflectance from the canopy/soil composite surface. This study evaluated an existing computer model of radiative transfer in a canopy as a means to assess variability in measured canopy radiance resulting from non-nadir observation.

Comparison was made between model calculations of spectral canopy reflectance (reflectance = reflected radiance/incident radiance) and field measurements of marsh grass reflectance made using a portable radiometer. Comparisons were performed for angles of view ranging from nadir to 60° off nadir under a variety of Sun angle conditions. The model was effective in simulating both the sense and the magnitude of measured reflectance changes resulting from varying the angle of observation. However, the model did not reproduce the observed dependence of reflectance on solar elevation at the time of measurement. This discrepancy occurred as a constant bias and was corrected by normalizing model predictions using a single measured reflectance value obtained at the appropriate Sun angle. This procedure resulted in high correlation of simulations with measured reflectance and was extended to assess view angle effects on data acquired by an aircraft multispectral scanner. The figure shows the excellent agreement between aerial measurements and simulated response of infrared (top) and red (bottom) canopy reflectance to variable angle of view. Use of radiative transfer modeling can be applied to quantitative correction of measured reflectance values obtained from varying angles of view and to optimization of the choice of sensor/target/Sun geometries for vegetation analysis.

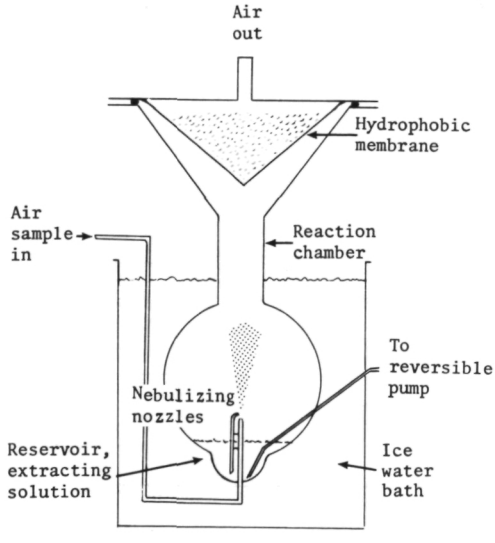


The effect of angle of view (measured from zenith) on vegetation reflectance measured by an aerial scanner (□) and simulated by radiative transfer model (O—O). Data for infrared (top) and red (bottom) spectral bands are shown.

D. S. Bartlett, 4345

Nebulization Reflux Concentrator

A new technique for the extraction and enrichment of water-soluble atmospheric trace gases has been developed at Langley. A representation of the nebulization reflux concentrator is illustrated. The gas concentrator utilizes a pair of small nebulizing nozzles to mix an incoming air sample with an aqueous extracting solution to form a mist. The mist provides an excellent interfacial surface area for phase transfer of soluble gases. The mist sprays upward through the reaction chamber until it impinges upon a hydrophobic membrane that blocks the passage of droplets but offers little resistance to the exiting gas flow. The droplets containing the scrubbed gases coalesce on the membrane and drip back into the extracting solution reservoir for further refluxing.



Schematic representation of nebulization reflux concentrator.

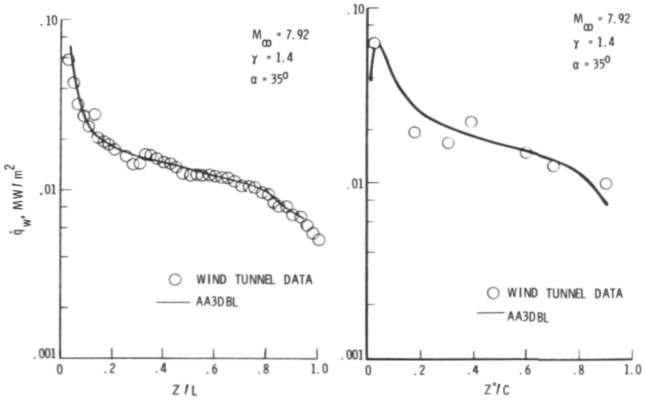
After a suitable concentration period, the extracting solution is withdrawn for chemical analysis. The nebulization reflux concentrator has been tested with calibrated mixtures of gaseous ammonia, hydrogen chloride, and sulfur dioxide, and was found to be more than a factor of 10 more efficient than conventional bubbler/impinger gas extraction techniques.

Wesley R. Cofer III, 4372

Calculation of Heating on Shuttle Lower Surface

An improved method (AA3DBL) has been developed at LaRC for calculating heating rates on three-dimensional configurations such as the Space Shuttle orbiter. It is based on the axisymmetric analog for three-dimensional boundary layers which reduces the three-dimensional boundary layer equations along a streamline to a much simpler form. This method has been coupled with HALIS (a three-dimensional inviscid flow field code) to provide boundary layer edge properties for the heating calculations. It has been used to calculate heating over the Shuttle orbiter lower surface at a Mach number of 7.92 and an angle of attack of 35°. These results are summarized in the figures.

The left figure shows a comparison of calculated results with AEDC wind tunnel data along the windward symmetry plane (Z/L) of the orbiter. The agreement with experimental data is excellent. The right figure shows a similar comparison over the wing at a semispan location of 50 percent ($2Y/B = 0.5$). These results are presented as a function of chord length (Z^*/C). Although there is more scatter in the experimental data for this case, the agreement is still very good. To the author's knowledge this is the only "near exact" method currently available that can be used to calculate heating on the Shuttle orbiter wing.

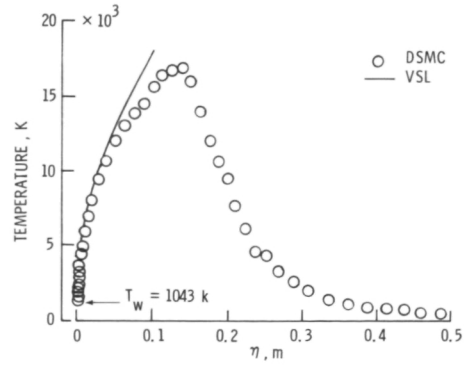


Heating rates along windward symmetry plane and wing of Shuttle orbiter.

Harris Hamilton, 3271

Direct Simulation of Transitional Flow for Hypersonic Reentry Conditions

The Direct Simulation Monte Carlo (DSMC) method has been used to calculate the flow field about the nose region of the Shuttle orbiter during reentry for an altitude range of 90 to 150 km (most of the transitional region). The DSMC calculations account for translational, rotational, vibrational, and chemical nonequilibrium effects. At the lowest altitude considered (92 km), the calculated heating is in agreement with the STS-2 flight data and the results calculated with a viscous shock layer (VSL) method (a continuum method). As the altitude increases, the continuum results for heating and drag depart rapidly from the DSMC results and flight data. Futhermore, the extent and magnitude of local thermodynamic nonequilibrium effects increase with increasing altitude. Chemical reactions within the flow field are evident up to an altitude of about 105 km, whereas at higher altitudes the gas composition is basically that of the free stream.



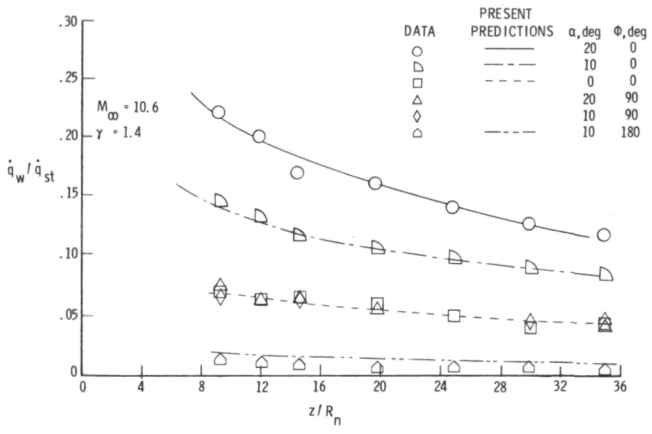
Comparison of stagnation line temperature profile for direct simulation Monte Carlo method and viscous shock layer method.

Even though the drag and heating results are in good agreement at 92 km, there are substantial differences in the flow field structures. The temperature for the stagnation streamline, as predicted by the DSMC and continuum methods, is shown in the figure. Within the shock layer ($\eta = 0.1$), the predicted temperatures are in close agreement, yet the DSMC method is required to provide a complete description of both the shock wave and shock layer formation. These results point out some of the limitations of continuum methods. A much thicker layer of high-temperature gases could have significant impact on calculated heating for entries where radiative heating is important.

James N. Moss, 3770

Engineering Flow Field Method With Angle-of-Attack Applications

An approximate flow field code has been developed at LaRC which adequately predicts the heat transfer distribution at hypersonic entry conditions over a range of analytic bodies and spherically blunted cones at 0° angle of attack and over sphere cones at incidence. Reliable approximate codes are of practical utility for parametric studies since the detailed codes typically require large computer run times and storage. The flow field calculations are based on either a constant gamma or an equilibrium-air model and may employ constant or variable-entropy flow assumptions to compute the local flow properties. For angle-of-attack applications, an approximate method that accounts for the impact of streamline spreading on calculated sphere-cone windward or leeward heating rates is included. The circumferential heat transfer is predicted with an empirical procedure which uses the predicted windward and leeward heating levels. Pressure distributions are computed along any meridian ray provided cross-flow separation has not occurred.



Comparision of predicted and measured heating rates.

In the figure, the predicted and measured heat transfer data to a 15° blunt cone are presented for a freestream Mach number of 10.6 and angles of attack α of 0°, 10°, and 20°. For 0° angle of attack, or for the windward ray ($\phi = 0$) at angle of attack, the method compares well with the data. The 90° ray heating data are shown to also be in good agreement with the 0° angle-of-attack experimental and predicted results. Several other experimental investigations have noted similar results.

E. Vincent Zoby, 2707

Experimental Investigation of A Transatmospheric Vehicle at Mach 20

A transatmospheric vehicle (TAV) is being proposed by the U.S. Air Force for use in the beginning of the next century. Mission requirements include the ability to re-enter from low Earth orbit to target and landing areas. Therefore, the TAV must be capable of operating across the total speed regime.

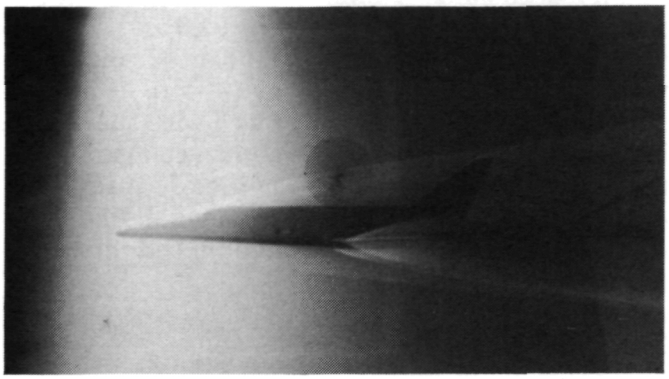
A model of one of the TAV concepts has been tested at $M = 20.3$ in the Langley Hypersonic Helium Tunnel facility to obtain hypersonic static longitudinal and lateral-directional characteristics. Data were obtained at 0° to 25° angle of attack and −3° to 0° angle of sideslip over a unit Reynolds number range of 2.5×10^6 to 6.8×10^6 per foot. Aerodynamic control effectiveness was determined by varying elevator, elevon, rudder, and combinations of elevator and elevon deflections.

Results showed that the maximum lift-drag ratio $(L/D)_{max}$ occurred at $\alpha = 12°$ for all control settings tested. With the center of gravity located at 64 percent of fuselage length, large positive control deflections were required for longitudinal trim at $(L/D)_{max}$, which would result

in high heating problems. This problem could be alleviated by moving the c.g. forward 1 percent of the body length.

This concept was shown to be directionally unstable over the angle-of-attack range with positive dihedral effect. The rudder had negligible effect on the lateral-directional stability of the vehicle for the entire angle-of-attack range tested. This vehicle will continue to be tested at other flight conditions in other Langley facilities.

Ronald S. McCandless, 2483



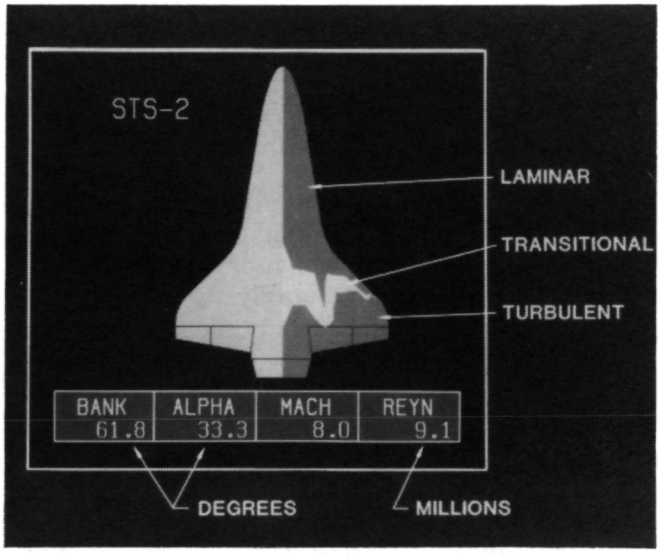
Electron beam flow visualization of TAV in Hypersonic Helium Tunnel facility.

Orbiter Boundary Layer Transition Visualization

Flights of the extensively instrumented Shuttle orbiter Columbia provided an unprecedented opportunity for the investigation of hypersonic boundary layer transition on a lifting entry vehicle. The onset and completion of the boundary layer transition process were indicated by "instantaneous" shifts in the value of the time rate of change of surface temperature measured at approximately 90 locations on the vehicle's lower surface. Using this information, the boundary layer state was characterized at any point in time, locally at each of the temperature measurement locations, as being either laminar, transitional, or turbulent. By "contour plotting" on this information, a "map" of the boundary layer transition front location was created for any selected point in time.

Computer graphic techniques were applied to the processing of the orbiter entry flight data in order to create a visual presentation of the in-flight boundary layer transition process. The location of the boundary layer transition front on the orbiter planform was automatically mapped and color shaded for each discrete time at which flight data were available. These images were also automatically annotated with trajectory information which describes the vehicle's flight environment at that point in time. These time-discrete images were then used to create "real-time" motion pictures. The results are real-time, animated, visual presentations of the movement of the boundary layer transition front over the orbiter lower surface for each of the first five flights of the orbiter Columbia. The computer graphic processing approach has allowed researchers to "see" the boundary layer transition process as it occurred in flight and relate the instantaneous transition location to pertinent freestream flow parameters.

David A. Throckmorton, 3984



Shuttle orbiter boundary layer transition "map".

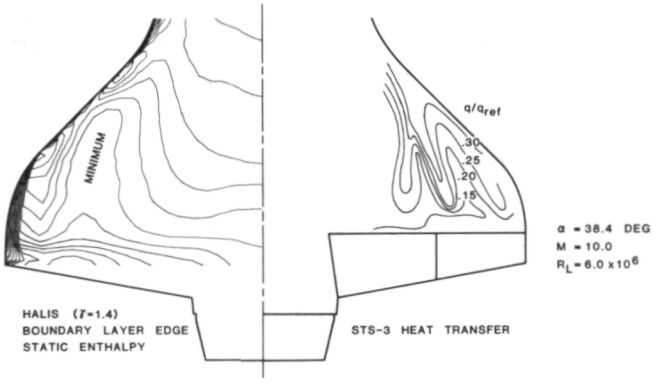
Orbiter Shock-Interaction-Induced Heat Transfer

Analysis of flight-derived heat transfer data from Space Shuttle orbiter missions STS-2, -3, and -5 have revealed clear evidence of an interference heat transfer region on the orbiter wing lower surface resulting from the downstream effects of the interaction of the vehicle's bow and wing shock waves. This interference heat transfer region develops progressively as the entry trajectory carries the orbiter deeper into the atmosphere and the flow field is transformed from that of a fully

viscous shock layer flow to one with distinct inviscid and boundary layer regions. The flight-observed heat transfer distributions have been compared with state-of-the-art computational flow field predictions of the boundary layer edge static enthalpy. The computational results were generated by a three-dimensional inviscid flow field procedure developed at Langley known as HALIS.

The flow field solution results indicate the presence of a distinct "minimum" in the spanwise distribution of boundary layer edge static enthalpy downstream of the bow/wing shock interaction region. The spatial location of this "minimum" correlates well with the location of a "maximum" streak in the flight-measured surface heat transfer. A "minimum" in static enthalpy at the boundary layer edge would be expected to relate to increased boundary layer edge velocity, increased shear in the boundary layer, and attendant increased surface heat transfer. Just such a relationship is observed in the flight data.

David A. Throckmorton, 3984

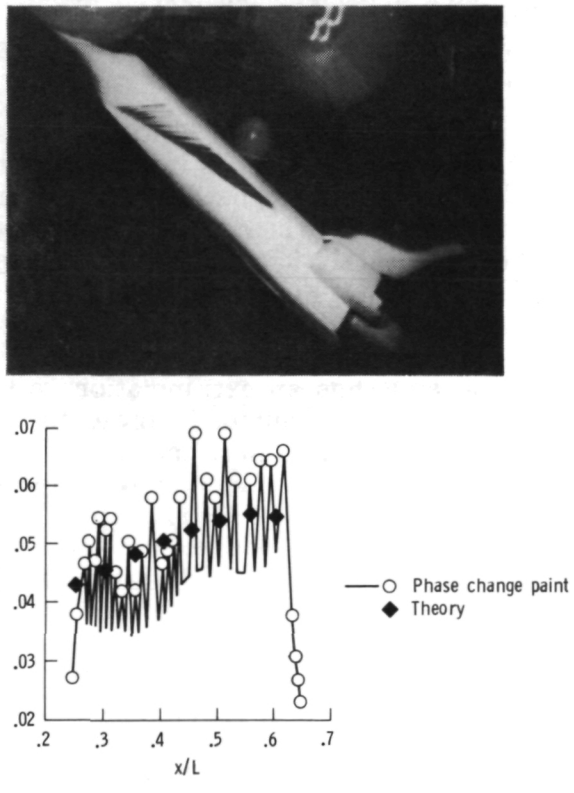


Comparison of computational and flight data.

Space Shuttle Orbiter Side Fuselage Heating Study

Flow reattachment on the Space Shuttle orbiter side fuselage during entry produces some of the highest heating rates observed on the orbiter's leeward surface. Since current three-dimensional flow field codes cannot accurately treat leeside conditions, an empirical technique was developed at LaRC to predict side fuselage reattachment heating using oil flow and phase change paint data obtained in Langley's 31-Inch Mach 10 Tunnel and in the 20-Inch Mach 6 Tunnel. This method was derived from an empirical leeward centerline heating technique previously developed for the Shuttle orbiter. Both methods use the same form of turbulent heating equation, with appropriate modifications for differences in geometry and the source of local flow, and each is incorporated with a correlation between changes in local surface oil flow directions and axial variations in heating distributions which was developed during the course of this work. The side fuselage reattachment heating predictions provided by this method are generally within 10 percent of wind tunnel measurements and a preliminary comparison with a selected STS-3 trajectory point indicates similar agreement with flight data.

Heating due to embedded vorticity in the form of narrow, evenly spaced streaks of locally higher heating was observed at the high Reynolds number, high-angle-of-attack wind tunnel test conditions. An example of a streak heating pattern and its effect on the side fuselage reattachment line heating distribution is shown in the figure.



Streak heating pattern in phase change paint. Side fuselage reattachment line heating distribution compared with empirical predictions for $M_\infty = 6$, $\alpha = 40°$, *and* $Re_\infty = 7.3 \times 10^6$.

The photograph was taken during the first seconds of a wind tunnel test in order to emphasize the streak heating pattern. Individual heating peaks along the side fuselage reattachment line caused by each streak are shown in the graph. Also included are empirical heating predictions which indicate the level that side fuselage reattachment heating would have if the streaks were not present. For those test conditions that produce numerous streaks, as in the photograph, the vorticity-free predictions of the empirical heating technique represent an average of the resulting fluctuations in reattachment line heating rate. STS-3 entry heating data also reveal the presence of streak heating in flight, with associated temperatures that are raised as much as 300°F above local undisturbed levels.

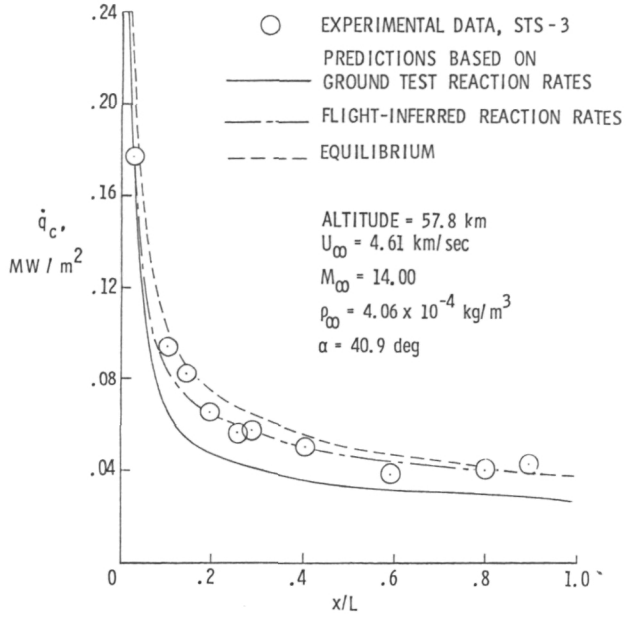
Vernon T. Helms III, 3984

Temperature-Dependent Reaction Rate Expression for Oxygen Recombination On Shuttle Heatshield Tiles

Shuttle heating data for altitudes above 50 km where the shock layer is in nonequilibrium have shown a trend of somewhat higher heating than the predictions. These predictions have been based on wall catalytic recombination rates obtained in an arc jet. For oxygen, the arc jet data were obtained at temperatures considerably higher than the wall temperatures for the orbiter centerline, and thus an extrapolation to lower temperatures was required. In order to assess whether the flight data were consistent with an alternate set of oxygen reaction rates, a few sample flight conditions were used to infer a best-fit variation of oxygen reaction rate with wall temperature. This new inferred relation was then used throughout the nonequilibrium range for flights STS-2 and STS-3.

The figure illustrates the comparison of heating distribution along the lower fuselage centerline for the two oxygen reaction rate assumptions. The solid curve, which used oxygen rates extrapolated from the arc jet data, significantly underpredicts the flight data, whereas the flight-derived rates fit quite well. The significance of this work is that the flight data are shown to be consistent with an alternate expression for the oxygen wall recombination rate, and thus additional ground tests on the wall reaction rates are needed.

E. Vincent Zoby, 2707



Comparison of predicted and experimental heating rates for different assumed surface conditions.

Box Truss Antenna Structure

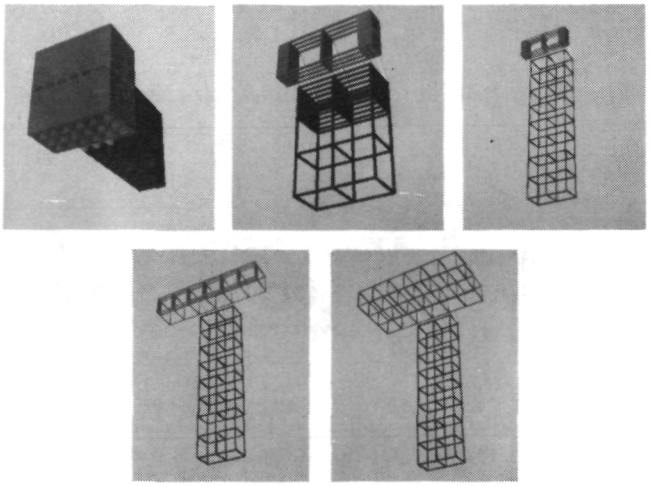
Several recent systems studies of advanced antenna missions have employed the box truss structural concept as the core or primary structure for the spacecraft. These missions have ranged from various communication needs to Earth observational radiometers and have required antenna reflectors from 50 to 200 m in diameter. The box truss concept is a sequentially deployable structure of graphite composite material with excellent operational characteristics and high packaging efficiency ratios. The figure shows an antenna concept in various stages of deployment.

Comparative analyses have been conducted to establish the performance of this concept relative to other deployable structures. Although some of these comparisons have been necessarily qualitative, quantitative analyses have established significant dynamic performance, packaging, and deployment advantages. The inherent

strength and stiffness significantly reduce the attitude and vibrational control requirements while expanding the range of applicability of the concept. The efficient packaging and reliability deployment mode reduce the technological risk while enhancing the operational performance.

The deployable box truss design has progressed to the stage where the technology is now near that of other deployable concepts. Experimental laboratory hardware has provided test data to corroborate design and analysis results. A scaled flight experiment has been designed to provide comprehensive flight validation of many of the technical analysis and ground test results. As a direct result of this research, deployable box truss antenna technology and design concepts can compete for many large space antenna applications.

U. M. Lovelace, 2486

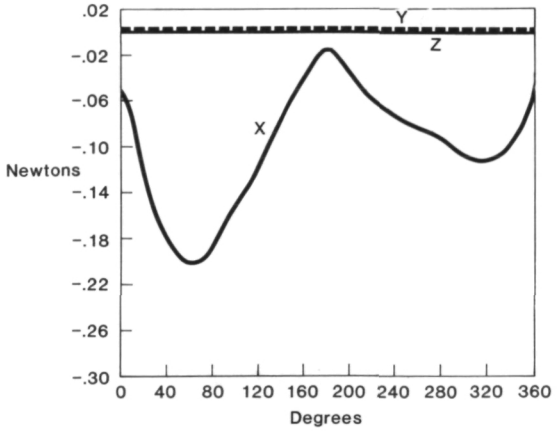


Box truss deployment sequence.

An Analytical Method For Assessment of Space Station Rigid Body Control Dynamics With Articulating Appendages

During the space station conceptual configuration study phase, four configurations were proposed which consisted of large (20,000 ft^2) solar array areas and large heat dissipating radiator areas (3000 ft^2) which rotated with respect to the station's core body relative to the position of the sun. (These concepts were known as the axial-radial, planar, race track, and power tower.) Because of the relatively large areas associated with these rotating appendages, changes in solar array panel or radiator orientation with respect to the orbital velocity vector and/or the sunline significantly alter the resulting aerodynamic and solar radiation pressure-induced forces and torques acting on the station. Likewise, appendage articulation gives rise to changing mass distribution properties which must be accounted for. These changes in turn affect orbit maintenance as well as attitude control requirements; hence the need to properly model space station articulation characteristics to obtain accurate attitude control system resource sizing requirements.

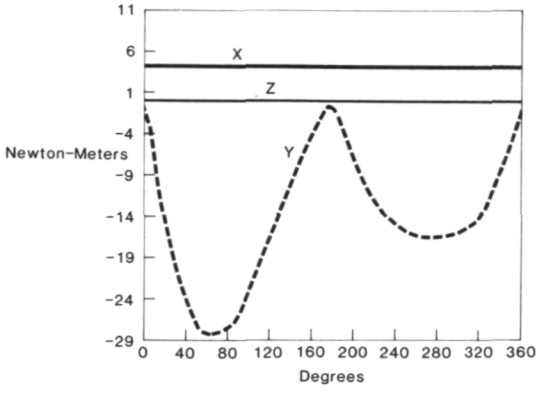
A new analytical methodology has been developed that treats the articulated appendages as free-rotating bodies subject to joint constraints associated with connecting them to the core body of the space station proper. This is accomplished by modifying the controller torques obtained from the attitude equations of motion to account for both the sum of all the external torques acting on the space station and the sum of all torques resulting from the forces created by the articulation of each individual appendage. Computer code implementation of this technique determines the constant moment-of-inertia matrix for each articulating appendage in its own unique and separate coordinate system. The forces and torques acting through each articulating appendage are also determined in the articulating part coordinate system, rotated to the space station core proper coordinates and summed. Accurate forces, torque, and momentum time histories can now be obtained for space station solar array and thermal radiator articulation characteristics, which can include sunline tracking and cable unwrap rotations.



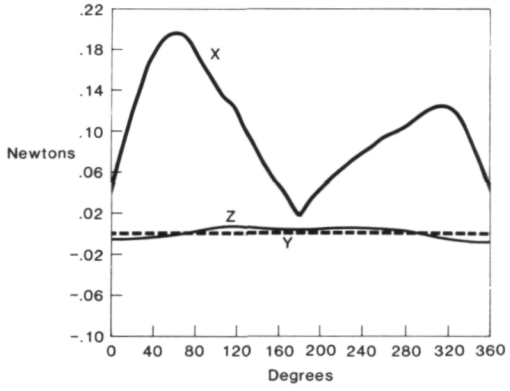
Environmental forces vs true anomaly.

These can be modeled as shown in the figures for the space station reference configuration illustrated.

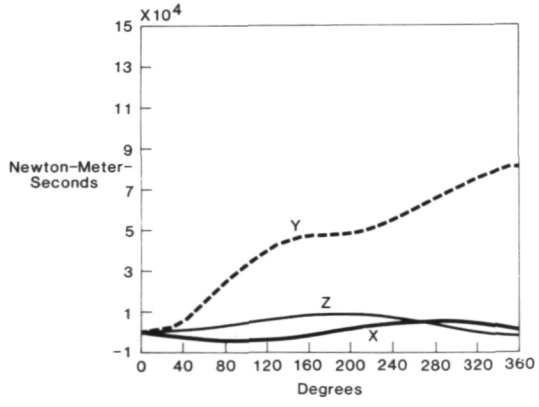
L. J. DeRyder, 2486



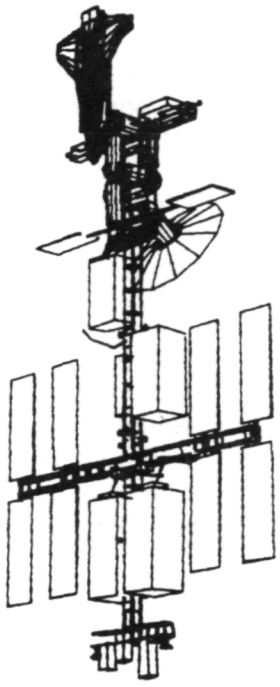
Control torques vs true anomaly.



Control forces vs true anomaly.



Angular momentum requirements vs true anomaly.



Space station reference configuration.

Atmospheric Model Implementation for Space Station Orbital Control and Decay Assessments

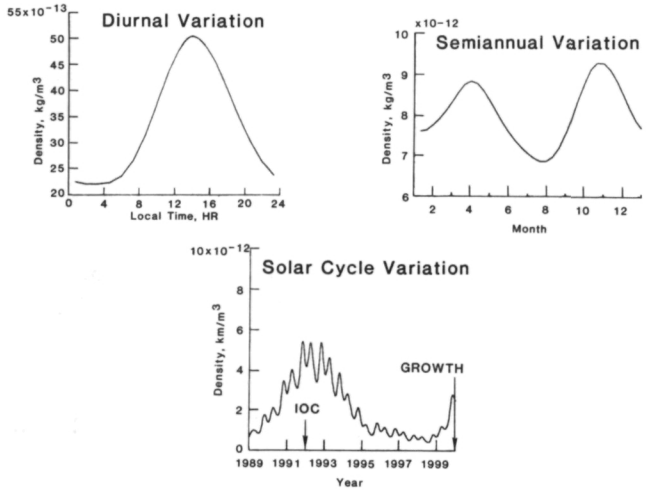
Current space station concepts are large-area space systems with solar arrays which are envisioned to grow up to an acre in area. Thus, interactions with the upper atmosphere at orbital altitudes (i.e., drag and associated torques) must be taken into account in controllability and orbit maintenance studies. To account for this atmospheric effect, the Jacchia 1970 (J70) atmospheric density model was implemented for use in in-house computer-aided analytical capabilities and studies. This model of the neutral upper atmosphere includes variations in density with altitude, with the 11-year solar cycle, and with geomagnetic activity, as well as the semiannual, seasonal-latitudinal, and diurnal variations.

For space station attitude control and stabilization studies, the J70 model was incorporated into the IDEAS Rigid Body Control and Dynamics (RBCD) computer program which analyzes spacecraft dynamics throughout the orbit. With the implementation of the J70 model, space station control system analysis can now in-

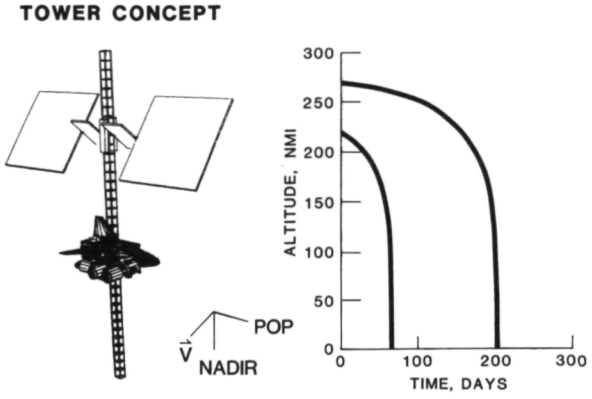
clude the effect of the diurnal variation in atmospheric density, which can vary by a factor of 2 within a single orbit, and which significantly affects the single-orbit torque time history and momentum buildup profiles. In addition, a dual-density modeling capability has been included in the computer program which permits atmospheric density to be calculated separately for attitude control calculations (for which extreme density values are considered) and orbit maintenance calculations (for which average density values are relevant). The two density calculations are controlled by the 10.7-cm solar flux level, which may be input separately for control and orbit maintenance.

For space station orbital decay studies, the J70 model was included in an update of the LaRC Orbital Lifetime program, which is used to determine decay rates and total lifetimes in the absence of reboost. Solar cycle density variations are included through use of predictions of monthly average 10.7-cm solar flux values. Nominal (50th percentile) or $\pm 2\sigma$ (97.7th percentile) predictions may be chosen for average or worst-case densities, respectively, to determine expected ranges or orbital decay rates.

Lynne H. Orr, 2486



Atmospheric density variations over time.

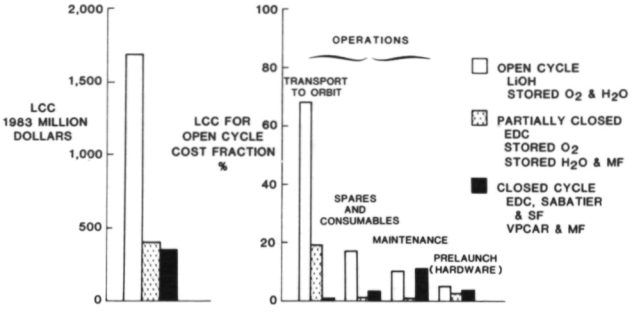


Space station orbital lifetime (no reboost).

Space Station Environmental Control and Life Support System Technology Assessment Analysis

The formulation of system concepts to meet evolving space station requirements has become more difficult and time consuming over the last several years. This is due largely to the increase in technology options available for space station considerations and the demand for improved space station performance imposed by the user community. Advances have been made at LaRC in developing and refining an assessment methodology for the selection of the most promising technologies for various space station systems. This methodology has significantly enhanced the evaluation of competing technology options for space station application. The analysis methodology consists of a data base and algorithms which provide the basis for the assessments as functions of space station design requirements.

The data base consists of design loads associated with space station functions as well as engineering design parameters for each technology option. Cost data are included to provide candidate life cycle cost comparisons. Computer-generated assessment products provide the information required for the technology assessment analysis. Results from the assessment



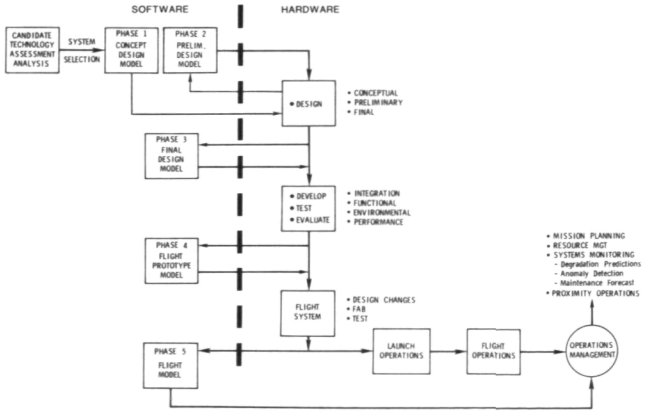
Life cycle cost (LCC) distribution for 1982 space station (crew size, eight; resupply interval, 90 days; mission duration, 3650 days).

of Environmental Control and Life Support System (ECLSS) technology options for providing metabolic oxygen and potable water to an eight-person crew are shown in the figure. Significant life cycle cost reductions can be realized by closing these cycles with regenerative processes. These reductions are shown as decreases in launch weight, launch volume, resupply consumables, and transport-to-orbit costs.

John B. Hall, Jr., 2486

Space Station Systems Analysis Through Phased Emulation/Simulation

The development and operation of a manned space station will be one of the most demanding engineering challenges undertaken by NASA. In addition to the existing stringent requirements that are characteristic of aerospace systems, other requirements have been added which include a 20-year mission life, growth provisions to accommodate improved technology revisions, a high degree of autonomy, and flexibility to support a diverse range of mission experiments. LaRC has implemented a program focused toward the development of subsystem emulation/simulation models to aid in assessing the impact of the requirements on space station design and performance. The major objectives of developing such models are to analytically evaluate and assess the engineering design, expedite realization of the design and identify design improvements, reduce costs, and provide an ongoing capability that can accommodate design changes for use during all phases of space station design, fabrication, testing, and operations. The philosophy of this approach is to have the emulation/simulation models for each step in the design process precede the hardware development in order to receive optimum design, operations, and cost benefits.



Space station phased emulation/simulation systems analysis concept.

The methodology developed is applicable to all space station systems. For demonstration of the methodology, a model has been developed for a space station humidity control and CO_2 concentration subsystem which has shown the usefulness of these models for design enhancement. Evaluation of the demonstration model will continue in order to determine its utility to examine performance capabilities, investigate failure modes and corrective actions, and identify critical subsystem interfaces.

Lawrence F. Rowell, 2486

MAPS Shuttle-Borne Remote Measurements of Carbon Monoxide

The MAPS (Measurement of Air Pollution from Satellites) Experiment flew on the Shuttle orbiter in November 1981 and obtained 32 hours of nadir-viewing data between 38°N and 38°S latitude. A technique has been developed and applied to produce the meteorological data required for measurement data reduction based on temporal and spatial interpolation of gridded time-specific data available from the U.S. Naval Fleet Numerical Oceanographic Center. Since the cold upper surfaces of some clouds introduce errors in the MAPS data, another requirement was for the development of a cloud filtering algorithm. This algorithm was developed and then adjusted by subjectively comparing the data traces with cloud cover as documented by color photography from the MAPS camera. In addition, a postflight instrument characterization has been conducted in a thermal/vacuum chamber. During the characterization, instrument responsivity as a function of instrument temperature, scene temperature, and carbon monoxide volume mixing ratios was determined.

With the instrument characterization data, the cloud filtering algorithm, the meteorological data interpolation technique, and radiative transfer models previously developed, the entire

data set has been reduced. A 12-hour segment of the data has been studied in some detail.

Comparisons of measurements over the same geographical areas taken at times separated by 1½ to 3 hours indicate a repeatability in the data of about 6 to 10 percent. The data clearly show variations of 50 percent or more in the tropical CO mixing ratio as a function of longitude, with the high mixing ratio region stretching from the western coast of South America eastward toward central Africa. Latitudinal variations in CO of a factor of two can be seen, with the highest values occurring in the vicinity of the eastern Mediterranean Sea and the lowest values occurring near southern South America. Efforts are now being concentrated on development of optimum techniques for display of the data and on application of the data to studies of global tropospheric chemistry.

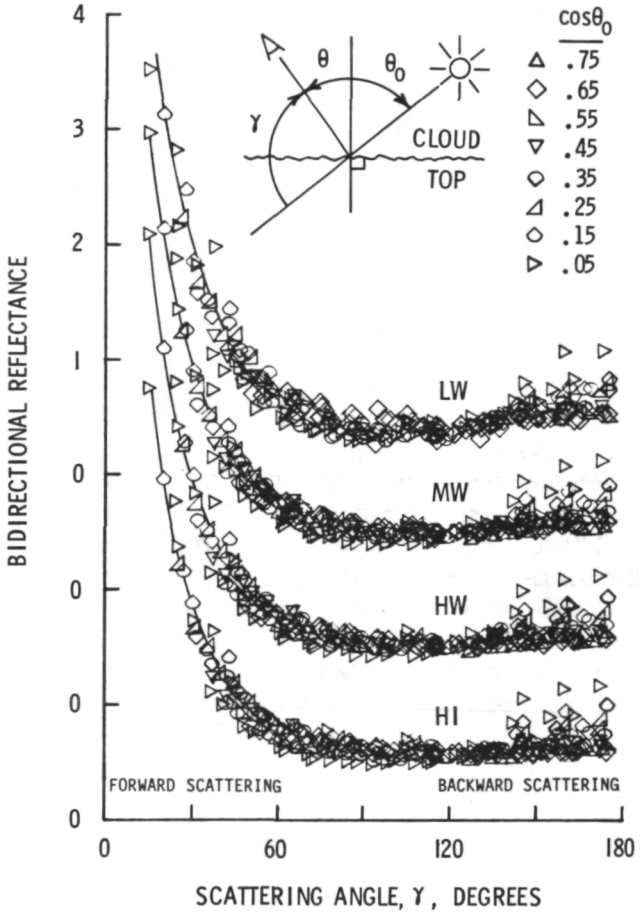
Henry G. Reichle, 2576

Bidirectional Cloud Models

Three Earth Radiation Budget Experiment (ERBE) missions will be launched during the 1984-1986 time period to study the regional, zonal, and global radiation properties of the Earth. The ERBE scanners will normally scan in the crosstrack direction, and thus will provide only limited angular sampling of surface scenes. Bidirectional models for a number of scene types will be needed to convert these data into useful exitance parameters. These models are determined primarily from a data set obtained by the Nimbus 7 Earth Radiation Budget (ERB) scanner, which had a multi-axis scanning capability and provided measurements over a wide range of angular parameters required for directional modeling.

Clouds are the most predominant single scene type (45 percent), and are the major regulators of energy, providing long-term stability for the Earth's radiation balance. The Nimbus 7 ERB scanner obtained about 4 million sets of broadband shortwave and longwave measurements of overcast, cloudy scenes taken globally during the period from November 1978 to May 1980. These cloud data were separated into low, middle, or high water clouds or high ice clouds. Plots of the bidirectional reflectance as a function of scattering angle for the four cloud types are quite similar; there is a strong forward-scattering peak, followed by a minimum in the 90° to 120° range, and a slight increase in the backward-scattering direction. These general patterns are typical of large-particle scattering and have been seen in previous theoretical and experimental cloud studies. Results from the present study will be used to provide cloud models for utilization during the ERBE mission.

W. Frank Staylor, 2977



Bidirectional scattering patterns for low, middle, and high water clouds and high ice clouds.

Airborne Lidar Observations of Polar Stratospheric Clouds Over the North Pole

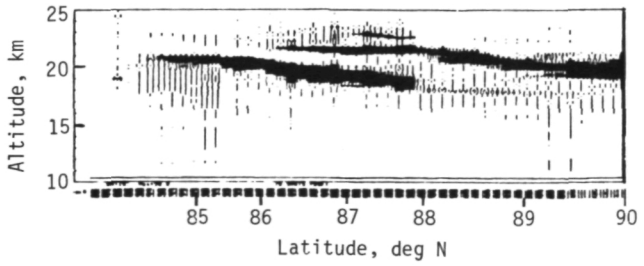
Polar stratospheric clouds (PSCs), a phenomenon that occurs during the Arctic and Antarctic winters, were first observed by the SAM II

(Stratospheric Aerosol Measurement) satellite instrument in 1979. PSCs are thought to be ice clouds that form during the polar winters by freezing of diluted sulfuric acid-water aerosol droplets at temperatures less than 200 K (−73°C).

During the period January 19-28, 1984, an airborne lidar mission was flown on the NASA Wallops Electra aircraft from 37°N to the North Pole. The primary objective of the mission was to provide correlative stratospheric aerosol measurements for the SAM II instrument. A flight was conducted on January 24, 1984, from Thule Air Base, Greenland, (76.5°N, 68.7°W) to the North Pole along the 60°W meridian to determine the northerly extent of the El Chichon volcanic material in the stratosphere and to search for PSCs. This was the first time that PSCs had been observed by lidar, confirming the previous satellite observations. The PSCs were ubiquitous over the full latitude range from 85°N to 90°N and varied in altitude from 19 to 23 km. A second mission was conducted on January 25 from Thule to 86°N, and PSCs were again detected within the temperature region of −85°C from 81°N to 86°N. A third flight was conducted on January 27 to 87°N with no indication of PSCs, which correlated with stratospheric temperature data showing that the low-temperature region had moved over the North Pole toward Siberia.

These first-time lidar measurements of PSCs, which indicated their vertical as well as horizontal extent, provide a unique data set to allow a more complete study of the formation of these clouds. Furthermore, these data, coupled with the SAM II measurements, will provide a better understanding of the effect of PSCs on the polar climate.

William H. Fuller, Jr., 2064



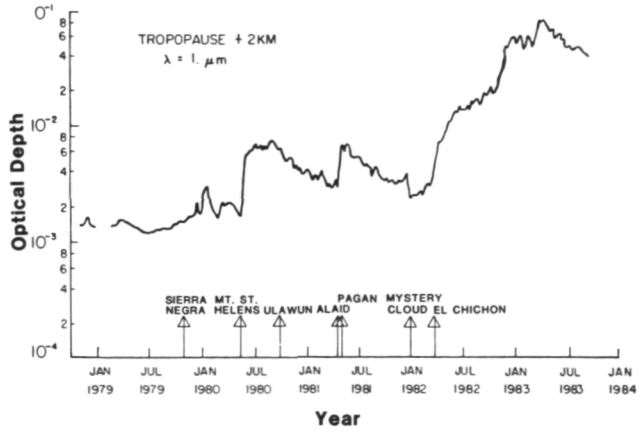
Lidar backscatter intensity versus altitude from airborne lidar data taken on January 24, 1984. Dark layers are indications of polar stratospheric clouds (PSCs).

Aircraft Window Crazing Explained by SAM II Observation of Volcanic Material in Polar Stratosphere

The SAM II satellite instrument was launched on the Nimbus 7 spacecraft in 1978 in an orbit that constrains its measurements to the polar regions between 64° and 82° latitude. Since 1979 a series of volcanic eruptions have perturbed the stratospheric aerosol in an additive manner. The time of arrival of the volcanic material in high latitudes has depended upon the location of the particular volcano and the season in which it erupted. Significant increases in total optical depth were observed in the polar regions by SAM II following the eruptions of Mt. Saint Helens in 1980, Alaid in 1981, and El Chichon in 1982.

In 1982, commercial airlines throughout the world noticed that the acrylic windows in some of the larger aircraft were being mysteriously clouded over with minute cracks. After a preliminary study, it was discovered that the damage, called crazing, occurred only on those airplanes flying polar routes. SAM II data were provided to the airline industry to help explain this phenomenon.

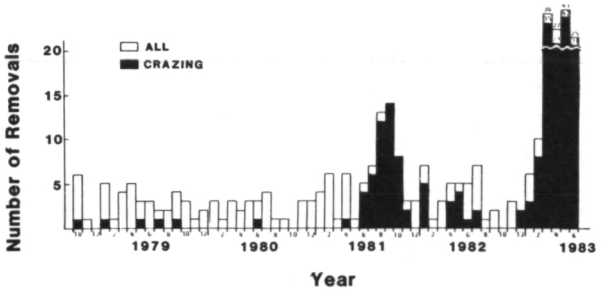
Airplanes flying polar routes at cruising altitudes of 30,000 to 35,000 ft are clearly in the stratosphere and are flying in the volcanically enhanced aerosol layer. The stratospheric aerosols resulting from volcanic eruptions are predominately sulfuric acid-water droplets, which are reacting with the acrylic windows to cause the observed damage. The figures dramatically show the correlation between increased aerosol loading observed by SAM II in the Arctic and the recent airline window replacement. LaRC is continuing to pro-



SAM II derived stratospheric optical depth versus time for the Arctic.

vide SAM II stratospheric aerosol data to the airline industry to predict the magnitude and duration of this effect on window replacement.

M. Patrick McCormick, 2065



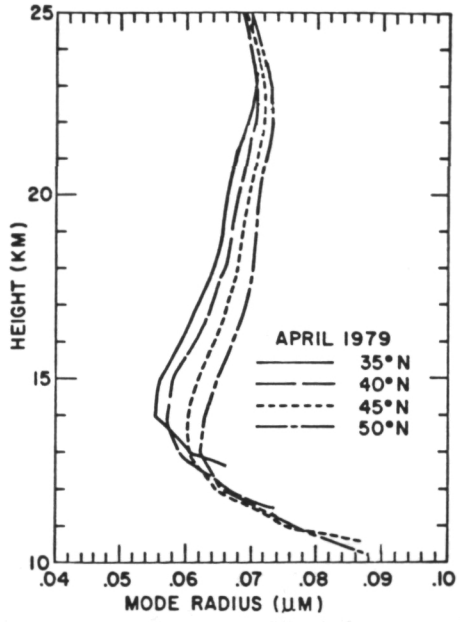
Japan Airlines 747 no. 2 and 3 window replacement experience. (From Boeing Airliner, *April-June 1984, p. 21)*

Altitudinal and Latitudinal Variation of Aerosol Sizes Inferred From SAGE Data

The SAGE satellite experiment provides extinction coefficients of stratospheric aerosols at wavelengths of 0.45 and 1.0 μm. It was found that the ratio of these two coefficients is not very sensitive to either the composition or the radii limits of stratospheric aerosols, but is quite sensitive to the parameter governing the size distribution of aerosol particles. If we assume that the size distribution of background stratospheric aerosol particles follows the log normal expression, there is a one-to-one correspondence between R (the ratio of aerosol extinction at two wavelengths) and the mode radius r_g (a parameter that describes the near radius of the size distribution). Consequently, the global distribution of the value R measured by SAGE can be inverted to obtain the altitudinal and latitudinal variation of aerosol sizes.

In this study the atmosphere is divided into a grid consisting of 1-km intervals in altitude and 5° intervals in latitude. The altitude considered here ranges from the tropopause to 25 km. The figure illustrates the results of this analysis. It was found that in the midlatitude regions of the Northern Hemisphere, the larger particles are concentrated in the higher altitudes and their sizes gradually decrease to minima at about 12 to 14 km as altitudes decrease. There is also a gradual increase of aerosol size as latitudes increase. Although the actual change varies from one month to another, the trend is the same for other months. Results of this analysis are consistent with the suggestion that tropical regions are the source of stratospheric aerosols, which grow to larger sizes as they move to higher latitudes.

Glenn K. Yue, 2065



Profiles of mode radius for midlatitudes in Northern Hemisphere.

Aerosol Measurements in the Arctic

In late January 1984, a NASA research aircraft (Wallops Electra) flew several sampling missions between Thule Air Base, Greenland, ($\sim 76°$N) and the North Pole at altitudes ranging from ~ 2.2 to 8.8 km. A quartz crystal microbalance (QCM) cascade impactor was operated to measure aerosols and in particular to characterize arctic haze aerosols.

Generally the aerosols at the higher altitudes (above about 6.5 km) consisted mostly of liquid acid droplets on the order of 0.5 μm diameter with mass loadings on the order of 1 μg or less per cubic meter, which is similar to stratospheric aerosols. Scanning electron microscopy and energy-dispersive X-ray analysis showed a significant number of sparsely scattered, irregularly shaped, solid particles ranging up to several μm

in size having the same morphology and chemical makeup as previously sampled volcanic particles. These solid particles are very likely the remains from the 1982 El Chichon eruption which were transported into the Arctic region.

In addition to the volcanic particles, patches of highly concentrated material in widely spaced layers at lower altitudes were clearly defined by an on-board downlooking lidar system. As the aircraft passed through the layers, the QCM indicated aerosol enhancements in the 0.5- to 1.0-μm size band. Energy-dispersive X-ray analysis showed these particles to be quite complex chemically, consisting of traces of Al, P, S, Cl, K, Ca, Fe, Cu, and Zn, but Auger spectroscopy indicated that they are dominated by carbonaceous material. An abundance of carbon among particles in an optically active size range, as these particles are, suggests that the particles may be highly absorbent. It is possible, therefore, that arctic haze aerosols could significantly influence climate in the polar region.

David C. Woods, 2065

Lidar Measurements of Arctic Haze During the 1984 Winter Polar Mission

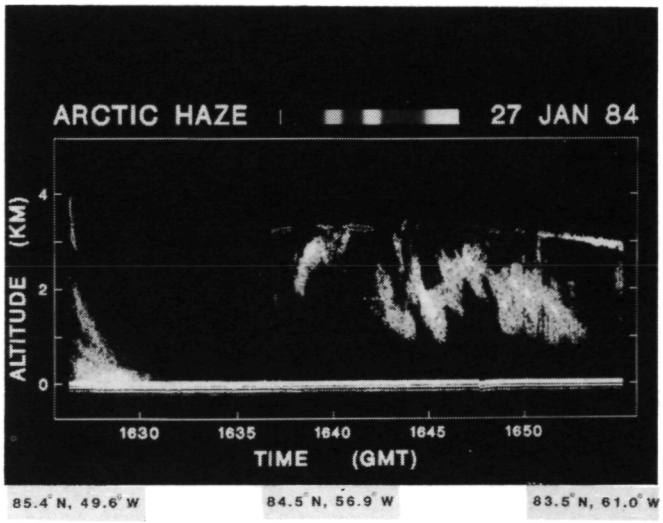
Arctic haze is a widespread air pollution phenomenon that has been observed in the Arctic region mainly during the winter and early spring. Although the main source areas of the material that makes up arctic haze have not been determined, chemical and meteorological data indicate it to be of probable Siberian origin. Aircraft and ground-based measurements in the past have shown that the pollution component of the aerosol is dominated by sulfates, organics, and black carbon.

During the period January 19-28, 1984, an airborne lidar polar mission was flown from 37°N to 90°N to provide correlative measurements for the SAM II satellite instrument. A downlooking 8-in. lidar system operating at 1.06 μm was assembled and installed on the Wallops Electra aircraft as a piggyback experiment. The lidar was designed to provide high-resolution mapping of the expected haze layers below the aircraft and to operate simultaneously with the prime uplooking lidar.

The first indications of haze layers were observed on the SAM II "ground truth" flight path north of Sondrestrom Air Base (67°N, 50.7°W) in Greenland on January 21, 1984. Three polar flights were also conducted north of Thule Air Base, Greenland, (76.5°N, 68.7°W) on January 24, 25, and 27. Arctic haze was observed on each of these flights, with the most prominent layering observed on January 27, 1984, as shown in the figure. Good correlation with a quartz crystal microbalance (QCM) aerosol sampler was obtained on the January 24 flight, as discussed in the preceding highlight.

The first-time lidar measurements of arctic haze, showing distinct layering of material, demonstrates the usefulness of this technique. Another aircraft could easily be directed into these layers to provide in situ sampling of the subvisible material.

William H. Fuller, Jr., 2065



Lidar backscatter intensity versus altitude, January 27, 1984. Black is minimum intensity and white is maximum.

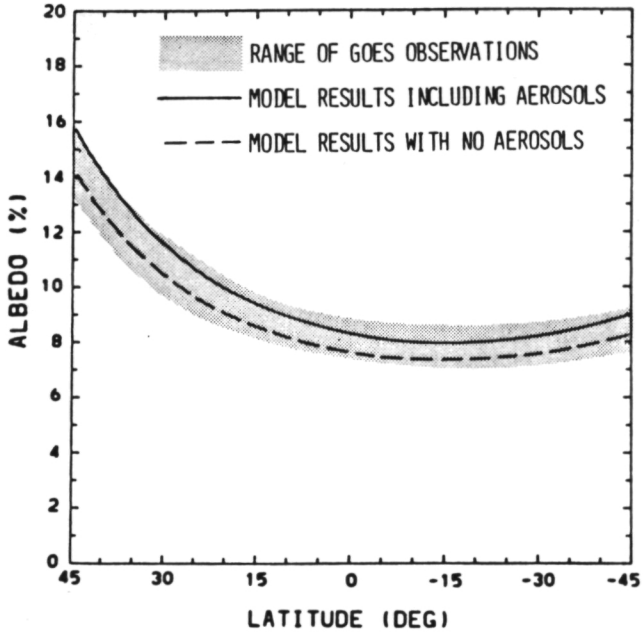
Comparison of Satellite-Observed and Modeled Clear-Sky Albedos

One of the primary uses of satellite-measured Earth radiation budget data is the verification of climate model parameterizations of radiative pro-

cesses in the atmosphere and at the Earth's surface. Accurate modeling of the Earth's albedo in cloud-free conditions is a prerequisite to the more complex modeling of albedo for partly cloudy or overcast skies. Thus, verification of a given clear-sky albedo scheme is essential before the radiative effects of clouds can be confidently incorporated in predictive climate models. Researchers at NASA Langley, in cooperation with scientists at the National Center for Atmospheric Research (NCAR), have compared regional clear-sky albedos derived from high-resolution visible data from the Geostationary Operational Environmental Satellite (GOES) with those computed with an albedo parameterization used in global circulation models.

A plot of the zonal variations of clear-sky albedo over ocean for November 1978 shows good agreement between the calculated and observed values for a range of atmospheric conditions. The model effectively follows the observed poleward increase in albedo due to its inclusion of the solar zenith angle dependencies of ocean and atmosphere albedos. Differences between the observed and computed albedos were generally within the accuracies of the measurements and the model inputs. Comparisons using data from other seasons will continue to help improve the computation of albedo in climate models.

Patrick Minnis, 2977



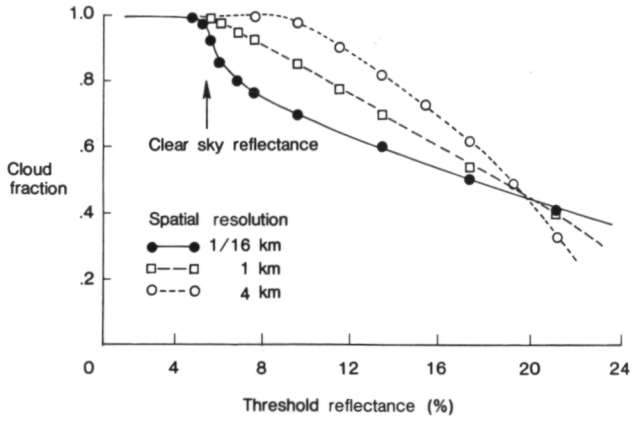
Clear-sky albedo over ocean for November 1978.

Cloud Remote Sensing

Major efforts are being devoted to quantify Earth's cloud cover from space observations. The International Satellite Cloud Climatology Project (ISCCP) will use measurements of reflected solar radiation and emitted thermal radiation averaged over 8- by 8-km areas to derive fractional cloud coverage and cloud height over the Earth for the next 5 years. Because cloudiness can vary substantially, even in an 8-km area, research is under way to intercalibrate this global cloud measurement system with much higher spatial resolution data, such as those of Landsat.

Landsat data provide a spatial resolution of 57 m, or about 1/16 km. This resolution is sufficient to resolve individual cloud cells, which are commonly ½ to 2 km in size for cumulus and stratocumulus cloud fields. Using the Landsat data as cloud truth, comparisions were made of cloud fractions derived from satellite sensor spatial resolutions of 1/16, 1, and 4 km. The figure shows cloud fraction for the eastern Pacific Ocean as a function of the visible reflectance threshold, where measurements above the threshold are cloudy and below are clear. The full-resolution Landsat data give a cloud fraction of 0.75 for a threshold of 8 percent, while the 1-km data give 0.95 and the 4-km data give 1. These results indicate that sensor spatial resolution has a substantial impact on cloud cover determination. In addition, the variation of cloud fraction with changing threshold for the Landsat data is found to be caused by an unexpectedly large variation in cloud field reflectance, even within individual cloud cells.

Bruce A. Wielicki, 2977



Dependence of satellite-determined cloud fraction on sensor resolution.

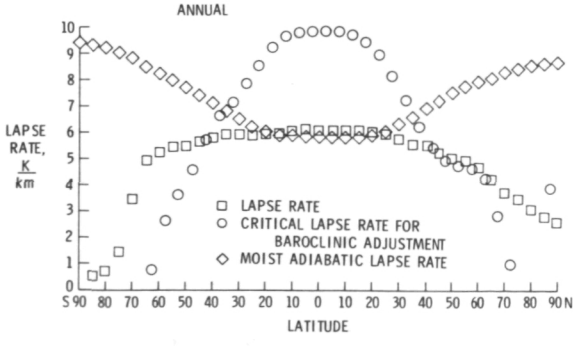
Atmospheric Lapse Rate Regimes

The change of atmospheric temperature with altitude is called the lapse rate. The lapse rate is a fundamental characteristic of the atmosphere and is strongly coupled to dynamic and radiative processes that govern our weather and climate. Using data supplied by the National Center for Atmospheric Research, the global distribution of lapse rate has been computed.

The annual average of the zonal average lapse rate is shown in the figure as a function of latitude. The lapse rate is shown as squares. Two other important parameters, the critical lapse rate for baroclinic adjustment and the moist adiabatic lapse rate, are shown as circles and diamonds, respectively. A lapse rate greater than the critical lapse rate for baroclinic adjustment would result in air mass movements (creating storms) which transport heat to higher latitudes and, in turn, reduce the lapse rate. A lapse rate greater than the moist adiabatic lapse rate would result in the air overturning, carrying heat to higher altitudes. In low latitudes, the lapse rate is approximately the same as the moist adiabatic lapse rate. In the northern hemispheric midlatitudes, the lapse rate can be approximated by the critical lapse rate for baroclinic adjustment.

Computations have also been made of the lapse rate as a function of longitude and altitude as well as latitude and month of the year. These show that the lapse rate at low altitudes is governed by land-ocean differences, but that these effects vanish by midtroposphere. Future work will investigate the effects of these lapse rate variations on atmospheric processes. This research should provide insight into the relationships of radiation budget at the top of the atmosphere and at the surface with weather and climate.

G. Louis Smith, 2977



Annual average lapse rate as a function of latitude.

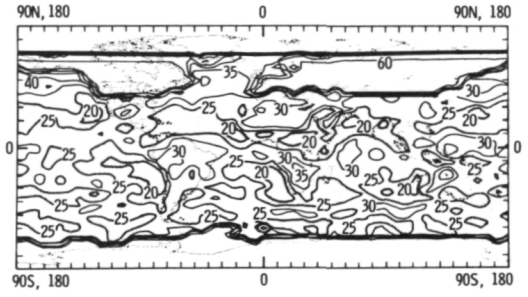
Clouds in Climate Models

General circulation models (GCMs) are complex mathematical formulations of global weather and climate. GCMs are used to predict climatic changes, such as those anticipated for increases in the concentrations of CO_2 and other "greenhouse" gases. One critical factor in the GCM climate—and the real climate—is cloudiness. An increase in the average thickness of clouds would result in the reflection of more incoming solar radiation back to space, cooling the planet.

Although GCM predictions of climatic change have accounted for variations in cloud area and height, they have not accounted for variations in cloud thickness. Climate models which are simpler than GCMs have shown that although CO_2 increases will warm the planet, the warming will place more water vapor in the atmosphere, possibly resulting in an increase in the average thickness of clouds and a cancellation of some of the warming.

The figure shows the albedo (reflectivity) in a GCM that has been modified to interactively compute the thickness of clouds as a function of the liquid water content (LWC). A comparison of the GCM albedo with satellite observations is favorable, indicating that new cloud thickness formulation constitutes an advance in the field of climate modeling.

T. P. Charlock, 2977



Albedo computed by cloud LWC GCM (January).

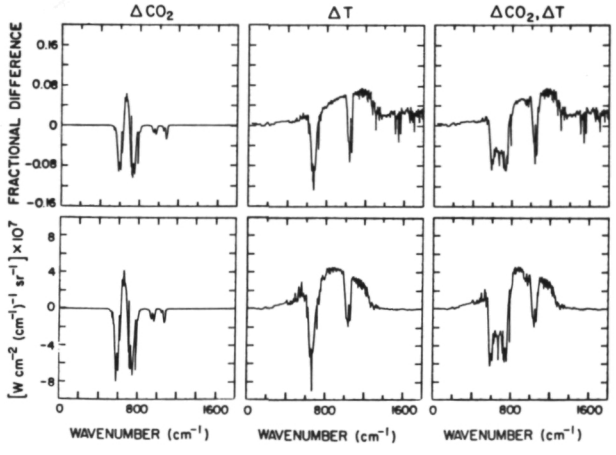
CO_2 Greenhouse Effect and Infrared Radiation

The global climate is the result of a delicate balance between the absorption of incoming solar radiation and the emission of terrestrial infrared

radiation to space. Increases in the concentration of CO_2, a "greenhouse" gas, will impede the emission of terrestrial infrared radiation and warm the planet. The left-hand section of the figure (ΔCO_2) shows how a hypothetical doubling of CO_2 would affect the emission of infrared radiation to space at various wavenumbers in the terrestrial spectrum.

Mathematical models of climate indicate that an increase in CO_2 will warm the surface and troposphere, and also cool the stratosphere. Such a temperature change would affect the emission of infrared radiation as indicated in the center section (ΔT). The right section ($\Delta CO_2, \Delta T$) shows the combined effect of changed temperature and increased CO_2. This constitutes a spectral fingerprint of the climatic change caused by an increase in CO_2. The climate models, which predict the CO_2 temperature changes, are probably accurate to within a factor of 2. Langley scientists are presently formulating a strategy to measure the CO_2 fingerprint from space and provide meteorologists with both an early warning of the effects of CO_2 and a validation tool for the tuning of climate models.

T. P. Charlock, 2977

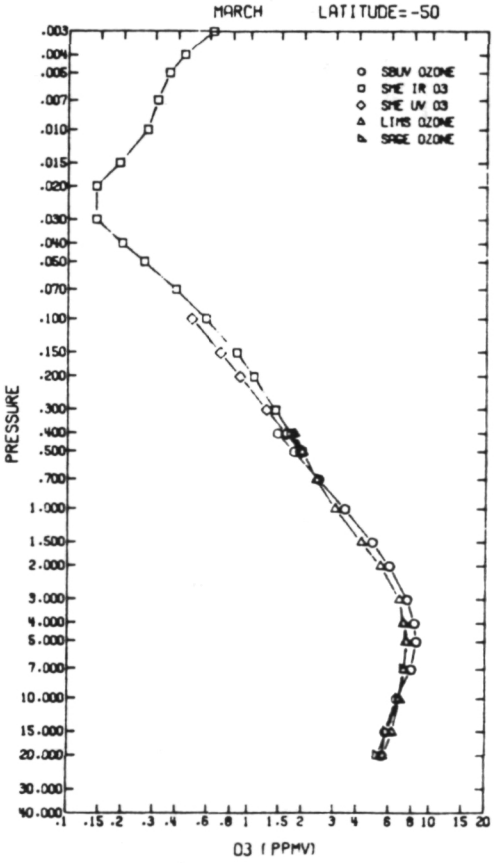


Radiance differences for CO_2 scenarios.

Ozone International Reference Models for the Middle Atmosphere

Reference models of ozone have been generated for the first time from multiple satellite data sets. Use of the reference models is important for studies of atmospheric circulation, dynamic processes, and the radiation balance and photochemistry of the atmosphere. COSPAR (of the International Council of Scientific Unions) invited NASA Langley scientists to generate these ozone reference models for the next International Reference Atmosphere. The present International Reference Atmosphere does not include ozone.

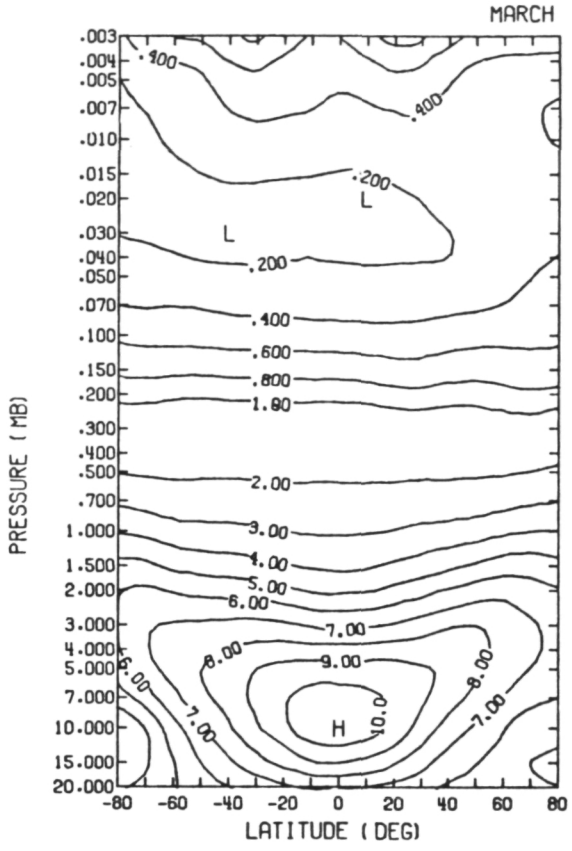
Monthly models were developed of the latitudinal and altitudinal variations in the ozone mixing ratio from 25 to 90 km using five satellite experiments (Nimbus 7 SBUV and LIMS, AEM-2 SAGE, and SME IR and UVS). Considering that these five experiments used five different measurement techniques (IR limb, BUV nadir, solar occultation, airglow, and BUV limb, respectively), the agreement between measurements was found to be excellent. Shown in the first figure is a sample comparison between the five experiments for March at 50°S latitude. Standard deviation and interannual variability were also quantified and at middle and low latitudes were found to be only a few percent. Shown in the second figure is the reference model for the ozone vertical structure for March. The reference model based on satellite data



Five satellite measurements of ozone.

was found to be in excellent agreement with the standard midlatitude mean annual model based on rocket and balloon data.

Gerald M. Keating, 2084

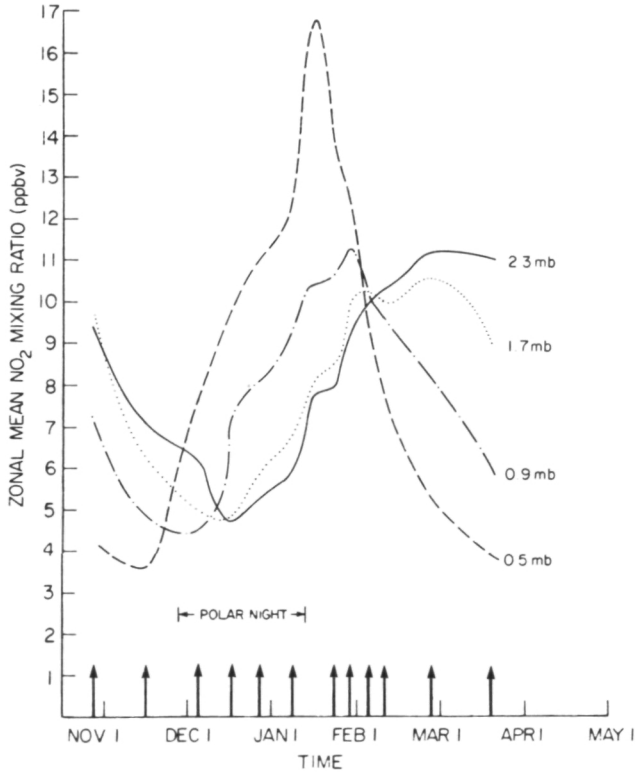


Ozone mixing ratios (ppmv).

Polar Night NO_2 Measurements From LIMS

The Limb Infrared Monitor of the Stratosphere (LIMS) experiment was launched aboard Nimbus 7 on October 24, 1978, for the purpose of sounding the upper atmosphere composition and structure. The LIMS instrument is a 6-channel infrared limb-scanning radiometer that employs cryogenically cooled detectors. Cooling was by a solid cryogen containing NH_3 and CH_4, which limited the experiment to 7 months. One of the LIMS channels was located in the 6-μm spectral region to provide data on vertical profiles and the global distribution of nitrogen dioxide (NO_2). This gas is a catalyst in a chain of nitrogen compound photochemical reactions that cause destruction of ozone.

One of the important questions suggested by theory but, before LIMS, not verified experimentally is whether the polar night thermosphere/mesosphere could act as a source for stratospheric NO_2. Special processing using radiance averaging was performed on the LIMS data, allowing the polar night region to be sounded from the middle mesosphere (~ 70 km) down to the tropopause (~ 10 km) so that this question could be examined. When this was done, it was discovered that deep in the polar night, the NO_2 level reached 170 ppbv at 70 km compared to only 20 ppbv in the stratosphere. Furthermore, the NO_2 was found to have a longitudinal variability at 70 km of about a factor of 8, and regions of maxima and minimia were highly correlated with highs and lows in geopotential. This suggests that downward transport of NO_2 is occurring and is quite localized. The notion of downward transport is given additional credence by the NO_2 time series at four pressure levels shown in the figure. The pressure levels of 0.5, 0.9, 1.7, and 2.3 mb were chosen to cover from the lower mesosphere to the



Time dependence of nighttime NO_2 mixing ratio at 76°N for 0.5, 0.9, 1.7, and 2.3 mb. Arrows indicate measurement points.

stratosphere. Careful study of the figure shows that at the highest altitude (0.5 mb pressure), the NO_2 level begins to increase in mid-November, followed by the next highest altitude (0.9 mb) in early December, and so on. The increases occur for the most part during polar night, when in the absence of sunlight NO_2 is formed high up and is transported undisturbed down to the stratosphere. Once sunlight returns around mid-January, the increases cease and NO_2 levels decline or remain nearly constant, depending on photochemical time constants at the various altitudes. These results represent the first experimental evidence that the mesosphere is an NO_2 source for the stratosphere, and they provide a key data base for tests of theory, establishment of vertical velocities, and determination of photochemical time constants. This information, coupled with other Nimbus 7 data, will allow important studies to be conducted of the nitrogen budget in the stratosphere.

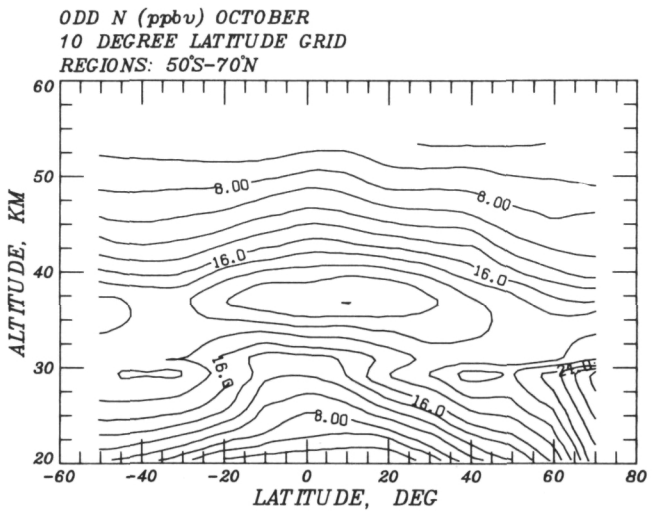
James M. Russell III, 4789

Distribution of Total Odd Nitrogen in the Stratosphere

With the availability of the LIMS, SAMS, SBUV, SAGE, and SAM II satellite data, there is an unprecedented opportunity to use models and data to develop a better understanding of stratospheric phenomena. Knowledge of the odd nitrogen (ON) chemical family ($NO + NO_2 + HNO_3 + 2 \times N_2O_5 + HNO_4 + NO_3$) is of central importance in developing an understanding of these processes. The ON family is a nearly inert tracer within the stratosphere, and knowledge of its distribution with time, derived from measurements, may be used to shed light on important stratospheric transport processes and can provide a powerful means to validate model calculations used to assess the impact of man's activities on the stratosphere.

The ON field in the stratosphere has been inferred at Langley from the LIMS satellite experiment measurements of NO_2, O_3, HNO_3, H_2O, and T used with a contemporary photochemical code. The figure indicates the ON mixing ratio field for October between 50°S and 70°N and 20.5 and 53.5 km. Most interesting is the presence of maximum ON mixing ratios of 30 ppbv in the high-latitude lower stratosphere. These maximum values are located away from the middle-altitude middle-latitude source region for odd nitrogen. This suggests the presence, at the lower levels, of a mesospheric source of odd nitrogen, and is thought to be the first measurement-derived indication of this effect. The presence of such high levels of ON in the lower stratosphere may have a significant impact on the photochemistry of the higher latitudes during winter and will shed interesting light on the respective roles of one-, two-, and three-dimensional models in stratospheric analysis.

Linwood B. Callis, 2985



Distribution of odd nitrogen mixing ratios derived from LIMS satellite measurements and photochemical models.

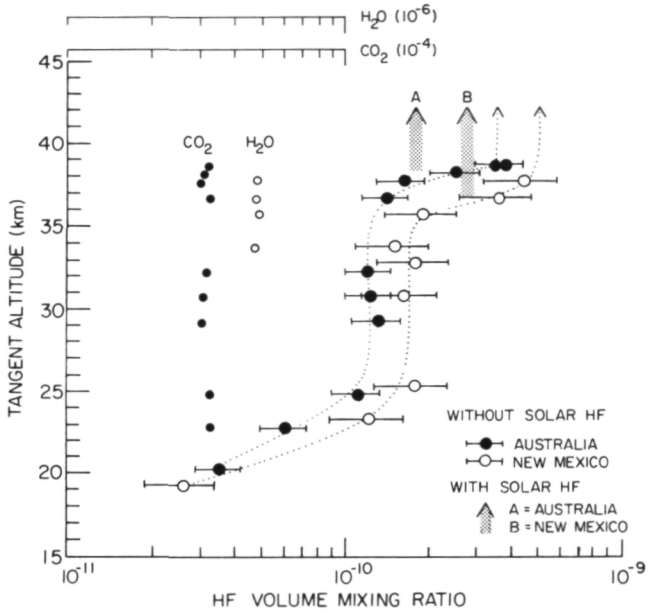
Analysis and Application of Fourier Transform Spectroscopy in Atmospheric Remote Sensing

Spectra obtained by balloon-borne Michelson interferometers over South Australia in 1977 and New Mexico in 1978 have been analyzed to obtain HF mixing ratios using an advanced analysis method for Fourier transform spectroscopy. This method, developed at Langley Research Center, is based on nonlinear least-squares fitting of the interferometric spectra and allows accurate determination of spectral distortions due to errors in measured interferograms.

As illustrated in the figure, the stratospheric HF mixing ratio appears to be significantly larger

in the Northern Hemisphere than in the Southern Hemisphere for similar respective latitudes. The profiles have a similar vertical shape; the HF mixing ratio increases from 20 to 25 km, stays approximately constant between 25 and 35 km, and increases above 35 km. The large differences in the HF mixing ratio reported earlier by other investigators have been shown to be less than previously indicated.

Jae H. Park, 2576



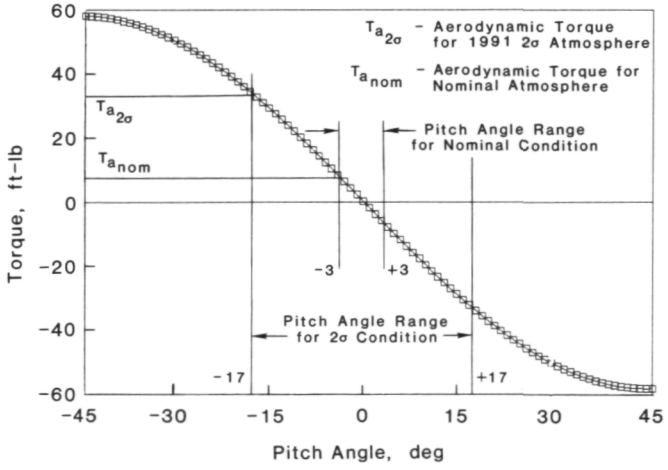
HF mixing ratio profile retrievals for Northern and Southern Hemispheres.

Computer-Aided Controllability Assessments of Space Station Conceptual Configurations

Computer-aided rigid body control dynamics methodology has been used to assess the salient controllability characteristics and resource requirements for eight generic space station configurations. This analysis effort was part of an agency-wide in-house conceptual configuration definition study effort led by NASA in which aerospace contractors participated on a voluntary basis as part of the study team. LaRC analysis tasks consisted of developing analytical computer models of each of the eight proposed configurations using the Interactive Design and Evaluation of Advanced Spacecraft (IDEAS) computer-aided design system. The initial tasks required the creation of three-dimensional geometry models of each configuration normalized to a set of specified functional module definitions to establish dimensional requirements for module connectivity, payload accommodation, and orbiter, OTV, and OMV berthing clearances. Configuration models were generated from each geometry model to determine the mass, center of gravity, inertias, and aerodynamic drag areas of each concept. These data were used along with mission requirements to assess and size the momentum storage system and determine propellant requirements for attitude control, orbit maintenance, and momentum storage desaturation.

An investigation was also performed to determine the preferred flight attitude of each station configuration. This preferred flight attitude is an orientation in which the normal to the solar array plane has the smallest deviation from the solar flux and provides the minimum resources for controlling peak cyclic environmental torques as a function of momentum desaturation requirements. Trim angle assessments of configurations with large center-of-gravity and center-of-pressure distances (which create large control torques) were made to provide off-setting aerodynamic and gravity gradient torques to minimize the size of control system authority and resources needed for attitude stabilization.

L. J. DeRyder, 2486



Induced gravity torque as a function of pitch angle of power tower concept.

Structures Directorate

The Structures Directorate conducts basic research and develops technology in the areas of advanced aerospace materials and composites, structural loading and aeroelasticity, and noise generation by aircraft propulsion systems and structures. This technology development is directed toward reducing both weight and cost of aircraft and space structures while increasing their reliability and service life. The technology developed also provides improved design capability through more accurate prediction of aerostructural loads, vibration, and noise.

The Materials Division conducts research on advanced materials and their application to aircraft and space structures. The Division also develops novel polymeric, metallic, and ceramic materials for these applications. The materials processing and fabrication sciences are developed, and the application of materials to specific flight and space structures is demonstrated. The Division conducts research on thermal protection materials and systems for application to supersonic aircraft and to the Space Shuttle. The fatigue and fracture behavior of materials is studied in specialized laboratories to provide practical methods for insuring structural integrity. Specialized facilities are also used to study the behavior of materials under extreme conditions of high and low temperature, pressure or vacuum, and electromagnetic radiation.

The Structures and Dynamics Division conducts research on structures for advanced aircraft, space vehicles, and the space station. Analytical methods are developed for the prediction of static and dynamic stresses and strains in complex structures. Research is conducted on transient response of structures to aircraft control systems and landing dynamics. Specialized facilities are used to study the dynamics and deformations of aircraft crashes. The Division develops new structural systems for aircraft and space structures. It is also active in research and development of advanced computational methods for structural analysis and design.

The Loads and Aeroelasticity Division conducts research in aeroelasticity, aerothermal loads, high-temperature structures, unsteady aerodynamic loads, and aeroservoelasticity. Analytical methods are developed for calculating aeroelastic deformations and instabilities, for dynamic, vibratory, and thermal response of structures, and for the active control of aeroelastic and dynamic behavior of aircraft. Unique facilities are employed in experimental studies of unsteady aerodynamics, aeroelastic behavior, and aerodynamic heating.

The Acoustics and Noise Reduction Division conducts research on the generation and propagation of aircraft noise. It seeks to understand the relationships between unsteady aerodynamics, structural dynamics, and noise generation by the interaction of fluids with solid surfaces. This research is directed toward predicting and reducing the noise from helicopter rotors, conventional and advanced aircraft propellers, and turbofan engines. Research is conducted on the propagation of noise from its source through the atmosphere and through aircraft structures.

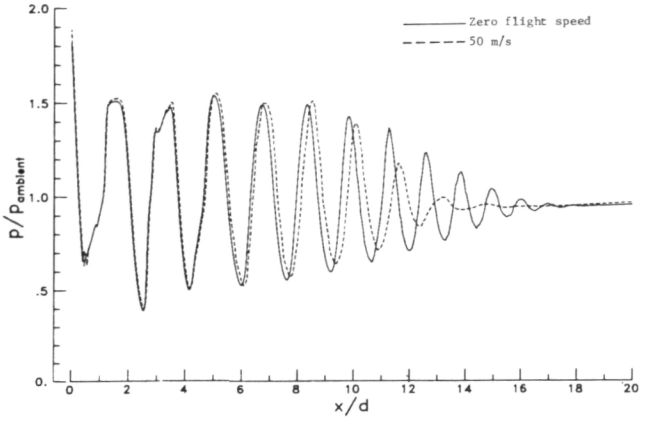
Effects of Flight on Shock-Associated Noise

The effects of flight on the noise radiated from a supersonic jet impacts both the far-field acoustic signature and the dynamic loads imparted to the aircraft structure in the vicinity of the exhaust nozzle. An experiment of flight simulation using an 18-in.-diameter free jet concentric with a 1-in. convergent nozzle has been conducted to determine the effects of aircraft motion on an underexpanded jet.

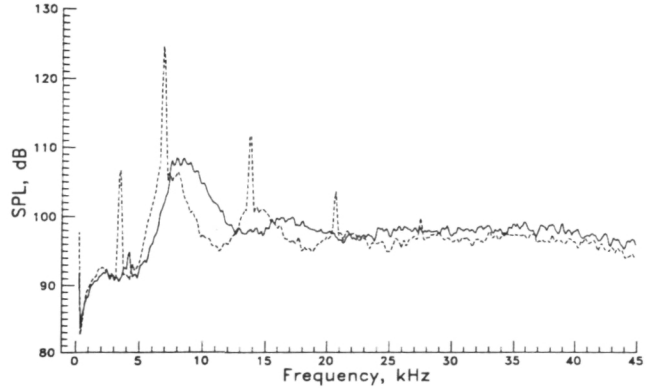
Mean pressure measurements within the jet plume show that when increased flight speed leaves the fundamental structure of the jet unchanged, shock cells in the downstream noise-producing region of the jet increase in length. Corresponding acoustic measurements yield predictably longer wavelengths of both the screech (discrete tones) and broadband components of shock-associated noise. Over a wide range of nozzle pressure ratios (NPR), however, a change in the flight speed can result in a different jet structure, causing large variations in the spread rate of the jet. Shown in the first figure is the measured mean static pressure variation along the plume centerline at NPR = 4.6 for static and flight conditions. Here, p/p_a is the static pressure normalized by the ambient static pressure, and x/d is the distance from the nozzle exit divided by the nozzle diameter. A significant reduction in the extent of the shock system can be seen between flight speeds of 0 and 50 m/sec. Large changes occur in both the amplitude and spacing of the shocks in the downstream, noise-producing region of the jet. Shown in the second figure is the narrowband

sound pressure levels (SPL) measured perpendicular to the jet. The changes in the entire spectrum, including large increases in the amplitudes of the screech tones for the flight condition, are evident. The results clearly show that knowledge of the flight-dependent screech mode of the jet is necessary to predict its structure and acoustic output.

Thomas D. Norum, 4304



Effects of flight on jet centerline static pressure.



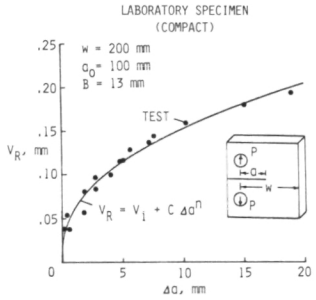
Effects of flight on radiated noise.

Improved Failure Prediction Method for Cracked Metal Structures

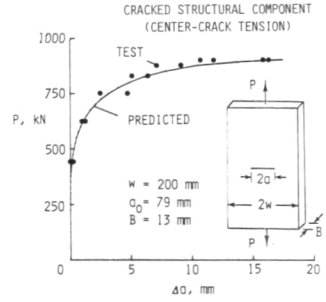
Fracture mechanics technology has developed to a point where the failure of brittle metals can be very accurately predicted just from elastic analyses. But the fracture of very ductile metals used in structures ranging from aircraft to nuclear reactors cannot be described by the same analyses. Concepts such as the K-resistance curve and the J-integral have been tried and often fail to correlate the fracture characteristics between the standard compact specimen and a realistic structure.

A new concept based on crack opening displacement, V_R, has recently been developed at Langley. It has the advantage of requiring only an elastic Dugdale model analysis (first figure) rather than an elastoplastic finite-element analysis. An empirical equation of the form shown in the first figure, where C, n, and V_i are coefficients determined from curve-fitting the data from laboratory tests of a compact specimen, leads to a displacement resistance curve which accurately predicts crack growth, Δa, and fracture for a panel with a central crack. Specimen dimensions are shown in the figures along with the location of the applied force P. Efforts are under way to develop the required Dugdale model analysis for any cracked configuration in a universal computer code. The data from the laboratory compact specimen will then be used to predict fractures for ductile materials in any configuration.

J. C. Newman, 3192



Determining material fracture resistance behavior.



Predicting load-against-crack-growth behavior.

Rapid Adhesive Bonding

Adhesively bonded components offer advantages to aerospace structures in weight, fatigue resistance, and part count. Adhesive bonding can also facilitate field repairs on damaged aircraft, thereby taking less time than many standard repair techniques. Thermoplastic adhesives and many thermosetting adhesives do not inherently require long processing times. A few minutes to heat the adhesive to a viscosity low enough to obtain flow and wetting of the adherend surfaces and a short time to cure, or form bonds with the adherends, are sufficient. However, the limitations of current equipment and techniques slow the bonding process considerably. Current techniques depend on thermal energy being generated and conducted through equipment, tooling fixtures, and layers of structural parts before reaching the adhesive in the bondline.

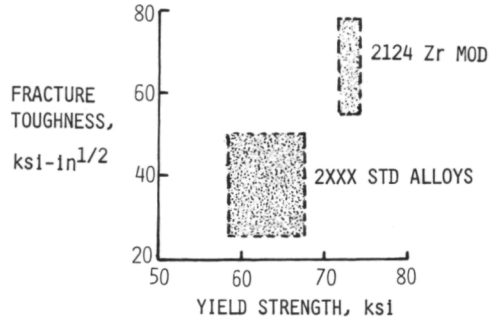
In contrast to the current state of the art in bonding, the rapid adhesive bonding technique developed at Langley heats the adhesive in the bondline directly, without heating everything else. In rapid adhesive bonding, high-frequency induction-heating toroids are used as the power source to rapidly heat a metallic susceptor (such as a steel screen or perforated steel foil) which is impregnated with a thermoplastic or thermosetting adhesive. Typical heatup time is about 1 minute for thermoplastic adhesives heated to around 600°F and less than 1 minute for thermosetting adhesives that need to be heated to the 400°F to 500°F range. A 2-minute hold is used to promote flow and adherend "wetting". The specimen is then cooled to room temperature in about 2 minutes. After this 5-minute cycle, the shear strengths of bonds on titanium and graphite/epoxy composite specimens are comparable to those achieved with conventional bonding methods. The electrical energy expended during a typical bonding cycle is less than 200 W for 5 minutes, no more than that of two light bulbs.

William T. Hodges, 3041

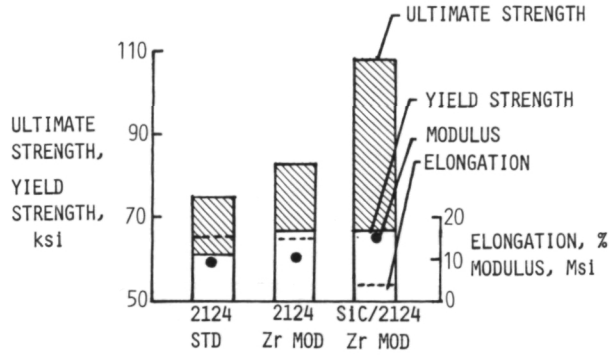
Improved Metal Matrix Composites

Selected lightweight aluminum alloy matrix composites have unique properties that make them good candidates for application to a variety of aerospace structures. The generally good blend of strength, stiffness, thermal stability, and formability could lead to high payoffs in terms of structural system weight, performance, and cost. However, the utility of these materials has been limited because of their low strain-to-failure and poor toughness. One approach to the resolution of these problems is to combine the high-strength, brittle reinforcement (usually silicon carbide) with a tough, ductile matrix to produce a useful engineering material with both high strength and toughness.

Lockheed-California Company, under contract to Langley, has investigated the effects of chemistry changes on mechanical properties of a number of powder metallurgy aluminum alloys. One very promising alloy, based on 2124 alloy chemistry with zirconium added as a stabilizer, has shown significant improvements in toughness and yield strength combinations over the standard alloys. The first figure shows the range of values obtained for the standard alloys and for zirconium-modified alloys. The second figure shows the tensile properties of silicon-carbide-whisker-reinforced composite prepared using a zirconium-modified



Fracture toughness — yield strength combination for PM 2xxx aluminum alloy extrusions.



Tensile properties of PM aluminum alloy extrusions with and without SiC whisker reinforcement.

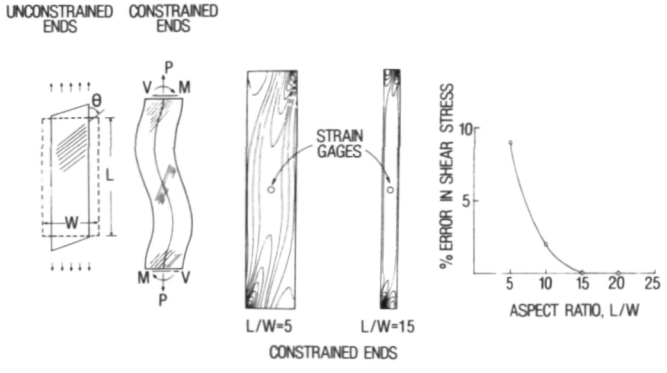
alloy. Composites with the zirconium-modified alloy matrix have been fabricated with ultimate strength of over 100 ksi, yield strength near 70 ksi, elastic moduli of about 18 Msi, and strains-to-failure approaching 5 percent. The property combinations demonstrated by the composites represent a good balance that could lead to improved structural efficiency for selected aerospace applications.

William D. Brewer, 4193

Off-Axis Tensile Coupon Requires High Aspect Ratio To Measure Shear Modulus Accurately

One way to measure the in-plane shear modulus of composite materials is by the "off-axis" tensile test. This test method is attractive in that it provides shear stress-strain data by a routine testing procedure. A finite-element analysis was used to determine the pointwise stress and strain distributions of graphite-epoxy off-axis specimens having aspect (length-to-width) ratios of 5, 10, 15, and 20 with fiber orientations $\theta = 15°$. A new optical method of high-sensitivity moire interferometry was used in laboratory tests to verify the accuracy of the finite-element results.

This study indicated very good agreement between finite-element results and experiment. Both experiment and analysis showed that the clamped end grips of the test machine introduce inplane bending, M, and shear, V, under tensile loading, P. This loading state results in non-



Deformation modes, shear stress coupons ($\theta = 15°$ off-axis coupon), and error in shear stress at strain gage.

uniform stress distributions at the test section where the strain gages are located. The extent of the stress distribution nonuniformity was found to be significant for aspect ratios smaller than 15 (see center of figure). This stress distribution nonuniformity causes errors in determining the shear modulus, G_{12}. The errors occur because the stresses at the strain gages cannot be determined exactly from the test data, but are calculated from the net load recorded by the testing machine. Hence, the presence of the stress distribution nonuniformity implies a difference in the actual stresses at the gages and the recorded values. The finite-element results indicate that as the specimen aspect ratio increases to 15 and beyond, the error in the shear stress (based on calculations using test data) due to the nonuniformity of the shear stress distribution diminishes substantially and a more reliable determination of G_{12} can be obtained.

Michael P. Nemeth, 4585

Fracture Criteria for Adhesives

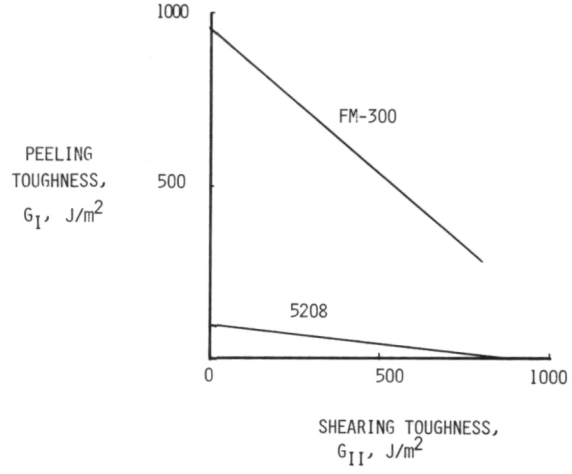
Most bonded joints are designed to transfer load between the bonded elements by a shear action, but peeling forces do develop in the process. Application of fracture mechanics thinking to the failure of bonded joints is relatively new and is beginning to provide insight into the behavior of both composite resin matrices and adhesives because it can analytically separate the peeling and shearing actions.

The figure shows results obtained for a typical brittle resin system (5208) and a tough adhesive (FM-300). The lines represent the combined peel and shear load induced strain energy release rates (G_I and G_{II}, respectively) required for static fracture. The slopes of the lines indicate that the brittle system (5208) is more sensitive to peel stresses, whereas the tougher system is almost equally sensitive to peel and shear stresses, as indicated by the 45° slope of the FM-300 curve. Volume expansion (dilation) is required in order to produce high peeling toughness. Brittle matrices obviously have limited ability to expand because of their high degree of crosslinking. Tougher polymers, such as FM-300, can exhibit dilation through crazing and void formation due to rubber toughening mechanisms. Other tough polymers, such as poly-

sulfone, have linear molecular structures which allow them to dilate under plane strain peel.

The failure criteria for mixed-mode fracture toughness will be dependent on the toughness of the polymer system. Brittle systems will be more G_I dependent while the tougher systems may depend equally on both G_I and G_{II}.

W. S. Johnson, 2715



Mixed-mode fracture for two polymer systems.

Optically Transparent/Colorless Polyimide Films

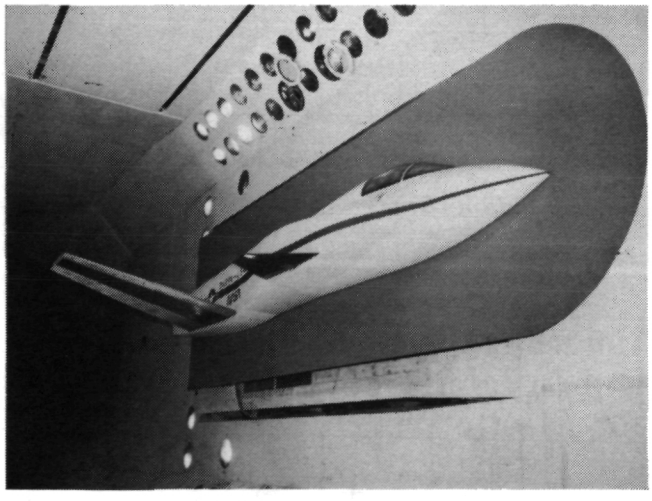
Research is being conducted to synthesize aromatic polyimide films and coatings having improved optical transparency in the visible region of the electromagnetic spectrum. These materials are needed for transmitting solar energy on space components such as antennas, solar cells, and thermal-control coating systems. Although there are other polymers available which are highly transparent, most have limited long-term thermal stability. Linear aromatic polyimides exhibit excellent thermal stability but are bright yellow in color and only 60 to 70 percent transparent at the solar wavelength of interest, about 500 nm. Recent work at Langley has succeeded in modifying aromatic polyimide materials in a way that produces fully transparent (colorless) films while retaining thermal stability.

Two approaches have been used to produce aromatic polyimide films that are 90 percent transparent in the 450- to 600-nm range. First, highly purified starting materials are used to prevent discoloration of the final polyimide film. The second and most important condition for providing maximum transparency includes the incorporation of bulky electron-withdrawing groups, such as $-C(CF_3)_2-$ or $-SO_2-$, into the polymer molecular structure. These groups separate chromophoric centers, reduce inter- and intra-chain electronic interactions, and reduce the intensity of color in the resulting film. Although incorporation of a $-C(CF_3)_2-$ group into the dianhydride portion of the polymer reduced the overall color intensity of resulting films, the use of such groups in both parts of the polymer was necessary to produce colorless films.

Anne K. St. Clair, 3041

Forward-Swept-Wing/Body-Freedom Flutter Studies at Transonic Speeds

Body-freedom flutter is known to be one of the fundamental aeroelastic problems to be avoided on forward-swept-wing (FSW) aircraft. This phenomenon is caused by adverse coupling of rigid-body pitching and wing-bending motions. Although rare on aft-swept-wing aircraft, this mechanism is generic to FSW configurations due to the tendency of the wing effectively to destiffen (or aeroelastically diverge) with increasing dynamic pressure. To assist in better understanding body-freedom flutter, a 0.5-scale aeroelastic model of a FSW airplane was tested in the Langley Transonic Dynamics Tunnel. The purposes of this

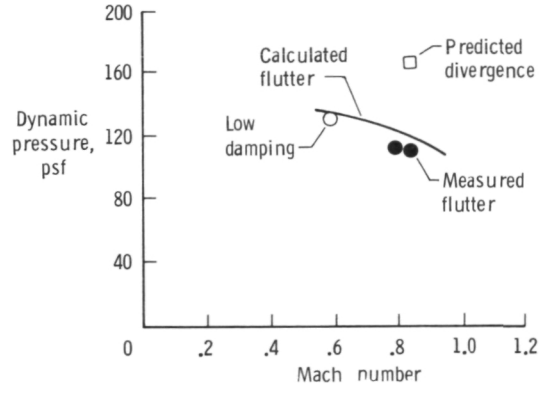


FSW airplane model sidewall mounted in tunnel test section.

study were to investigate this phenomenon of a realistic FSW configuration in the flutter-critical transonic speed regime and to ascertain the ability of existing analytical tools to predict its occurrence. The model is shown sidewall mounted in the tunnel test section. A special model suspension system provided rigid body pitch and plunge degrees of freedom. The model was tested both in a statically stable condition and with relaxed static stability (RSS) up to -25 percent static margin. A stability augmentation system which employed an active canard was used to stabilize the RSS configurations.

Measured and calculated results obtained for the statically stable model configuration are shown as functions of Mach number and dynamic pressure. The body-freedom flutter calculations as shown agree fairly well with the measured data; however, the calculated results are slightly nonconservative in the transonic region. Additionally, a static divergence instability was predicted using a subcritical response technique applied to data measured below the flutter boundary. This instability is shown as the square symbol. By comparison, the flutter occurred at about 70 percent of the divergence dynamic pressure.

Rodney H. Ricketts, 2661

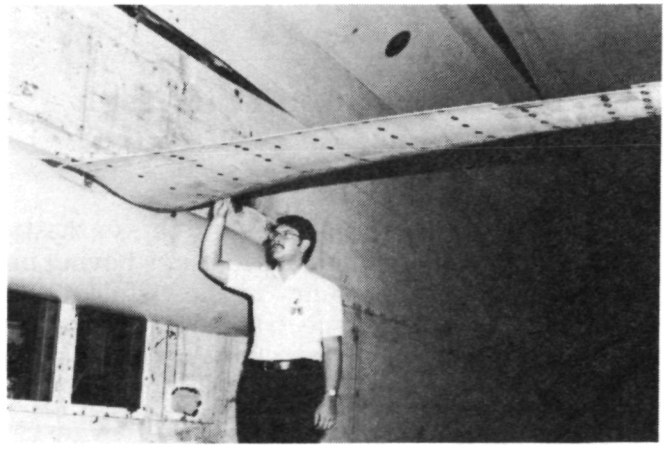


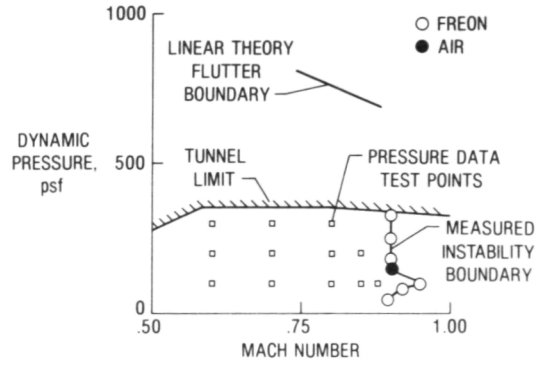
Body-freedom flutter of a forward-swept-wing model.

Unsteady Aerodynamic Pressures and Instability Boundary Determined for Elastic Wing

The accurate prediction of aeroelastic effects at transonic speeds for modern aerospace vehicles requires knowledge of the interaction of unsteady aerodynamic loads and elastic deformations. Although unsteady forces and pressures have been measured previously on oscillating rigid surfaces, these results have not provided all the needed information. Consequently, the present study was undertaken in the Langley Transonic Dynamics Tunnel to determine the unsteady aerodynamic characteristics of an elastic wing and the relationship between the aerodynamic loading and the elastic deformations. This relationship can be determined because both quantities are measured. The wing tested was from the NASA Drones for Aerodynamic and Structural Testing (DAST) program, which involves flight testing of several Aeroelastic Research Wings (ARW) on a drone aircraft. In particular, the ARW-2 right wing was used because it was instrumented for unsteady pressure measurements. This wind tunnel study was undertaken to complement the flight program and to obtain transonic unsteady pressure data on an aeroelastic wing.

Measured pressure and deflection data were obtained for a wide range of wing angles of attack, control surface deflection angles, and tunnel flow conditions, as shown by the small square symbols in the figure. In the course of the tests an unex-





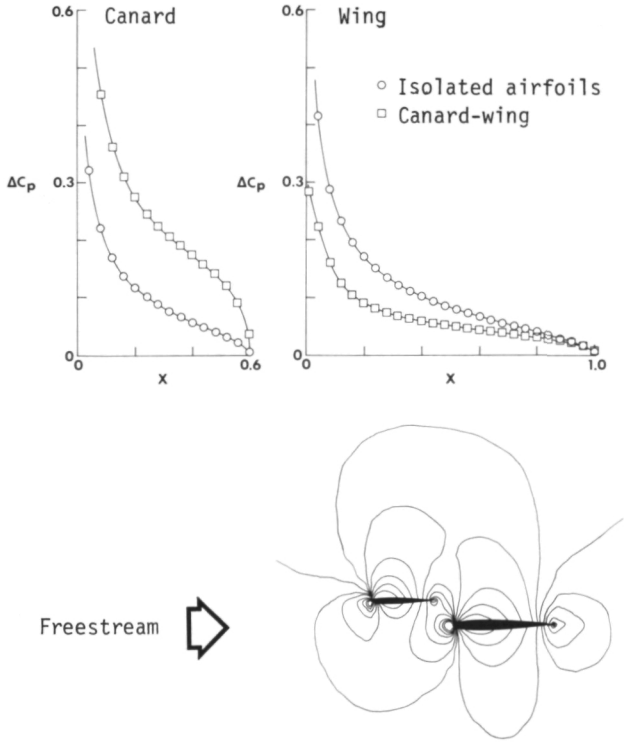
Unsteady pressure test of DAST ARW-2 shows unusual transonic instability boundary.

pected instability was encountered and the boundary was defined as shown by the circle symbols. The unstable behavior (dominated by wing first bending motion) occurs above the DAST vehicle's flight regime, which is limited to Mach numbers less than 0.86. However, it is of great interest from a research point of view because it was not anticipated, because the phenomenon is not well understood, and because the dynamic pressures involved are extremely low and fall well below the flutter boundary predicted by linear theory (shown as a solid line in the figure).

Maynard Sandford, 2661

Transonic Code Extended to Multiple Airfoil Configuration

The two-dimensional finite-difference computer code XTRAN2L, which provides a time-marching solution to the nonlinear small-disturbance potential equation for transonic flow, has been extended at Langley to apply to combinations of airfoils such as canard-wing configurations. The figure shows results of an application



Canard-wing lifting pressure distributions and Mach number contours.

of the extended code to a closely coupled canard-wing system. Both airfoils are NACA 0010 sections, the freestream Mach number is 0.5, and the angle of attack is 1.0° for both canard and wing. The lifting pressure coefficient distribution, ΔC_p, along the airfoils is plotted for both isolated and canard-wing configurations. For each airfoil, the distance between the two curves represents the steady aerodynamic interference of one airfoil on the other. The Mach number contour lines, also shown in the figure, clearly illustrate the aerodynamic interaction between canard and wing.

The study has further assessed the effects of canard-wing separation distance on transonic unsteady airloads and flutter. For the configuration considered, inclusion of the canard in the transonic flow field increased damping in the aeroelastic system, which delayed the onset of flutter.

John T. Batina, 4236

Method For Reducing Stress Concentration in Diffusion-Bonded Joints

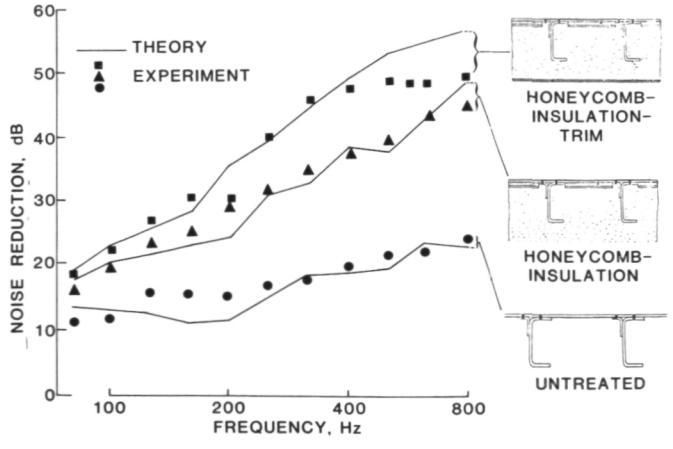
The diffusion bonding process for box-stiffened panels produces a sharp corner at the stiffener-skin interface. A method is needed to reduce the high stress concentration at this corner in order to provide sufficient fatigue life for the joint. Using simple photoelastic techniques, the severity of the stress concentration at the junction of the cap of the box-stiffened stringer and the panel skin was identified. Experimental fatigue test data from actual hardware specimens quantified the stress concentration in terms of cycle life at stress for the sharp corner of the diffusion-bonded joint. Various joint concepts were investigated using the photoelastic technique, and the better joints were identified. These joints were made in titanium specimens and fatigue tested to verify the results of the photoelastic study. A "diffusion bonded square-edge doubler" produces a fatigue stress concentration factor K_T of about 7.0, a flanged-edge cap (the geometry of interest) produces a K_T of about 3.5, which is too high for aircraft application, and a one-step chem-mill produces a K_T of about 1.5; however, a flanged-edge cap is necessary for panel stability.

The photoelastic results show that for the one-step chem-milled skin, a region of zero stress is produced at the corner of the step. By diffusion bonding the stringer flange to the skin at this step, the sharp corner of the diffusion-bonded joint can be positioned at this point of zero stress. At this position, the sharp corner produces no damaging stresses in the panel structure. Cycle life test data from titanium specimens show a substantial improvement at a given stress with this type of joint, and the K_T has an acceptable value of 2.5.

Randall C. Davis, 2291

Validation of Sidewall Noise Reduction Theory

Theoretical methods for interior noise prediction and optimization were developed at Langley for a turboprop Commander 1000 aircraft under flight conditions. The analytical model uses modal solutions to account for structural modes of the panel and the acoustic modes of the receiving space. The forcing function is a convecting surface pressure caused by propeller and turbulent boundary layer noise. However, for laboratory conditions it is taken to be a random reverberant noise field. The additional noise losses due to acoustic treatments such as porous materials and trim panels are calculated by the impedance transfer method. The theoretical methods have been used to design sidewall acoustic treatment configurations for reduced cabin noise with minimum weight.



Reduction of transmitted noise.

To validate the theory, a specially designed panel which closely represents a segment of the Commander 1000 aircraft sidewall was constructed for laboratory testing using the Transmission Loss Apparatus at Langley Research Center. For the laboratory studies the noise reduction was defined as the difference between the measured sound pressure levels of microphones in the source and receiving rooms. Theoretical and experimental noise reductions are shown for an untreated condition and for two add-on treatments. These treatment configurations were developed theoretically as potential candidates for noise control in the Commander aircraft. The results indicate generally good agreement between theory and experiment. Substantial reduction of noise transmission can be achieved with the new proposed optimized treatment composed of honeycomb stiffening, "insul shield" acoustic material, and limp trim panel. The surface density of such a treatment is about 2 psf, which is about 80 percent of the weight of some current aircraft treatments.

John S. Mixson, 3561

Transmission Loss of Finite Composite Panels

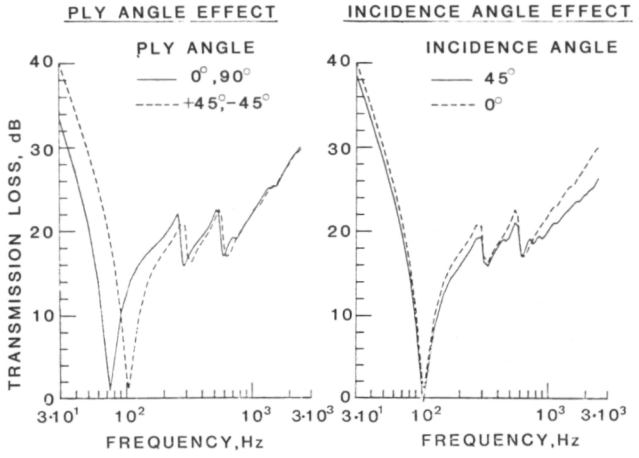
Noise transmission on aircraft with composite fuselages (for example, advanced turboprop) is expected to occur at low frequency. Because the flexural rigidity of a composite panel has variable directionality depending on ply angle layup, panels with different ply angle layups or different orientations with respect to the incident noise could have markedly different low-frequency noise transmission characteristics. Therefore, calculations using a new theoretical method have been performed to obtain an indication of the magnitude of these effects on transmission loss.

Results illustrating ply angle effect are shown for a 14- by 8- by 0.04-in. graphite-epoxy panel and for the case of normal incidence. The curves show that a panel made of +45°,-45° plies has significantly higher transmission loss (6 to 14 dB) in the stiffness-controlled low-frequency region than a panel made of 0°,90° plies. At frequencies immediately following the fundamental resonance, the 0°,90° panel has 2 to 9 dB more transmission loss. Since the panels weigh the same, the transmission loss curves merge together in the

high-frequency mass-controlled region. In comparing the transmission loss for the +45°,-45° panel for two different angles of incidence, very little difference (less than 2 dB) is seen to occur in the stiffness- and resonance-controlled regions, while in the mass-controlled region the normal incidence curve reaches a maximum of 3 dB above the 45° incidence case.

These predictions indicate that the ply angle layup of a composite panel can significantly affect the low-frequency noise transmission characteristics, but that the effect of varying the angle of incidence is not as important at low frequency. The ply angle effect merits further study.

Clemans A. Powell, 3561



Transmission loss of finite composite panels.

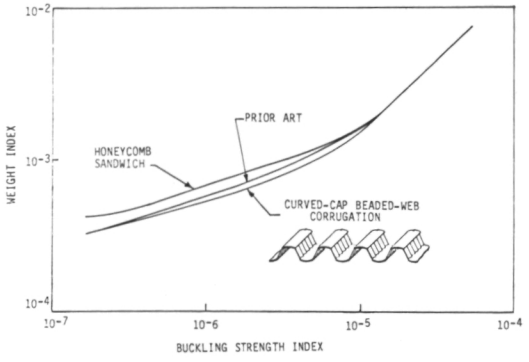
Curved-Cap Beaded-Web Corrugation

The need for lighter and stronger primary structures for high-speed aircraft and for spacecraft has motivated the search for minimum-mass fuselage and tank structures. Such craft normally require an external thermal protection system; therefore, the underlying primary structure does not have to be aerodynamically smooth. The limiting load in such structures is primarily compression buckling of the wall sections. A new structural concept is proposed that offers a significant weight saving potential over previous concepts for a wide range of loading. This is illustrated in the figure, which shows the buckling strength/weight payoffs.

The curved-cap beaded-web corrugation makes use of superplastically formed and diffusion-bonded (SPF/DB) technology for its construction. A thin-gauge metal sheet is superplastically formed to make the beaded web and to form cap areas for bonding the cap strips. The caps are separate strips bonded to the SPF corrugated segment. The cap strips carry the compressive load, and the thickness-to-width ratio of this curved cap determines its ability to resist local buckling. Beading the web prevents local buckling in the web while allowing maximum separation between the cap strips with a minimum amount of material. The separation between the cap strips determines the stiffness of the corrugation structure for resisting overall buckling. The curvature significantly increases the buckling strength of the curved cap over that of flat caps. The attachment of the beaded web to the cap strips is also unique. The attachment of the beaded web to the cap strip is moved under the cap strip edge to spread the web attachment over a portion of the face of the cap strip. The width of this attachment area between the beaded web and the face of the cap strip is determined by the depth of the beads in the beaded web. This new beaded web/cap joint provides rotational restraint to the cap, enabling the cap to carry its design load without edge rotation or premature buckling.

Structures of any width can be made by repeating any number of corrugation segments. Alternate configurations include the cap strips being curved inward to improve the damage resistance of the curved-cap beaded-web corrugation. Also, the edges of the cap strips can be extended and crimped over the beaded webs, improving the damage resistance of the caps and further stabilizing the caps against buckling.

Randall C. Davis, 2291



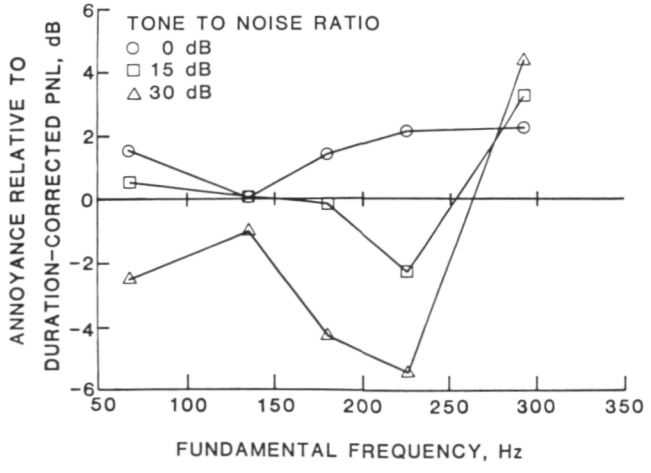
Structural efficiency potential of curved-cap beaded-web configuration.

Annoyance of Advanced Turboprop Aircraft Flyover Noise

Advanced turboprop (ATP) noise is unique in that the pure-tone harmonic content occurs at frequencies higher than those generated by conventional propeller aircraft. The understanding and quantification of annoyance caused by ATP flyover noise is required in order to predict and/or assess its effects upon community response. An experiment was conducted to determine the annoyance effects of the pure-tone harmonic content characteristics, such as fundamental frequency (blade passage frequency), frequency envelope shape, and tone to broadband noise ratio.

A computer synthesis system was used to generate 45 realistic time-varying simulations of ATP aircraft flyover noise in which the harmonic content was systematically varied to represent the factorial combinations of five fundamental frequencies ranging from 67.5 to 292.5 Hz, three frequency envelope shapes representing helical tip Mach numbers of 0.63, 0.73, and 0.78, and three tone to broadband noise ratios of 0, 15, and 30 dB. The simulations were based on takeoff conditions and assumed a single-propeller tractor configuration using a thin, highly-swept, twisted blade. Sixty-four subjects judged the annoyance of the 45 synthesized flyover noises presented at various levels.

envelope shape (blade tip Mach number) did not significantly affect annoyance. However, as shown in the figure, the interaction of fundamental frequency with tone to broadband noise ratio did have a large and complex effect on annoyance. Other results of the study indicated that the addition of duration corrections to the noise measurement procedures improved prediction ability and that duration-corrected A-weighted sound pressure level (simulating the response of the human ear) predicted annoyance better than any other measurement procedure.



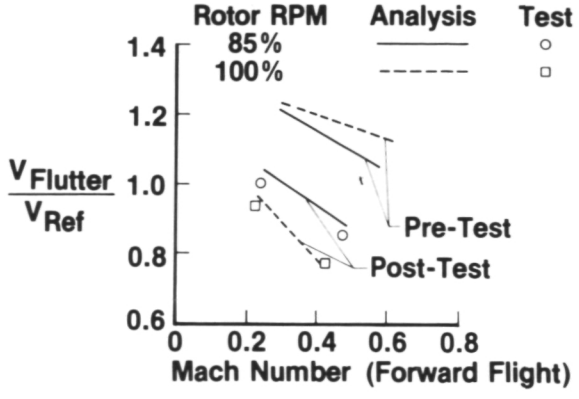
Interaction of fundamental frequency and tone-to-noise ratio.

David A. McCurdy, 3561

TDT Test Provides Essential Data Base for JVX Preliminary Design

To provide an experimental data base needed for the Joint Advanced Vertical Lift (JVX) design development, a 0.2-size aeroelastically scaled semispan model of a preliminary JVX design was tested in the Langley Transonic Dynamics Tunnel (TDT). Specific test objectives were to determine wing/rotor stability in the airplane mode, measure rotor and control system loads and vibration data primarily in the helicopter-to-airplane conversion mode, correlate these results with analysis, and therefore validate analytical methods applicable to tilt rotor configurations. The model consisted of a scaled, cantilevered wing and pylon/rotor system that could be operated with the rotor either powered or windmilling. The model was tested in both air (low Mach number operation) and Freon (high Mach number operation) over a range of simulated altitudes. Model parameters tested included pylon-to-wing locking (on and off downstop), rotor RPM, wing aerodynamics, wing spar stiffness, rotor pitch-flap coupling, and rotor control system stiffness.

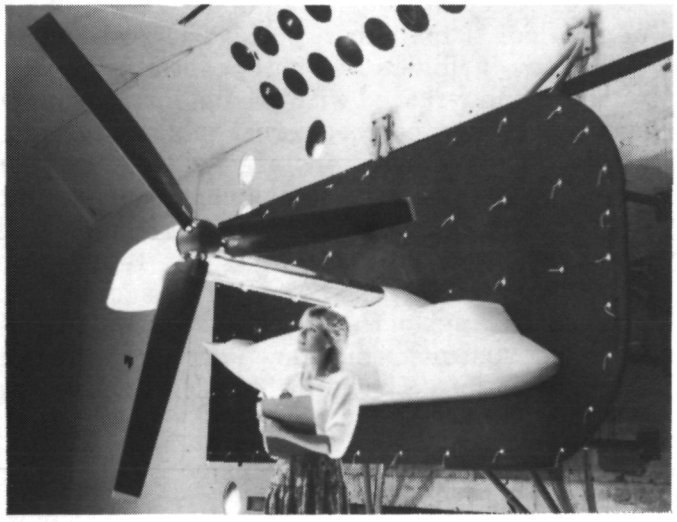
Wing beam mode instabilities were critical (lowest flutter speed) for most model configurations tested, although some wing chord mode in-



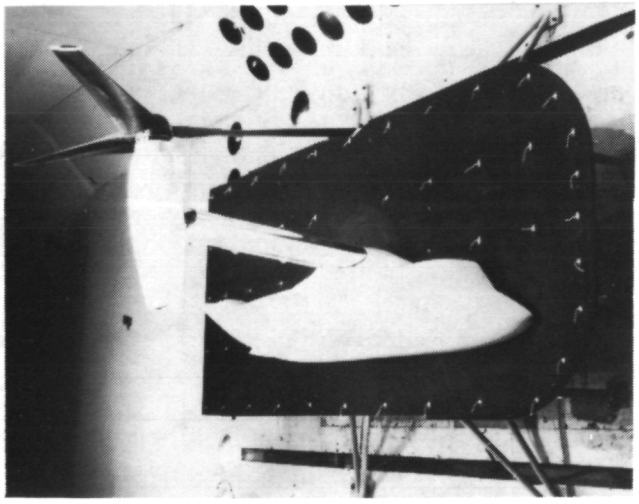
Airplane mode instabilities.

stability data were also obtained. Rotor and fixed system loads were measured for the helicopter-to-airplane conversion corridor. Because the experimental aeroelastic instabilities occurred at scaled speeds considerably below those predicted by pre-test analysis, a major impact of this test was to cause a detailed re-examination of, and changes to, the inputs and degrees of freedom used in the analytical methods. The figure shows both illustrative pre-test and post-test analytical results compared to test data for an airplane configuration with windmilling rotor at both 85 and 100 percent of scaled operational rotor RPM. The agreement between the current post-test analytical results and the test data is considered satisfactory.

William T. Yeager, Jr., 2661



Airplane high speeds.



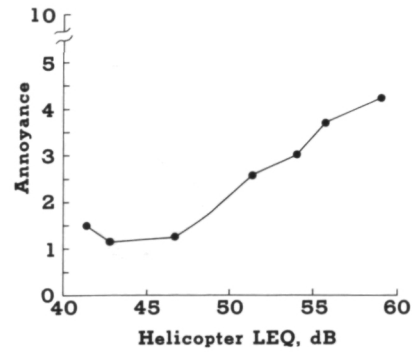
Helicopter low speeds.

Helicopter Community Noise Study

Because of the typically low number of daily operations at many heliports, there is uncertainty in the applicability of the energy-averaging noise metrics which are used to quantify community noise exposure around conventional airports. The present community noise study was conducted to determine relative annoyance effects of helicopter noise levels and number of flyovers at low daily flyover rates and to provide information to the FAA for the development of criteria for heliport operations, siting, and land use guidelines.

The study, conducted in the fall of 1983 in the Denbigh area of Newport News, VA, consisted of an initial face-to-face survey of general noise annoyance and a series of repeated telephone surveys of daily noise annoyance of helicopters, jet and propeller airplanes, and road traffic. On 17 of the 23 telephone survey days, the community helicopter noise exposure was controlled by planned flights of Fort Eustis helicopters over a prescribed flight path within the survey community. Measurements of the noise exposures were made on each flight day at three locations in the community and the telephone surveys were conducted during the early evening following the exposures. In both the face-to-face and telephone surveys, annoyance to each noise source was scored on a scale of 0 (not annoying at all) to 10 (extremely annoying). The figure indicates the relationship between the obtained annoyance ratings and the energy average metric, LEQ, which is currently used to assess conventional airport community noise exposure. A consistent trend for increasing annoyance with increasing LEQ is shown for LEQ above 45 dB, thus indicating the applicability of this energy-averaging noise metric.

Clemans A. Powell, 3561



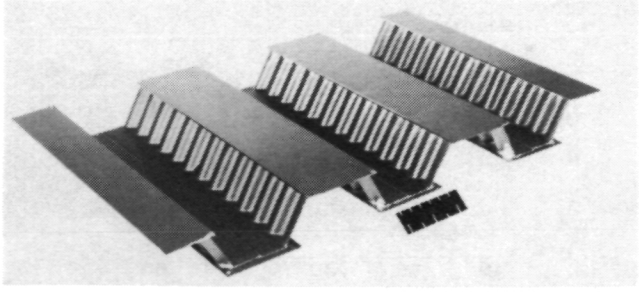
Annoyance correlated with energy-average metric.

Superplastic Forming and Weldbrazing of Titanium Compression Panels

Superplastic forming (SPF) of titanium alloys permits the formation of unique configurations to exacting tolerances. When heated to temperatures near 1700°F and subjected to low stresses (2 ksi), titanium alloys can be strained in excess of 1000 percent without significant property degradation. As a result, titanium can readily be formed into deep cavities and complex shapes using argon gas pressure. Prior studies have shown that SPF can be used to fabricate highly complex stiffener configurations. The stiffeners can be incorporated into compression panels by a number of different joining techniques and offer substantial improvements in structural efficiency. Some configurations have shown improvements of approximately 50 percent when compared to conventionally stiffened panels on a weight-equivalent basis. As a follow-on to the earlier work, a study was conducted to assess the potential of SPF and weldbrazing as a joining process for fabricating multiple-stringer compression panels employing unique stiffener configurations for improved structural efficiency.

Analytical studies were conducted to design a minimum-mass structure. The 10- by 18-in. corrugated beaded-web panel illustrated was selected for demonstration of the total fabrication process and evaluation of structural efficiency. The multiple-stiffener panel consisted of half-hat segments formed by SPF and weldbrazed to cap segments. Following fabrication, the panel was tested to failure in compression. The failure load was within 3 percent of the calculated theoretical load, verifying that superplastic forming can achieve controlled tolerances and that the weldbrazing process is a highly effective technique for joining panel elements.

Thomas T. Bales, 3405

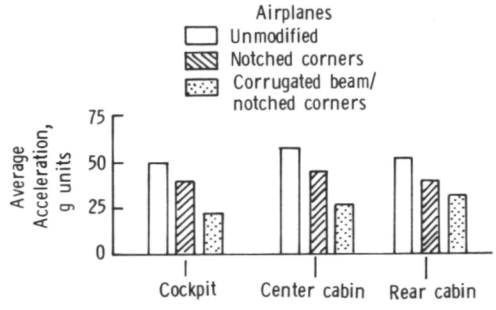


SPF weldbrazed half-hat multiple-stringer titanium compression specimen.

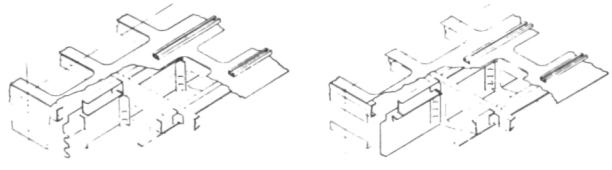
Load-Limiting Subfloor Concepts Reduce Aircraft Crash Loads by 50 Percent

Within the recently concluded crash dynamics research program conducted at the Langley Impact Dynamics Research Facility, a specific research area involved the development of structural concepts to limit the crash loads transmitted to the occupants of an airplane. Two of three identical twin-engine general-aviation aircraft were structurally modified to incorporate a different load-limiting (energy-absorbing) subfloor concept into the fuselage structure for full-scale crash test evaluation and comparison to the third, unmodified airplane. The fuselage subfloor structure was replaced from the main wing carry-through spar to aft of the rear cabin door, with only the upper floor panel left in place. The keel beams, bulkheads, stringers, and lower contour skin were removed and replaced with the notched-corner or corrugated-beam/notched-corner subfloor concepts shown. Seat tracks were installed on all upper floor panels to provide seat attachment capability.

All crash tests were conducted at 80 mph with a sink speed of 30ft/sec and a -15° flight path angle. The average peak normal crash acceleration pulses measured on the airplane structure for the three test specimens are shown for three different fuselage stations. The normal accelerations for the



Load-limiting subfloor concepts reduce crash loads by 50 percent while maintaining seat/floor integrity.



Subfloor concepts.

unmodified airplane reached appoximately -50 to -55 g's, whereas the accelerations for the notched-corner structure, which allowed some crushing, were reduced to approximately -25 g's, or about 50 percent of the acceleration of the unmodified airplane.

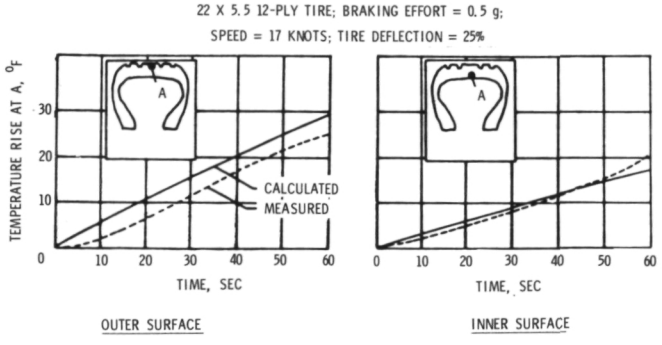
Huey D. Carden, 3795

Analysis Predicts Tire Carcass Temperature During Braked Rolling

Experimental and analytical studies have been conducted to determine temperature profiles in aircraft tires under a variety of operating conditions to help define the strength and fatigue limitations of aircraft tire carcass structures. The analytical effort to model the heat generation mechanisms, which was conducted by the University of Michigan under NASA grant, employs a finite-element representation of the tire cross section. The heat generated within the tire is treated as a function of the strain energy associated with the predicted tire flexure and the energy dissipation associated with the slippage in the footprint under braked rolling conditions. The experiments were conducted on 12-ply size 22 × 5.5 aircraft tires with thermocouples embedded in the tire carcass, and temperature data were acquired during braked rolling conditions on an actual runway surface.

The agreement between calculated and measured temperature rise is quite good for the moderate braking conditions shown in the figure. Only two of many thermocouple locations are shown, for the outer and inner surface of the tire carcass along the tire tread centerline. The data indicate a more rapid temperature rise along the outer surface, as would be expected for these conditions. The analytical effort is continuing to explore the yawed rolling (cornering) tire both with and without braking.

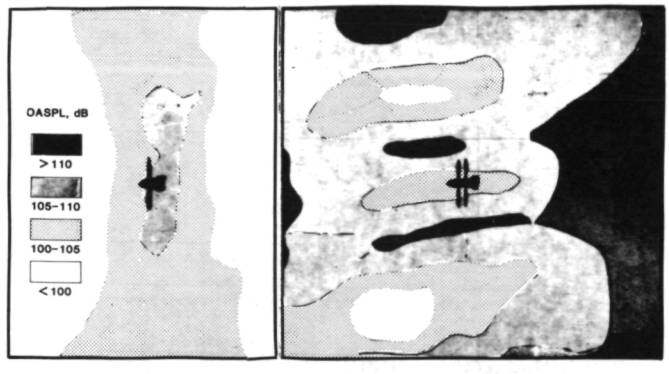
John A. Tanner, 2796



Tire carcass temperature during braked rolling conditions.

Single- and Counter-Rotation-Propeller Noise Comparison

To provide the technology base for incorporating noise tradeoffs into propeller installation design for subsonic aircraft, experiments have been conducted which provide a data base from which to infer noise trends for various installations and validate existing analytic noise prediction methods. Noise measurements of several propeller installations have been made in the Langley 4- by 7-Meter Tunnel. These installations include single- (SR) and counter-rotating (CR) propellers in strut-mounted pusher and tractor configurations as well as at pitch and yaw. These measurements were made at 143 positions to define the noise radiation patterns of these configurations on a square covering 60° in front of and behind the propeller disk and 60° on either side of the axis. This summary addresses the noise from the SR and CR propellers in the tractor mode at 0° pitch and 0° yaw. The overall sound pressure levels (OASPL) are presented here in contour format. The data have been corrected to free field and normalized to a constant radius from the propeller plane axis. The comparison is given between an eight-bladed SR propeller and a 4+4-bladed CR operating at the same pitch setting and rotational speed. The data show that the noise radiation patterns for the two propeller configurations are very different. The



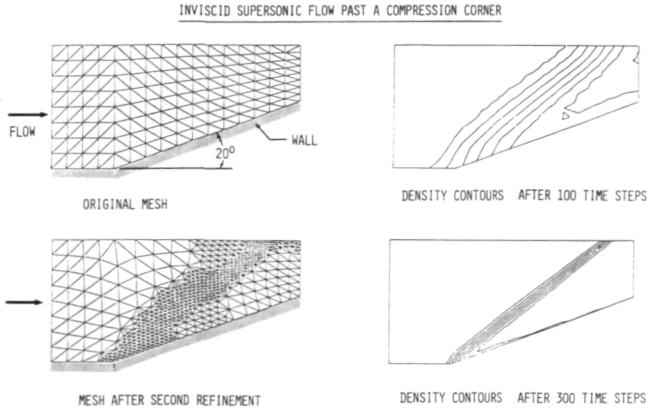
Noise radiation from model SR and CR propellers.

noise from the SR appears to radiate in the plane of the propeller and decreases in the upstream and downstream directions. On the other hand, the CR propeller produces noise in streamwise bands. These regions of high noise levels correspond to the directions in which the propeller blades of the front and back row are aligned. High noise levels are also generated upstream and downstream from the propeller disk. This noise is attributed to the flow interaction occurring between the two propeller rows. On the other hand, in the propeller plane the noise levels from the SR and CR are about equal. However, upstream and downstream from the propeller disk, the noise from the CR exceeds that of the SR by more than 15 dB.

P. J. W. Block, 2645

Automatic Finite-Element Mesh Refinement

Solutions of compressible flow problems are characterized by discontinuities such as shock waves. Numerical techniques must be able to accurately resolve such phenomena. Since the analyst does not know the exact location of these large gradients, the ideal algorithm should automatically refine the mesh in these regions throughout the computation. Using the finite-element method because of its inherent ability to handle complex geometries and capture shocks, the University of Wales under NASA grant has developed and implemented an automatic mesh refinement technique.



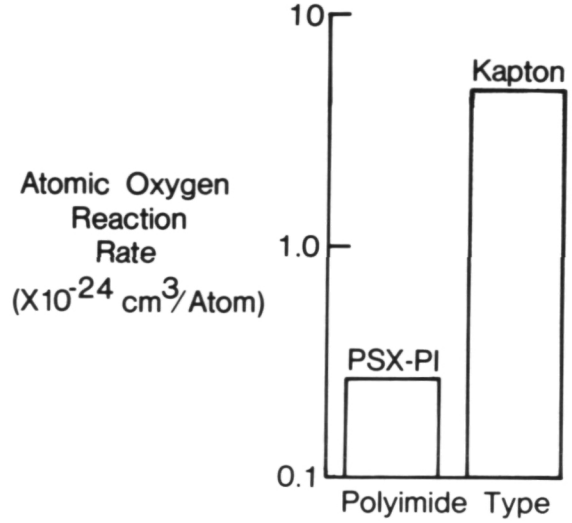
Automatic gradient-sensitive finite-element mesh refinement algorithm demonstrated.

This mesh enrichment technique adds elements to the mesh at certain times in the solution, based on regions of high gradients, to evenly distribute (or minimize) the solution error. The effectiveness of this technique has been demonstrated for a number of inviscid compressible steady flow problems. The results for flow past a compression corner are shown. The solution is started with a crude and fairly uniform mesh. After every 100 timesteps the algorithm adds elements in the shock region, so that after 300 timesteps there are many small elements near the shock, giving good resolution unobtainable with the original mesh.

Siloxane-Modified Polyimide for Space Applications

Early Space Shuttle flights revealed substantial mass loss of organic materials, including Kapton, a polyimide used for thermal-control blankets in the payload bay. Experiments conducted on subsequent flights determined that this mass loss was due to erosion of the surfaces caused by an interaction with atomic oxygen, a major constituent of the low-Earth-orbit environment.

To combat this problem, a siloxane-modified polyimide copolymer was developed which would minimize atomic-oxygen attack and yet retain the toughness properties of Kapton. Two siloxane polyimide copolymer films, containing 7 and 25 percent by weight of siloxane, were flown on STS-8, accompanied by Kapton and a series of Kapton-



Siloxane polyimide and Kapton reactions with oxygen.

like polyimides. The polyimides exhibited approximately the same reaction rate to the atomic-oxygen environment as the Kapton. However, the siloxane polyimide copolymers exhibited much lower reaction rates. The siloxane polyimide containing 7 percent siloxane had a reaction rate of 0.6×10^{-24} cm^3 per 0 atom and the 25-percent siloxane polyimide had a rate of 0.28×10^{-24} cm^3 per 0 atom, compared to 4.7×10^{-24} cm^3 per 0 atom for Kapton. Thus, a reaction rate of almost one-twentieth that of Kapton was obtained with the siloxane-modified polyimide. Because of this reaction rate, it is expected that siloxane-modified polyimides will be more durable in the low-Earth-orbit environment of space.

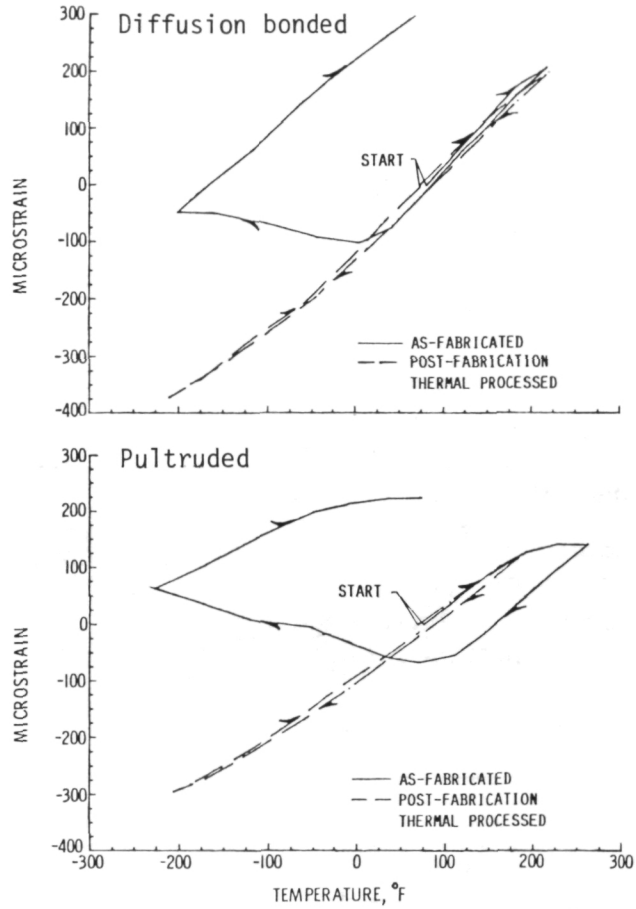
Beatrice Santos, 4555

Metal Matrix Composite Processing To Minimize Thermal Strain Hysteresis

Graphite-reinforced metal matrix composites (MMC) represent the next generation of high-stiffness low-thermal-expansion materials for structural applications on dimensionally critical spacecraft. These materials offer many advantages over the resin matrix composites, such as higher electrical and thermal conductivity, better radiation resistance, and no outgassing. Currently, the 6061 aluminum alloy is one of the primary metals being considered as the matrix for MMC. However, composites made with this alloy exhibit large hysteresis during thermal cycling and residual dimension changes induced by thermal cycling. This behavior is unacceptable for the reliable performance of dimensionally critical spacecraft.

The thermal expansion of a P100/6061 graphite/aluminum material as fabricated is shown in the figure. The expansion is characterized by a large hysteresis loop and residual strain. Samples fabricated by both diffusion bonding and pultrusion exhibit essentially the same expansion behavior. A post-fabrication process has been developed which significantly reduces the hysteresis loop and eliminates the residual strain. Thermal expansion after processing is also shown in the figure. The post-fabrication processes consist of standard heat treatments followed by cryogenic prestraining (i.e., cryogenic soak). A different heat treatment is required for samples fabricated by each of the two methods. Different treatments are required because the fabrication techniques cause different and significant magnesium depletion within the aluminum matrix. This change in chemistry alters the heat treatment required to strengthen the matrix alloy.

Stephen S. Tompkins, 4558



Thermal expansion of P100/6061 before and after processing to minimize thermal strain hysteresis.

Durable Thermal Protection System Concepts

Although the Reusable Surface Insulation (RSI) currently used on the Space Shuttle is an excellent insulation, it is very fragile. The goal of the durable thermal protection system (TPS) program is to develop metallic TPS taking advantage of the inherent durability associated with metals, the opportunity for mechanical attachments, and

the ability to cover gaps between panels while remaining mass-competitive with existing RSI systems. The approach is to develop the candidate concepts and verify them through thermal-pressure, wind tunnel, vibration, acoustic, water absorption, and lightning strike tests.

Two metallic concepts and one advanced carbon-carbon (ACC) concept have been developed covering the temperature range from 700°F to more than 2300°F. The titanium multiwall concept, which consists of alternate layers of flat and dimpled foil joined dimple-to-dimple, is limited to a maximum surface temperature of 1200°F. The superalloy concept, which consists of fibrous insulation contained between an outer Inconel 617 honeycomb sandwich and an inner titanium honeycomb sandwich, is limited to a maximum surface temperature of 2000°F. Both concepts have beaded edge closures which form panels nominally 12 in. square, and both are mechanically attached. The ACC concept consists of a nominally 3-ft-square ACC skin capable of withstanding temperatures in excess of 2300°F, supported on MA 965 (oxide-dispersion-strengthened iron alloy) posts. The ACC skin protects fibrous insulation packaged in Nextel ceramic cloth.

Test results indicate that the titanium multiwall concept is viable and mass-competitive with RSI. Vibration, acoustic, and thermal-vacuum tests on the superalloy concept have also yielded positive results.

John L. Shideler, 2425

Emittance/Catalysis Enhancement of Superalloys for TPS Applications

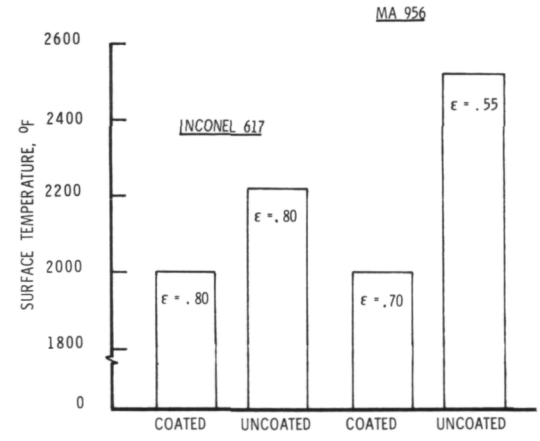
Superalloys in metallic thermal protection system (TPS) applications must have good resistance to dynamic oxidation, high emittance, and low catalysis for the recombination of dissociated oxygen and nitrogen. A number of superalloys have been found to have good oxidation and/or emittance characteristics; however, the naturally occurring oxides of most metals tend to catalyze the recombination of oxygen and nitrogen. Two alloys of interest are Inconel 617, a nickel-chromium-based alloy, and MA 956, an oxide-dispersion-strengthened iron-based alloy.

Inconel 617 has a high-temperature emittance ϵ greater than 0.8 under simulated reentry conditions; however, MA 956 has a low emittance (about 0.55) and very high resistance to oxidation. The low emittance of MA 956 results from Al_2O_3 that forms at the surface, shielding the alloy from oxidation.

Chemical-vapor-deposited coatings have been successfully applied to statically oxidized Inconel 617 and MA 956 superalloys by reacting silane and borane in the presence of hydrogen gas. The coatings were formulated to have a high emittance and a low catalysis. Results from simulated reentry testing of coated specimens indicate that the coated MA 956 has both increased emittance and low catalysis and the coated Inconel 617 has low catalysis after 5 hours (30 cycles) of exposure at 2000°F.

The figure shows that the effect of coating MA 956 for the 2000°F exposure conditions is to reduce the surface temperature by 525°F compared to that of the uncoated MA 956. The effect of coating Inconel 617 is about half that for MA 956 because of interaction between the coating and alloy oxide and because the high emittance of Inconel 617 is not improved by the coating.

Ronald K. Clark, 4557



Effect of chemical-vapor-deposited coating on equilibrium surface temperature in TPS applications.

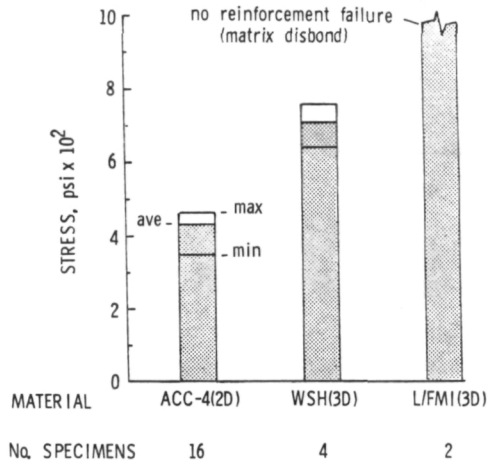
Three-Dimensional Architectures Improve Mechanical Properties of Carbon/Carbon Composites

Langley is conducting a research program to improve out-of-plane tensile and interlaminar shear strengths of carbon/carbon composites. One approach is to use three-dimensional reinforcement

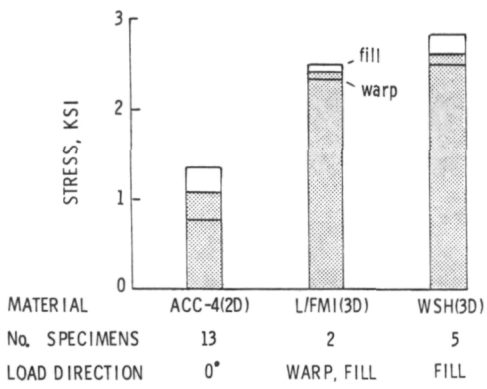
schemes in the fabrication of thin panels. To date, two types of three-dimensional carbon/carbon composites have been fabricated and tested along with two-dimensional advanced carbon/carbon (ACC-4(2-D)).

The first three-dimensional materials were fabricated at Langley using a three-dimensional preform of polyacrylonitrile yarns obtained from Fiber Materials, Inc.; hence the designation L/FMI(3-D). The architecture is a true three-dimensional orthogonal weave with fibers in the warp, fill, and thickness (*Z*) directions. The second three-dimensional material was fabricated by Woven Structures-Hitco (WSH(3-D)). The architecture is described as an angle-interlock system and has no fibers oriented parallel to the through-thickness (*Z*) direction. The warp yarns pass through the thickness at about 45° angles and contain fewer fibers than in-plane yarns.

The figures show out-of-plane tensile strength and interlaminar shear strength comparisons of the three materials. For both properties, the three-dimensional materials had much higher strengths. For out-of-plane tensile strength, WSH(3-D) was 65 percent stronger than ACC-4(2-D). The true strength of the L/FMI(3-D) material was not determined due to cohesive failures of the matrix on specimen surfaces. These failures occurred at stresses up to 975 psi, which is 130 percent stronger than ACC-4(2-D). For interlaminar shear strength, the three-dimensional materials were twice as strong. Thus, inclusion of fibers in the out-of-plane direction significantly improves out-of-plane mechanical properties.



Out-of plane tension strength of two- and three-dimensional carbon-carbon.



Interlaminar shear strength of two- and three-dimensional carbon-carbon.

Craig W. Ohlhorst, 4412

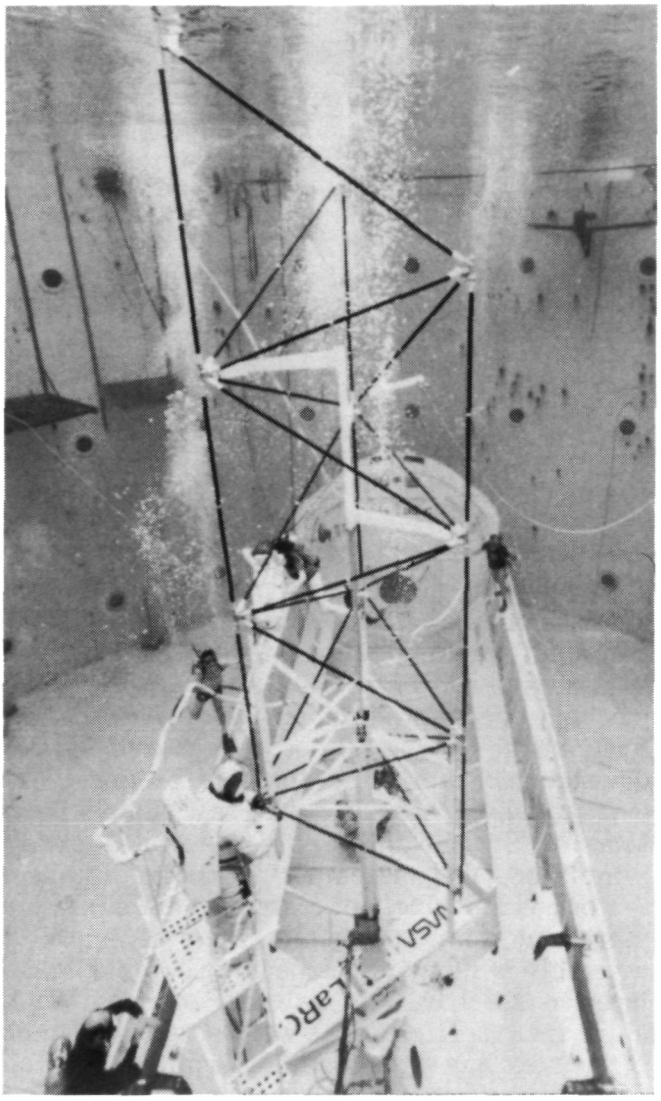
Underwater Neutral Buoyancy Tests Prove One-Man Assembly Concept Effective

An effective concept for assembly of an erectable beam-like space structure by a single astronaut would combine the intellect, versatility, and dexterity of man in combination with the mechanical advantage of a machine. An assembly fixture called swing arm beam erector (SABER), devised and fabricated for this program, was evaluated by a pressure-suited test subject in the Marshall Space Flight Center Neutral Buoyancy Simulator. The assembly fixture features a motorized movable foot restraint that eliminates astronaut manual translation tasks. When assembly of a bay of the beam is completed, the beam is mechanically indexed one bay length along its axis to clear the work site for assembly of the next bay. This method permits a constant assembly rate that depends only on the length of individual struts and not on the length of the beam being assembled.

Five consecutive assemblies of a three-bay beam were performed in one simulated EVA lasting 1 hour and 44 minutes, including four 10-minute rest periods. The pressure-suited test subject is shown at work on the structure in the Neutral Buoyancy Simulator. The total amount of structure assembled was equivalent to an 85-ft. 15-bay beam consisting of 150 struts and 48 nodes. The four rest periods, required in the test procedure, were not requested by the test subject, nor was reduction in productivity due to astronaut fatigue a factor within the limits of the data taken.

An average assembly rate of 26 seconds per strut was determined based on actual assembly time of 1 hour and 4 minutes.

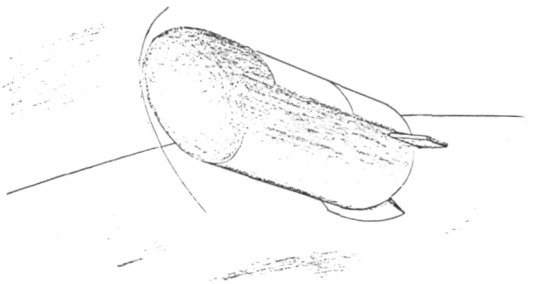
Judith J. Watson, 3596



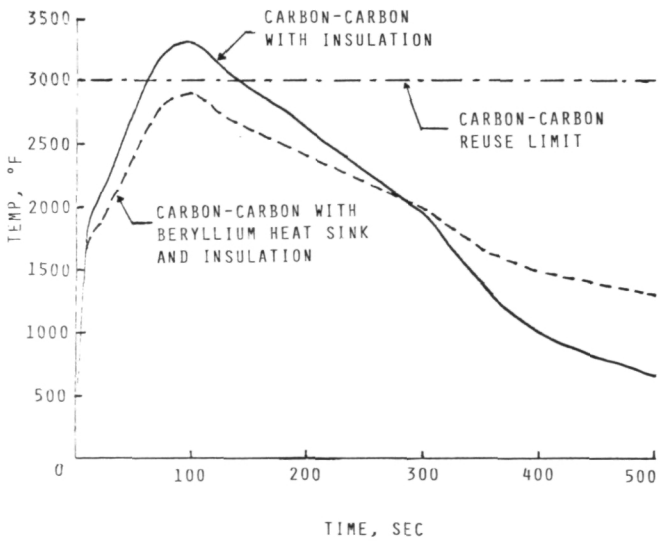
One-man structural assembly concept.

Thermal Protection System for Nose Cap of Aeroassisted Orbital Transfer Vehicle

The performance of an aeroassisted orbital transfer vehicle (AOTV) is greatly improved by passing the vehicle through the upper atmosphere and using the resulting lift and drag, rather than a rocket propulsion system, to dissipate most of the energy necessary to transfer from a high Earth orbit to a lower one. The nondeployable AOTV shown consists of a cylindrical body with a sloped, elliptical nose and fits in the cargo bay of the Shuttle orbiter, which allows the vehicle to be assembled and checked on Earth. As the vehicle passes through the atmosphere, the nose is subjected to high heating at the stagnation point. To accommodate this heating, either a nonreusable ablation system or a transpiration cooling system (a more complicated active system) has been proposed. A carbon-carbon heat shield is a more attractive alternative which is both passive and reusable. However, an insulated carbon-carbon heat shield, cooled only by radiation from its outside surface, would reach a peak temperature of 3300°F, which exceeds its 3000°F reuse temperature. However, by use of a beryllium heat sink beneath the carbon-carbon with a gap between them, the carbon-carbon heat shield can be cooled by radiation from both its inner and outer surface.



Aeroassisted orbital transfer vehicle.



AOTV atmospheric pass carbon-carbon temperatures.

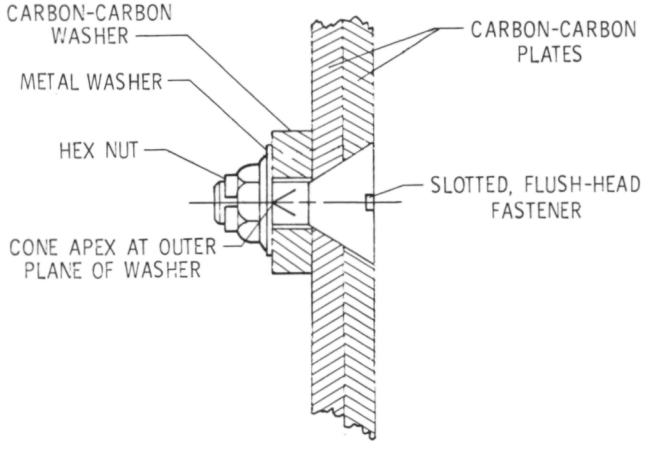
As shown, addition of a beryllium heat sink reduces the peak carbon-carbon temperature to below its reuse temperature. This system is comparable in weight to competing AOTV concepts. Thus, the combination of carbon-carbon heat shield and beryllium heat sink offers an attractive alternative for the nose cap of a nondeployable AOTV.

Max Blosser, 4295

Fastener Concept Developed for High-Temperature Composite Materials

For efficient design of high-temperature composite structures, joints must remain snug at all temperatures without producing large thermal stresses. Due to the large differences in the coefficient of thermal expansion for most high-temperature composites and metals, composite joints using conventional metal fasteners either become loose or generate large thermal stresses when heated. A metal fastener concept has been developed for joining high-temperature composite materials that provides a snug fit at all temperatures without producing large thermal stresses.

The thermal-stress-free fastener concept is shown in the figure. For a composite material with a uniform coefficient of thermal expansion in all directions, the fastener has a conical head with the vertex of the cone at the free edge of the pieces of composite material being joined together, as shown. As the joint is heated, the fastener and the composite material expand radially from the vertex of the cone. Any relative motion between the metal and the composite material (due to the difference in coefficient of thermal expansion) occurs along radial lines. Since both materials are free to expand, no thermal stresses are produced, yet the joint maintains good contact at all temperatures. For composite materials that have different inplane and through-the-thickness coefficients of thermal expansion, analysis shows that the thermal-stress-free fasteners must have a slightly curved shape. This shape depends on the coefficients of thermal expansion of the fastener and the material being fastened. If the coefficient of thermal expansion of the metallic fastener is considerably greater than that of the material being joined, a cone is a good approximation to the correct shape.



Thermal-stress-free fastener concept.

The thermal-stress-free fastener concept has been demonstrated for shear joints in carbon-carbon composite material using metal fasteners. The specimens, which were thermally cycled to 2000°F and held for 1 hour, did not show any evidence of thermal stresses or looseness of the joint. Shear tests conducted on specimens that had been thermally cycled showed static shear strengths that were equal to the shear strength for specimens that were not thermally cycled. The thermal-stress-free joints, mechanically loaded in shear, failed in bearing similar to composite joints using conventional fasteners.

James W. Sawyer, 2239

Carbon-Carbon Hot Structure Shuttle Body Flap Design

A carbon-carbon hot structure design of a replacement body flap for the Shuttle orbiter has been identified and analyzed. The baseline body flap design currently used on the orbiter consists of upper and lower honeycomb core panels which are supported by aluminum ribs every 20 in. and connected to a full-depth honeycomb core sandwich trailing edge. The aluminum structure is protected from entry heating on both upper and lower surfaces by thick reusable surface insulation (RSI) tiles, which comprise the majority of the body flap weight.

The carbon-carbon hot structure design, which eliminates almost all the RSI tiles, consists

of a torque box and tapered ribs which support the continuous lower skin. Because the leading edge of the body flap is sealed, no significant amount of air flows over the upper surface, and therefore the upper skin was removed to save weight. Removal of the upper surface also allows more heat to be radiated from the lower surface, thereby reducing its peak temperature from 2700°F on the baseline body flap to below 2400°F. The key considerations for the body flap design include high acoustic loads from the main engines during liftoff, low aerodynamic pressure loads, high entry heating, and ease of retrofitting the replacement body flap. Both static and dynamic analyses show the carbon-carbon design to be stiffer than the baseline body flap, and therefore a more effective control surface. Thermal stresses were found to be well below the material allowables and a detailed weight estimation indicated that this concept has the potential to save over half the 1460-lb weight of the existing body flap.

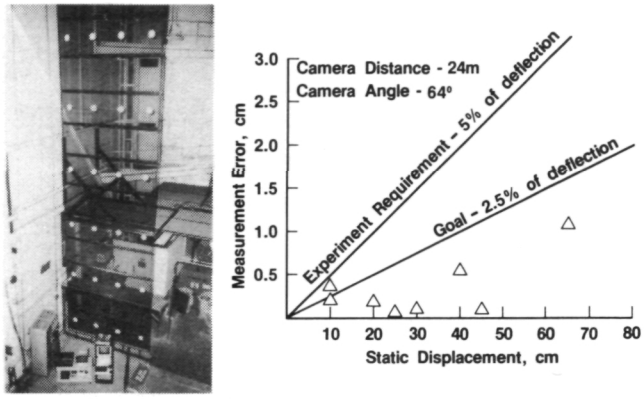
Max L. Blosser, 4295

Photogrammetric Measurement System Meets Solar Array Experiment Requirements

An experimental lightweight solar array for powering future space systems was tested on a Shuttle flight in September 1984, and the Shuttle closed-circuit television system was used to record video images of structural deformations of the solar array during orbital tests. A ground-based system has been designed to analyze these data by tracking the position change of specific targets from frame to frame. Data from four TV cameras will be merged in a triangulation program to determine a displacement time history of the solar array in Shuttle coordinates. This motion history will be analyzed using appropriate system identification techniques to determine the modal and frequency characteristics of the array in response to input excitations.

A full-scale ground-based mock-up of the solar array extended to the 70-percent deployed position was used earlier in a series of static displacement tests to determine the resolution capability of the video analysis system. The development goal was to achieve a resolution capability of 2.5 percent or less of the displacement. This goal is a factor of 2 better than the experiment requirement of 5 percent of the displacement. The system surpassed the goal in six out of seven test cases. The graph shows the results of the seven test cases compared to lines representing the experiment requirement and the development goal.

M. Larry Brumfield, 3196



Photogrammetric measurement system results.

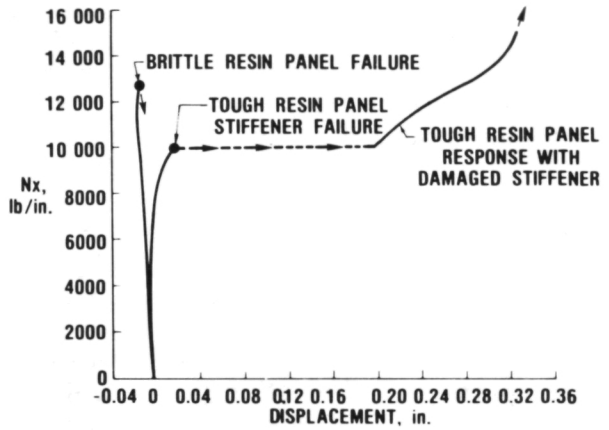
Damage Containment Demonstrated for Compression Panel With Tough Resin

As part of a research effort to study the failure mechanisms and damage containment capabilities of locally damaged compression components, a honeycomb blade stiffened panel was designed to satisfy heavily loaded wing panel requirements. Two specimens were fabricated, one using a delamination-prone brittle resin that has been used by industry for years and the other using a tough, delamination-resistant resin that has been shown (on the coupon level) to be less sensitive to impact damage. For these tests, local damage was simulated by 0.5-in.-deep sawcuts in the cap of an interior stiffener at panel midlength.

Test results indicate that the damaged stiffeners of both panels failed locally by a shear crippling failure mode when the strain gages near the end of the sawcuts recorded strains of approximately 1.1 percent. The local failure in the stiffener cap of both panels propagated across the honeycomb web to the skin-stiffener interface region in the same manner, but the global response of the two panels was different. In the brittle-resin panel, damage propagation continued by de-

lamination into and across the panel skin and failed the panel globally. For the tough-resin panel, local damage propagation was arrested at the skin-stiffener interface, and the panel subsequently carried a higher applied load Nx of about 15,000 lb/in. without failure. The graph compares out-of-plane deflections for the two specimens. These results indicate that a combination of damage-tolerant structural concepts and tough material systems is required to contain damage in heavily loaded structural components.

Jerry G. Williams, 4052



Damaged stiffener lateral displacement.

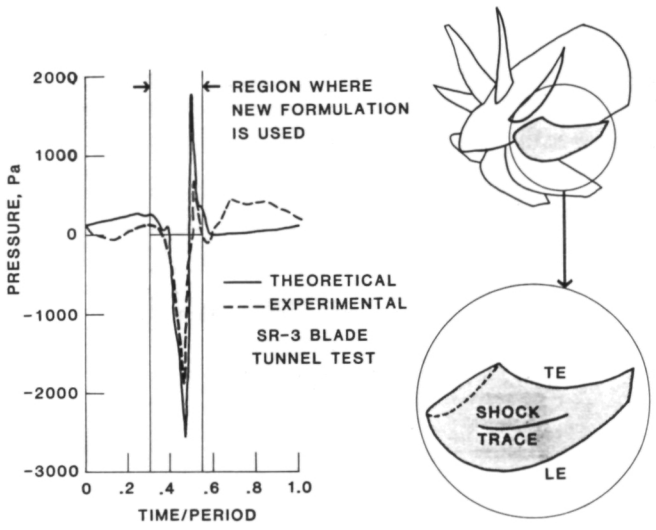
Prediction of Noise and Aerodynamics of Supersonic Propellers

Supersonic propellers with advanced blade geometry (propfan) can provide a significant improvement in the fuel efficiency of future commercial aircraft. Prediction of the aerodynamic performance and noise of supersonic propellers is an important problem which is under study at present. These propellers can produce high-level noise which affects both passengers and community. Understanding and hence predicting this noise can thus help in blade design (to reduce noise at the source) and also in fuselage structural design (to reduce interior noise). Accurate prediction of aerodynamic performance will ensure the efficiency of design and can also be used in noise prediction. The most current noise theories require knowledge of the blade surface pressure.

A new acoustic formulation particularly suited for prediction of the noise of transonic and supersonic propellers was derived at Langley. This is a solution of the Ffowcs Williams-Hawkings equation, which is the fundamental governing differential equation of noise generation. The main feature of the new solution is the avoidance of often troublesome singularities in previous solutions. In addition, high-frequency numerical error in an earlier formulation for high-speed propellers is also removed. The new solution consists of some surface integrals over the blade and some line integrals along the leading and trailing edges and the shock traces. A computer code for prediction of the noise of supersonic propellers has been developed which uses the new result when the blade approaches the observer at high speed. Another efficient formulation for subsonic blade motion is used whenever possible. Computed results indicate the superiority of the new formulation and are highly encouraging.

To obtain blade surface pressure, the observer location for acoustic calculation is moved onto the surface and a linear singular integral equation in terms of the unknown pressure is obtained. This integral equation can be solved numerically. It is compatible with analytic results for the aerodynamics of wings in compressible flow but is more general in scope and can be used for rotating bodies as well as wings. The new integral equation provides an alternative method for aerodynamic calculation to the existing highly complicated and time-consuming schemes based on the full-potential approach.

F. Farassat, 4308



Pressure generated by transonic propeller.

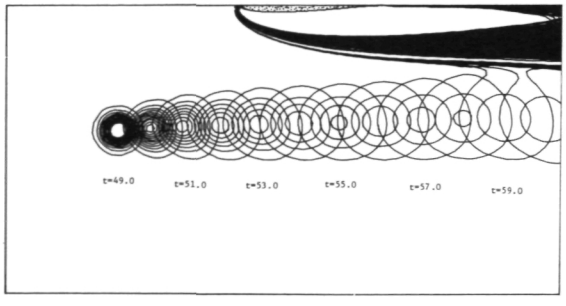
Aeroacoustic Computation of Blade/Vortex Interaction

An extensive in-house program is under way to understand and evaluate noise produced by the encounter of a distributed vortex with a lifting airfoil. Both analytical and experimental approaches are being pursued. Research into this phenomenon is motivated by the fact that such interactions result in the highly detectable "blade slap" noise radiation from the helicopters.

The computational apporach involves minimal solution of viscous-flow equations and produces results which are consistent with experimental observations. As a specific illustration of the calculations involved, the governing Navier-Stokes equations are solved at low Reynolds number in the stream function/vorticity form. A 100 $\times$ 256 boundary-fitted analytical grid is employed. The figure is a composite illustration depicting the temporal evolution of the calculated vorticity distribution during such an encounter. Solid lines indicate contours of constant vorticity. The airfoil can be seen in the upper middle along with its boundary layer and wake. The clear region surrounding the airfoil contains vorticity of higher magnitude than the values plotted. From such a time history, the noise radiation can be computed by standard aeroacoustic techniques.

Results of this research indicate the importance of the trajectory modifications and internal distortion of the vortex during a close encounter to the noise generation process. In addition, the apparent destruction of a vortex by such an interaction, which has been noted experimentally, has been observed in calculated results. Future work will evaluate methods of increasing the Reynolds number of the solution by approximate techniques for resolution of the boundary layer on the airfoil.

Jay C. Hardin, 4301

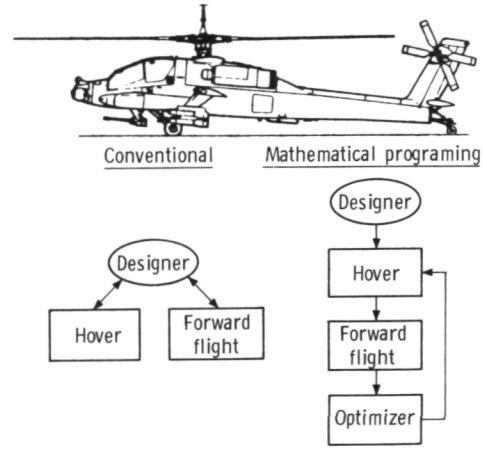


Vorticity contours during blade/vortex interaction.

Optimization Methods Applied to Rotor Blade Aerodynamic Design

One of the goals in helicopter design is to improve hover and forward-flight performance. A way of achieving this goal is through the use of advanced (nonrectangular) rotor blades. The design goal is to reduce hover horsepower without degrading forward flight performance. Designs are generated by determining the influences of rotor blade design variables (twist, percent taper or point of taper initiation, taper ratio, and solidity) on rotor performance and by adjusting these design variables to obtain desired performance. The conventional approach to the design of advanced blades combines a hover analysis program with a forward-flight analysis program. Although it has produced blade designs exhibiting improved performance, it is a tedious and time-consuming procedure.

Recently, formal mathematical programming techniques have been applied at Langley and elsewhere to the rotor blade design problem. The mathematical programming approach couples hover and forward-flight analysis programs with a general-purpose optimization program (CONMIN) to determine the blade taper ratio, percent taper, twist distribution, and solidity that minimize the horsepower required at hover while



Hover horsepower	1558 hp	1555 hp
Twist	-12^0	-10.6^0
Percent taper	.80	.85
Taper ratio	3.0	3.1
Solidity	.098	.092
Design time	5 weeks	2 days

Rotor blades designed by conventional and mathematical programming approaches.

meeting constraints on forward-flight performance. As shown in the figure, designs obtained using this approach for the blade of a representative Army helicopter compare well with those obtained using a conventional approach involving personnel-intensive parametric studies. Results from the present method can be obtained in 2 days as compared to 5 weeks required by the conventional procedure. Also, the systematic manipulation of the design variables by the optimization procedure minimizes the need for the researcher to have a vast body of past experience and data in determining the influence of a design change on the performance. Plans are to continue evaluation of the method for additional rotor blade configurations and to refine the procedure.

Joanne L. Walsh, 2887

Projects Directorate

The Projects Directorate is responsible for the implementation and management of specific tasks related to carrying out NASA Langley's research and technology role in aeronautics and space. These tasks include the following projects or functions: the Aircraft Energy Efficient (ACEE) Project, the Earth Radiation Budget Experiment/Stratospheric Aerosol and Gas Experiment (ERBE/SAGE II) Project, the Long Duration Exposure Facility (LDEF) Project, the Scout Project, the Aeronautical Systems Office (ASO), and the Space Technology Flight Experiments Office (STFEO).

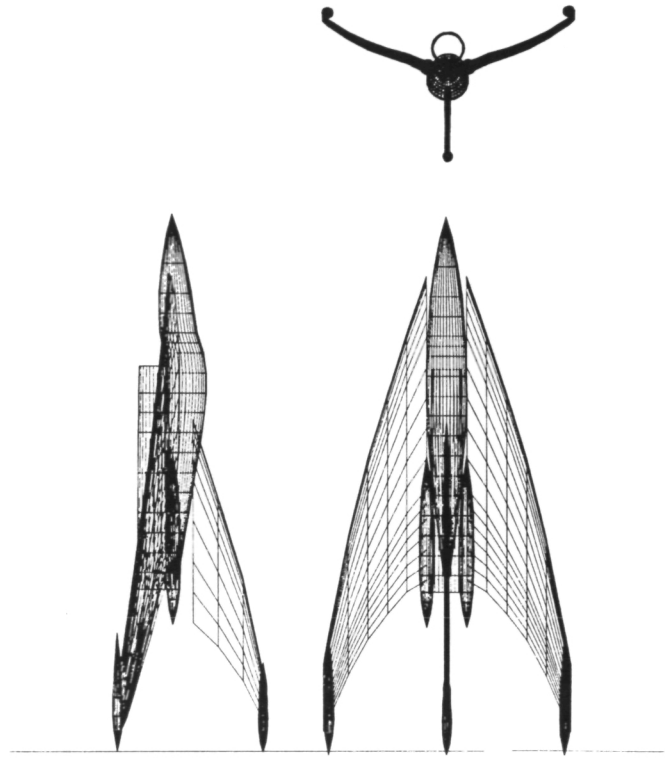
Management responsibilities explicitly include principal decisions concerning program content, scheduling, budgeting, operations planning, contract monitoring, and other aspects of project implementation. Responsibilities for assigned functions or projects include preparation of operating plans; negotiations with NASA Headquarters and other government agencies, universities, and industry; and administration of program funds and travel and manpower resources.

Technology Integration for Supersonic Cruise V/STOL Fighters

A new class of supersonic fighters under study has thrust-to-takeoff gross weight ratios of 1.4+ to provide exceptional sustained maneuverability across the Mach range, post-stall maneuverability, and, in addition, inherent capability for super-STOL (less than 500 ft) and/or vertical operation. Inherent super-STOL, STOVL, or VTOL can be achieved by either deflecting the primary exhaust near the aircraft's center of gravity or directing it vertically through the aircraft's center of gravity (vertical attitude takeoff and landing). The "tail-sitter" concept illustrated by the computer-generated drawings is one of the more unconventional in the new class of fighter aircraft.

The design incorporates many new technologies, including high-thrust-to-weight engines, all-axis vectored thrust control, reconfigurable fault-tolerant digital controls, advanced high-temperature lightweight metal matrix and composite materials/structures, active/passive variable wing camber and twist, and advanced high-Mach maneuver inlets. Preliminary systems integration studies indicate that this new class of fighter aircraft will be capable of sustained supersonic cruise, high sustained maneuver load factors across the Mach range, post-stall maneuverability, and super V/STOL operation, and it will be lighter and smaller than today's fighter aircraft while carrying more payload. Conformal fuel tanks will allow intercontinental deployment at supersonic speeds without refueling.

Samuel M. Dollyhigh, 4576



Thrust-vector control VTOL supersonic fighter concept.

Laminar Flow Control Technology

The most difficult problems in achieving laminar flow control (LFC) on commercial transports appear to be associated with the leading-edge region. Solutions to these problems will resolve many concerns about the ultimate practicality of laminar flow control. A flight program was initiated this year to evaluate the effectiveness of LFC leading-edge systems developed by the Douglas Aircraft Company and the Lockheed-Georgia Company under contract to the

Laminar Flow Control Project Office. Both companies designed and fabricated leading-edge test articles which have been installed on the NASA Jetstar at the Ames/Dryden Flight Research Facility. The test articles include all the systems that would be required in the leading-edge box for a future LFC transport: a suction surface and ducting system, a de-icing system, an anticontamination system, and a high-lift device in the Douglas test article.

The first flight of the aircraft was made in November 1983 to validate the aircraft flutter envelope. All systems installations were completed in March 1984 and acceptance flight testing has shown that all the systems are performing as expected and laminar flow has been achieved on each test article in flight. Research flight testing was initiated in August 1984 to expand the flight envelope for achieving laminar flow control. Early in 1985, the aircraft will be placed in a simulated service operation to evaluate the performance of the test articles in the airline operating environment.

Richard D. Wagner, 2045



Douglas leading-edge test article.



NASA Jetstar leading-edge flight test.

Advanced Composite Structures Technology

Five shipsets of NASA ACEE (Aircraft Energy Efficiency Program) composite horizontal stabilizers were installed on new Boeing 737 aircraft and delivered to airlines in 1984. This application represents the first composite primary structure to be certified for commercial aircraft in the free world. Revenue service began March 26, 1984. Composite transport wing key technology contracts have been successfully completed with tests to validate efficient designs with high resistance to damage, heavily loaded bolted joint concepts, and systems requirements for lightning protection and fuel containment. Four major contracts have been initiated to continue the development of technology for composite application to transport wing structures and to begin the development of fuselage design technology.

In a joint agreement with Lockheed, the redesign and construction of a composite center wing section of an advanced C-130 aircraft has begun. A significant data base is now available on second-generation composite materials using test procedures defined in NASA RP-1092, Standard Tests for Toughened Resin Composites. Tests conducted by NASA LaRC and the transport manufacturers show improvements in resistance to damage, but the improvements are not as pronounced as have been suggested by the material suppliers.

Herman L. Bohon, 3081



Advanced composite horizontal stabilizer installed on 737 aircraft.

Systems Engineering and Operations Directorate

The function of the Systems Engineering and Operations Directorate is to support ongoing aeronautical and space research at NASA Langley. This workforce is divided into four divisions with specific support functions. The Systems Engineering Division is responsible for structural, mechanical, electrical, and aeronautical systems engineering functions required to provide research models and flight hardware for aerospace research, applications, and technology. The Facilities Engineering Division is responsible for engineering and design of aerospace research and development equipment and institutional facilities for aeronautical and space research, such as special handling equipment, model supports, and special test equipment. The Fabrication Division is responsible for developing and fabricating aeronautical and aerospace research hardware related to ground support equipment as well as research facilities test equipment. This Division provides developmental manufacturing technology and electronics technical support, including communications systems and instrumented hardware. The Operations Support Division is responsible for providing the technical, mechanical, electrical, and maintenance services for research and institutional facilities. This Division operates laboratory equipment and wind tunnels, and collects, records, and interprets test data. In addition to the four divisions, the Facilities Program Development Office and the Systems Safety, Quality and Reliability Office are responsible to the Directorate.

Because of the unique requirements of some of the aerospace research performed at the Center, both engineers and technicians are involved in doing applied research in solving engineering and fabrication problems. These problems relate to support hardware and software in providing the experimental systems requested by research. The following contributions represent typical engineering and fabrication research and technology development activities in the Systems Engineering and Operations Directorate.

Nose Boom Development for the Global Tropospheric Experiment

In support of NASA's continuing effort to direct its applications program toward relevant national needs, NASA is conducting a Tropospheric Air Quality Program. The long-range objective is to apply NASA's space technology to assess and predict human impact on the troposphere on a regional and global scale. As a part of this effort, the Wallops Electra aircraft has been instrumented as a flight research vehicle to correlate directly measured data to those measured by satellite observation.

One aspect of this research involves the ability to measure the properties of minute air currents prior to disturbance by the aircraft. A highly specialized nose boom technology development program was undertaken to provide the means to make these measurements. To accomplish the design objectives, a high-modulus graphite epoxy prepreg material was selected and fabricated into a tapered, conically shaped 146-in.-long boom. Mounted to the boom is a conventional pitot static head with balsa vanes and close-coupled quartz pressure transducers to provide maximum data resolution. The base of the boom is attached to a support frame which houses the Inertial Navigation System, allowing the aircraft position to be closely correlated to the boom measurements, and a truss which attaches the systems to the aircraft. Extensive analyses were performed and special fabrication techniques were developed to build the boom in-house.



Nose boom installed on Electra aircraft.

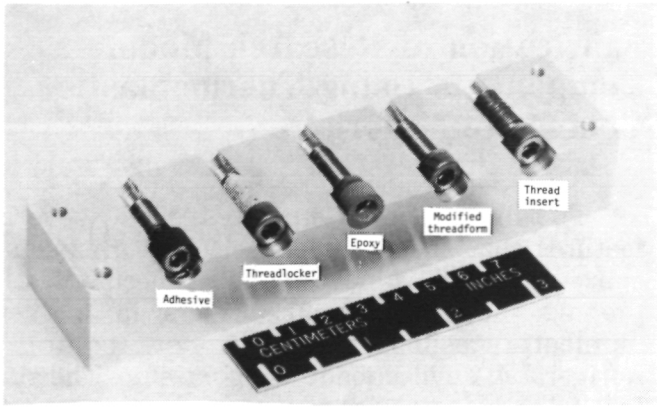
The recently completed flight test substantiated the structural capability of the installed nose boom; the Electra aircraft flew through its complete flight envelope and measured the vibration response of the nose boom to the aircraft vibration environment. The system provided significant vibration isolation from the low-frequency aircraft structural vibrations and provided good aerodynamic flow data for the minute atmospheric current measurements.

Robert K. Hedgepeth, 4666

Fastener Retention Systems for Cryogenic Wind Tunnel Models

Fastener retention systems tests were carried out as a part of the cryogenic models technology development activities at the Langley Research Center. Five fastener retention systems were tested by using A-286 screws with specimens made from the primary metallic alloys that are currently used for cryogenic models. Although fastener retention should always be a primary consideration in the design of wind tunnel models, this factor becomes even more critical for high-Reynolds-number testing at cryogenic temperatures and under high loads such as those which may be imposed on model systems to be tested in the new National Transonic Facility (NTF). The looseness, loss, or failure of a fastener could lead to structural component failures, which in turn could result in damage to the wind tunnel.

Self-locking thread insert, modified thread form, threadlocker sealant, adhesive, and an aluminum-filled epoxy were evaluated. The locking system effectiveness was examined by simple no-load cycling to cryogenic temperatures (-275°F) as well as by dynamic and static loading at cryogenic temperatures. It was found that cryogenic cycling (in the absence of mechanical loading) generally produced decreases in breakaway torque (loosening of screws). Also, tests at -275°F showed that cold temperatures act to improve screw retention. The modified thread form emerged as the best choice for cryogenic application, particularly for small screws. Differences between the devices with respect to application, cleanup, and reuse were evaluated. The results of this work have established a data base for choosing retention devices. These data are not limited to cryogenic model systems application; they have application to conventional wind tunnel models or other types of mechanical systems which require screw retention and in particular where the more conventional methods (such as safety wiring) cannot be used.



Fastener retention systems.

John W. Wallace, 4666

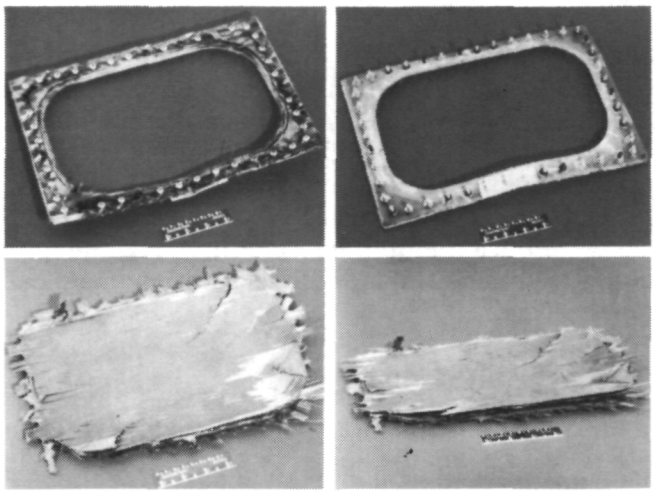
Explosively Severed Composite Panels for Aircraft Safety

Major accomplishments have been achieved in the conceptual development of explosively severed panels for emergency venting and egress from military and commercial aircraft. The U.S. Army is currently funding this program to increase the reliability and reduce the weight of an emergency ground egress system for the new Hughes AH-64A advanced attack helicopter. The helicopter application is to embed an explosive cord in composite frames of four side windows to allow (on initiation) egress of a two-member crew.

This principle is now being expanded to develop explosively severed composite panels for military and commercial aircraft for venting smoke (the greatest hazard) from the fuselage in case of fire and to provide passenger egress. The approach is to replace portions of the outer structure with composite panels containing a tiny, highly stable, unlimited-service explosive cord embedded in the panel. On initiation of the explosive cord, the panel is severed and jettisoned, as shown by the 10-by-14-inch graphite/epoxy specimen illustrated. The outboard side of the severed panel is shown at the upper left, the inboard side is at the upper right, and the 8- by 12-in. severed portion is shown in the bottom

photographs. The fiberglass frame on the inboard side eliminates potential harm to occupants. The goal is to make these panels as large as desired (with built-in reinforcing structure), and to allow installation in virtually any location with no loss in the structural integrity of the aircraft.

Laurence J. Bement, 4621



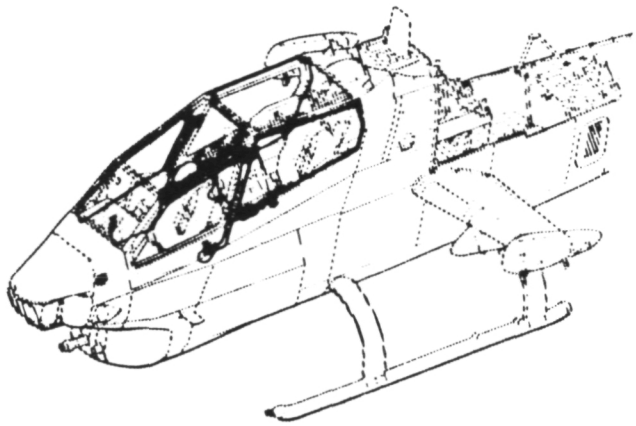
Development of severed composite panel.

Field Repair of AH-1G Helicopter Window Cutting Assemblies

The U.S. Army AH-1G helicopter utilizes explosively actuated window cutting assemblies to break the aircraft's four acrylic side windows for emergency ground egress. The Army procured this system as a complete package. A small explosive cord was installed in a plastic frame, which was mounted to the window frames. The system was designed and qualified to have the explosive cord in contact with the acrylic; no consideration was given to the possibility of cord-to-acrylic gaps. However, the plastic frames holding the explosive cord became distorted in service by heat and age, causing gaps up to 0.3 in. between the explosive cord and the acrylic. An inspection of 15 aircraft revealed that at least one of the four side windows on each aircraft had large gaps. Since this system was essential for crew survival, the entire fleet of over 300 aircraft was subject to grounding in order to replace the window cutting assemblies. The Army was faced with the problem of determining what gap, if any, was acceptable, and how to make this determination. Also, a field repair procedure was needed in order to reduce system costs and down time on the aircraft.

At the request of the Army, a research program was initiated at the Langley Research Center to address the problem. Past experience at LaRC has indicated that room temperature vulcanizing silicone compound (RTV) responds as an incompressible fluid under explosive pressure inputs. Therefore, RTV was installed in the gaps with a hand-held/operated injection gun to transfer the explosive energy to the acrylic. Functional tests with preset gaps between the explosive cord and the acrylic revealed that gaps up to 0.1 in. were acceptable without RTV; RTV-filled gaps of up to 0.25 in. achieved fully functional severance. This repair method was documented by LaRC and immediately incorporated into the Army's AH-1G aircraft service procedures.

Laurence J. Bement, 4621



Army helicopter in which four side windows are explosively severed for emergency ground egress.

Fabrication of Research Model Components Using Thermoplastic Composite Material

Thermoplastic composites have several features that suggest their selection over some epoxy composites now in use. Thermoplastic prepreg material (graphite fibers in a thermoplastic resin system) do not require a refrigerated environment as epoxies do. The surface adhesive qualities of thermoplastics are not affected by temperature or humidity, hence no

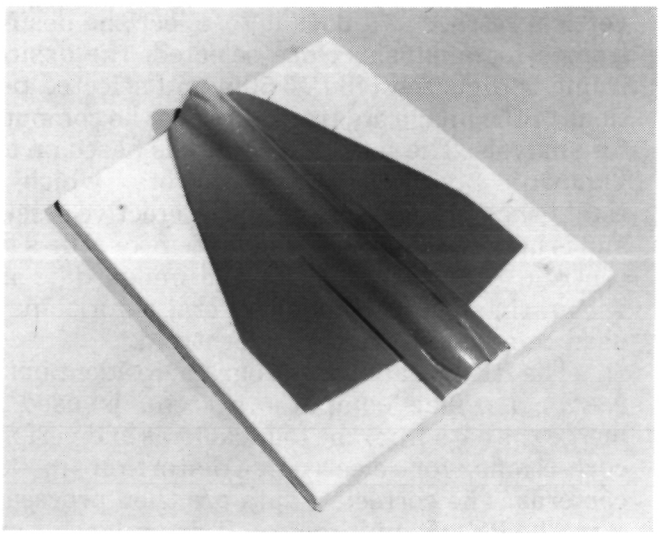
special air conditioning is required in the work area. With the remelt capability of thermoplastics, it is possible to tack ply laminates together using a soldering iron, assuring ply orientation during the cure cycle. Finally, thermoplastics can be recured if additional ply layup is required.

To research the fabrication techniques, a pattern of an advanced fighter aircraft was selected which included the wing and fuselage. A ceramic matched die mold was cast because ceramic was found to be economical, easily formed, and capable of withstanding the temperatures and pressures of the cure cycle.

Eight layers of the prepreg were placed in a quasi-isotropic layup. The layup method developed was to pre-form the shape to minimize bulk, thereby allowing the fiber orientation to remain true and constant. This was accomplished by stripping the correct length of prepreg, manually inserting the prepreg into the mold, and tacking successive strips together to acquire the shape of the mold and ultimately the part. This method is vital in the fabrication of complex-shaped pieces. Each layer is made in this manner until all eight layers are formed.

The mold is then heated to 800°F, the preformed thermoplastic is inserted into the ceramic mold and 700 psi pressure is applied by a heated press. After 10 minutes, the temperature is reduced to room temperature, pressure is reduced, and the part is removed. Thermoplastic material can be worked easily with normal shop equipment and all standard methods of repair and finishing apply to the component part.

Benjamin F. Guenther, 2651



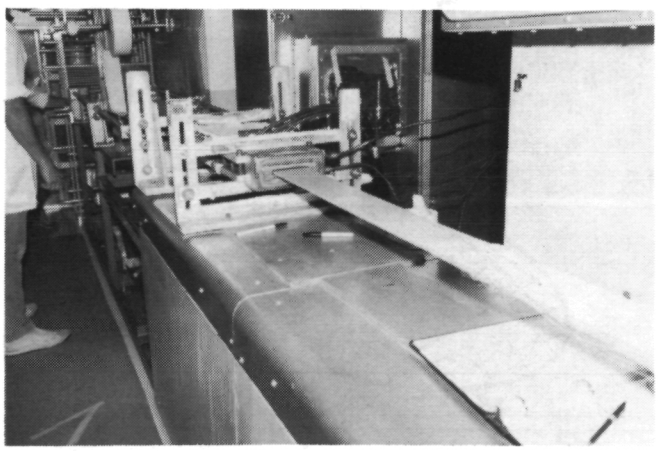
Thermoplastic composite model.

Pultrusion Fabrication Technology

Small airfoils having symmetrical and asymmetrical profiles are required for turbulent and viscous drag reduction research. These airfoils have 0.5- and 1.3-in. chord lengths and are 48 in. long. Because conventional machining methods are costly and produce marginal-quality structures, pultrusion techniques using reinforced plastic composites were tried and proved to be successful. The pultrusion materials used were polyester and vinyl ester matrices and fiberglass and Kevlar reinforcements. These airfoils are now being produced at a rate of 2 ft per minute. Wind tunnel test results of airfoils indicate that these pultruded materials, scaled up for retrofit on present aircraft, could result in fuel savings in the millions of dollars per year when used as large-eddy airflow breakup devices.

The pultrusion techniques are also employed in fabricating reinforced plastic structures using a new material concept in which fiberglass roving oriented in the 0°-90° directions is locked in position by polyester knitting. This orientation allows equal strengths to be obtained in both longitudinal and transverse directions. It is now possible to produce a long flexible structure for space boom models measuring ¼ in. by 4 in. by 32.8 ft. These components are produced at a rate of 1 ft per minute. These boom models were required to develop ground dynamic test methods for very large low-frequency space structures. This composite material is 34 percent lighter than 6061 aluminum alloy and 28 percent greater in tensile strength.

Maywood Wilson, 2781

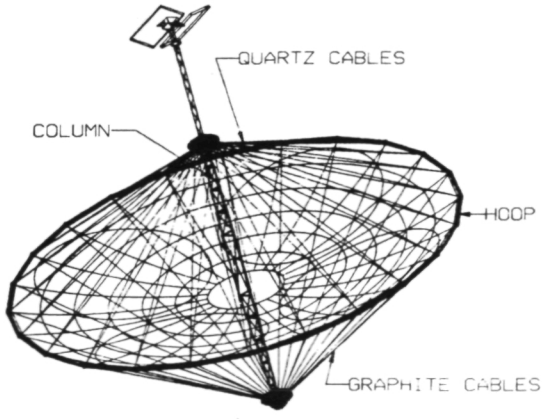


Long flexible space boom model composite fabrication by pultrusion.

Quartz Cable/Steel Bead Bond Joint for Hoop-Column Antenna

The hoop-column antenna structure has a column located in the center and perpendicular to a hoop, as illustrated. The location of the hoop relative to the column is maintained by a series of graphite and quartz cables. A bead end fitting secures each cable by seating on a nozzle, which is attached to the column. A good joint is required between the cable and bead for control of the hoop location and subsequent control of the antenna surface. The graphite and quartz cables are constructed of fibers held together by a Teflon matrix with a cross-wrap of Nomex which also acts as a protective cover. Because the bead size is constrained by the cable guide design, it was necessary to develop an efficient bond joint. The bond to the graphite cables was relatively simple because the Teflon could be removed from the bond area by heat (burning). However, since heat damages the quartz fibers, a different bonding technique was required.

A procedure was developed at LaRC which involved etching the Teflon matrix, selecting the bonding material, and controlling the process to achieve an efficient and repeatable bond. The bonding procedure involves coating the surface with Tetra-Etch to break down the surface of the Teflon. To insure a consistent bond, great care is taken to clean the bond area and to spread the bundles of the cords apart to maximize the bond area. The bead is then moved into place and epoxy (EA956) is applied with a hypodermic needle inside the bond area. This forces the EA956 to fill from the center of the quartz cord out to the bonding surface of the bead, insuring a mechanical and a chemical lock. The ends of the Nomex are then moved under the bead so no loose ends can unravel. This procedure has been proved by test data to satisfy all strength requirements without any damage to the quartz fibers.



Fifteen-meter hoop-column antenna.

Elvin Ahl, 4571

Video Processor for Dynamic Analysis of Large Structures

The Solar Array Experiment (SAE) video processor is a special-purpose automated video analysis system developed at NASA Langley to support the SAE of the OAST-1 package aboard STS-41D. During the dynamics experiment of OAST-1 the 100-ft-long solar array will be excited by paired firings of Shuttle vernier thrusters. The motion of the array will be recorded in the form of video tapes of the images from four Shuttle video cameras. Sixty-four targets mounted on both sides of the array provide identifiable features on the video images for tracking. Following the flight, the video tapes will be returned to NASA Langley for processing.

The first step in this process is for the SAE video processor to extract a time history of the position of each target in the camera image plane and store these coordinates on magnetic tape for further processing. Following a short interactive session, the system automatically processes the video from a single dynamic test (up to approximately 18,000 frames). The system reads the time code that the Shuttle video system places in the vertical retrace and uses it to select the desired frames for analysis. Once selected, the desired frame is digitized (480 × 500) and selected portions of the image are transferred to the computer for analysis. The selection of data is based on the "known" position of the targets, which is established initially during the interactive session and is updated each time the system identifies the centroid of a target. Once the image data are within the system, one of several algorithms is used to identify the target centroid.

The RIMS data base program, resident in the NASA Langley computer system, is used to merge the data from the four cameras and perform corrections for electronic distortion in the cameras. The corrected data are then processed by STARS (Simultaneous Triangulation and Resection System) to extract the camera

parameters and a time history of the target motion in three-dimensional Shuttle coordinates.

The SAE video processor was constrained to use existing Shuttle raster scan video as a data source. The system, as built, can provide noncontact measurements of the motion of other large structures. The technology developed in this program could be extended readily to cameras using addressable array sensors, permitting real-time operation, higher bandwidths, and the flexibility of using a mixture of active and passive targets.

James B. Miller, 4621



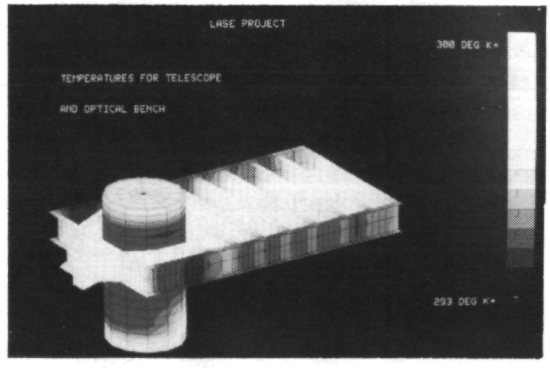
SAE video processor system.

Optimal Design of a Thermally Stable Optical Bench

The Lidar Atmospheric Sensing Experiment (LASE) will make high-altitude measurements using critically sensitive optical components. Conventional optical benches are designed to operate in a thermally controlled laboratory to minimize the thermal distortion effects on the optical components; thus, in order to maintain the integrity of the LASE's optics, a thermally stable optical bench is required. In a laboratory, the thermal effects of dissimilar materials can be controlled and calibrated out so as not to distort the optics. However, in a high-altitude flight, test calibration is made preflight, thermal excursions are impossible to control, and gross weight is a constant concern. A design for the optical bench was developed at Langley which utilizes a graphite-epoxy laminate and combines the optimal design aspects of light weight, high strength, and a near-zero coefficient of thermal expansion (CTE).

A thermal model of the experiment and the test bay of the ER-2 aircraft was used to determine component temperatures for the entire flight test envelope. Flight thermal measurements using the ER-2 aircraft were found to be in agreement with the model's predictions. The results from the model were used as thermal boundary conditions for more detailed thermal models of the telescope and optical bench. The temperature results from the thermal analysis were used with finite-element structural models to predict distortions. The finite-element models were also used to evaluate the coupled transient thermal and steady-state mechanical response of the instrument in the proposed flight environment. Results of the analysis indicated that for the design laminate the deformations were minimum and would not adversely affect the critical alignment of the optical components. The layup of the graphite-epoxy laminate was designed to achieve zero coefficient of thermal expansion while maximizing the stiffness in the primary direction for all members in the structure. Preliminary CTE test results on the proposed laminate correlate well with the analytical predictions.

D. Petley, 4508



Optical bench math model.

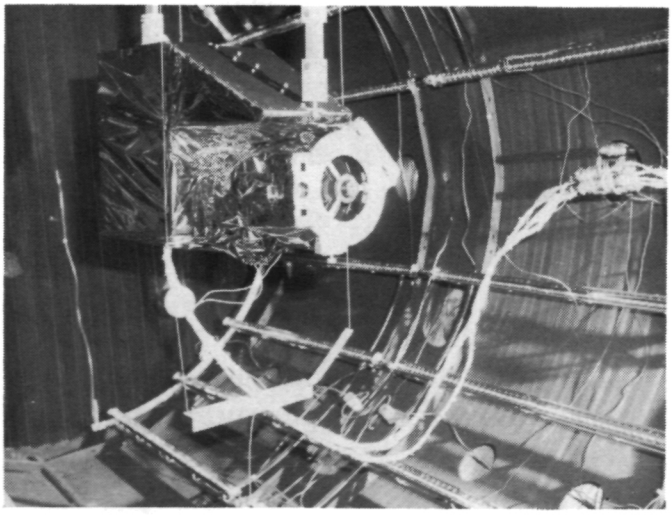
Thermal-Vacuum Testing and In Situ Optical Alignment Measurements of the HALOE Telescope and Sun Sensors

The Halogen Occultation Experiment (HALOE) will measure the amounts of various

halogen constituents in the Earth's stratosphere with an infrared telescope while in Earth orbit. In order to accomplish this mission, precise alignment (±1.35 arc minutes) of the telescope relative to the Sun sensors must be maintained during occultation as the optical components are subjected to rapid temperature changes while in orbit. A finite-difference thermal model and a finite-element structural model of the Telescope/Sun Sensor Assembly were constructed. Predictions of temperature changes and structural deflections and rotations were made for Earth orbital conditions. A determination of the prediction accuracy of the thermal and structural models was made by conducting a thermal-vacuum test on the flight hardware and measuring both temperature gradients and structural deflections in the hardware.

The thermal-vacuum test was unique in that optical alignment measurements were made in situ in the vacuum chamber by incorporating an optical viewing port in the chamber end wall for observation of the assembly with an alignment telescope located outside the chamber. Various temperature gradients were imposed on the hardware with the use of flight heaters on the telescope mirrors and Sun sensor and strip heaters mounted especially for the test. Optical alignment measurements were made under steady-state temperature conditions.

Comparisons of the temperature and optical alignment test data with predictions from the thermal and structural models were made. Modifications to the models were performed where necessary to obtain agreement with the test data. The models have been validated so that accurate predictions can be made for all flight conditions.



HALOE Telescope/Sun Sensor in 8 × 15 vacuum chamber.

The test results demonstrate a method of validating analytical models by testing hardware under a known set of ground test conditions that can be extrapolated to flight conditions.

Dewey M. Smith, 4508

Technology Utilization Program

One of NASA's Congressionally mandated responsibilities is to promote economic and productivity benefits to the nation by facilitating the transfer of aerospace-generated technology to the public domain. NASA's means of meeting this objective is its Technology Utilization Program, which provides a link between the developers of aerospace technology and those in either the public or private sectors who might be able to employ the technology productively.

One important facet of NASA's Technology Utilization Program is its applications engineering projects, which involve the use of NASA expertise to redesign and/or re-engineer existing aerospace technology to solve problems encountered by federal agencies or other public-sector institutions. Applications engineering projects originate in various ways. Some stem from requests for NASA assistance from other government agencies and some are generated by NASA engineers or scientists who perceive possible solutions to public-sector problems through the adaptation of NASA technology. In addition, NASA employs a multidisciplinary applications team which contacts public-sector agencies, medical and public-health institutions, and professional organizations to uncover significant problems in fields such as health care, public safety, transportation, and industrial processes which might be amenable to solution by the application of NASA technology. The projects reported on here are typical of the applications engineering efforts conducted at NASA Langley in support of the Technology Utilization Program.

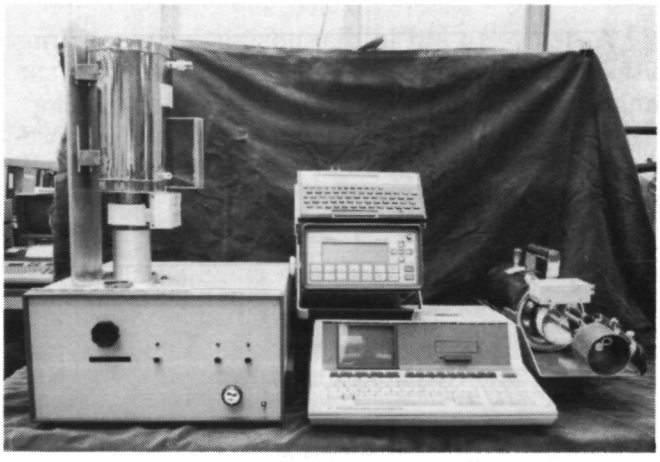
Water Quality Monitoring System

A prototype system for determining the elemental content of water and toxic wastes has been developed under LaRC direction in a collaborative NASA/EPA project. The system represents a modification of the X-Ray Fluorescence Spectrometer which was used to determine the inorganic constituents in Martian surface samples for the Viking missions to Mars in 1976.

The system, as designed to accomodate EPA's objectives, is intended to be sufficiently portable to be transported in a van to a source of water—lake, stream, estuary, or industrial effluent discharge channel—to sample and perform a series of analyses on site to determine the chemical content of the water. Of particular interest are the high-priority toxic metals, such as As, Hg, Pb, Cd, and Cr. Over 30 elements can be detected with accuracies in the 10 ppm range or less.

The overall water quality monitor system is comprised of a main electronics unit powered by rechargeable batteries, which includes a 1000-channel pulse height analyzer, spectrum display, and computer interface; a high-sensitivity sensor head containing a high-resolution cryogenic Si (Li) X-ray sensor and a ruggedized portable X-ray tube, all powered by an auxiliary battery pack; a data processor unit, including an HP-85 computer, CRT display, thermal printer, and tape recorder; and a sample handling equipment module. Delivery of the first prototype system to EPA is scheduled for December 1984. Field tests at three sites (to be selected) will be accomplished in 1985.

Warren C. Kelliher, 4641



Prototype elemental analyzer system.

Collagen Phase Transition in Thermal Skin Death

Recent studies of skin burns using an ultrasonic diagnostic technique being developed at LaRC for human patients have resulted in a significant breakthrough in the understanding of skin death (necrosis) due to high-temperature thermal exposures. The ultrasonic studies link thermal necrosis with the crystalline-amorphous (first-

order) phase transition of collagen. Collagen, which comprises 40 percent of the skin tissue, is found to undergo an abrupt increase in density (characteristic of such a transition) only at the necrotic tissue sites. Further, skin death occurs for high-temperature exposures only at those sites experiencing the collagen transition.

The study also reveals that an energy expenditure of 11.7 cal/g is required for the phase transition to occur. This value is found to be in agreement with independent in vitro calorimetric studies of extracted collagen. The present findings are the first direct in vitro confirmation of the dominant role of collagen in skin death, and they emphasize the sensitivity of the ultrasonic technique in diagnosing thermal injury to skin tissue.

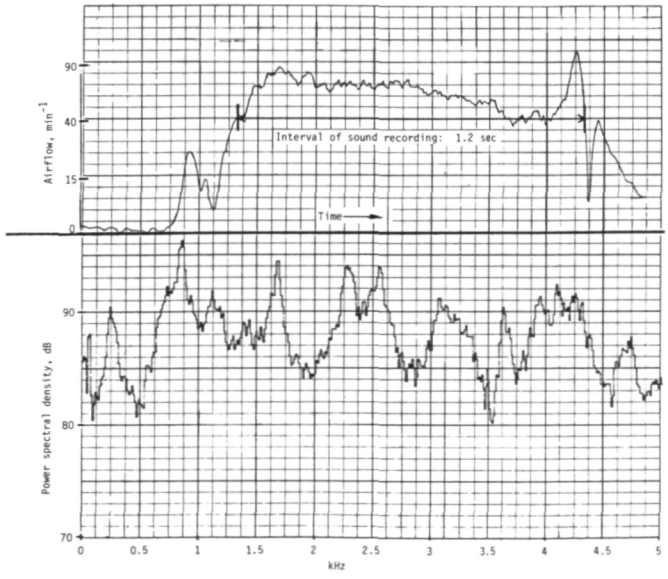
John H. Cantrell, Jr., 3036

Noninvasive Lung Diagnosis Through Sound

A device to aid in diagnosing incipient lung disease by analysis of sound radiation from the lung during expiratory airflow is under development. This work is being carried out in collaboration with the Medical College of Virginia in Richmond, Virginia. The technique employed is based upon a theory of sound generation in the human lung which was derived at Langley Research Center. The theory indicated that each order of bronchi within the lung radiates a characteristic frequency, dependent upon its diameter and the flow velocity through it. This theory has been validated experimentally on both glass lung models and animal lung bronchi in tests conducted at Langley Research Center.

The figure displays a typical recording obtained from a human subject tested at the Medical College of Virginia. The upper plot shows expiratory volume flow, in liters per minute, as a function of time. The lower plot depicts the spectral density of the sound radiation recorded by a microphone located proximal to the subject's mouth and taken over the time interval in which the velocity was nearly constant. The peaks seen in the spectrum are produced by the various orders of bronchi. Both the frequency and the amplitude of these peaks have been shown to be very sensitive to incipient lung disease. Characteristic signatures of various lung disorders are presently being catalogued at MCV.

Jay C. Hardin, 4301



Pattern of breathing during spectral sound recording (top) and sound spectrum during near-constant expiratory airflow (bottom).

1. Report No.	2. Government Accession No.	3. Recipient's Catalog No.
NASA TM-86321		

4. Title and Subtitle	5. Report Date
Research and Technology 1984 Annual Report of the Langley Research Center	November 1984
	6. Performing Organization Code
7. Author(s)	8. Performing Organization Report No.
	10. Work Unit No.
9. Performing Organization Name and Address	
NASA Langley Research Center Hampton, VA 23665	11. Contract or Grant No.
	13. Type of Report and Period Covered
12. Sponsoring Agency Name and Address	Technical Memorandum
National Aeronautics and Space Administration Washington, DC 20546	14. Sponsoring Agency Code

15. Supplementary Notes

16. Abstract

The role of the Langley Research Center is to engage in the basic and applied research necessary for the advancement of aeronautics and space flight, to generate new and advanced concepts for the accomplishment of related national goals, and to provide research advice, technological support, and assistance to other NASA installations, other government agencies, and industry. This Langley Research Center 1984 Annual Report on Research and Technology contains highlights of our major accomplishments and applications made during the past year. The highlights illustrate both the broad range of the research and technology activities at the Langley Research Center and the contributions of this work toward maintaining United States leadership in aeronautics and space research. For further information about the report contact Jerry C. South, Chief Scientist, Mail Stop 103, Langley Research Center, Hampton, Virginia 23665, (804) 865-3316.

17. Key Words (Suggested by Author(s))	18. Distribution Statement
Research and technology	Unclassified - Unlimited Subject Category 99

19. Security Classif. (of this report)	20. Security Classif. (of this page)	21. No. of Pages	22. Price
Unclassified	Unclassified	109	A06

For sale by the National Technical Information Service, Springfield, Virginia 22161 NASA-Langley, 1984

7/30/85 Keith Zeisel #113/HQ 63/672

National Aeronautics and
Space Administration

Washington, D.C.
20546

Official Business
Penalty for Private Use, $300

SPECIAL FOURTH CLASS MAIL
BOOK

Postage and Fees Paid
National Aeronautics and
Space Administration
NASA-451

U.S.MAIL

NASA

POSTMASTER: If Undeliverable (Section 158
Postal Manual) Do Not Return

McDONNELL DOUGLAS
LIBRARY
ST. LOUIS, MISSOURI
12 JUN 1985
21 0U